HIDRAULICA

HYDRAULICS-PNEUMATICS-TRIBOLOGY-ECOLOGY-SENSORICS-MECHATRONICS

2022

June

No. 2

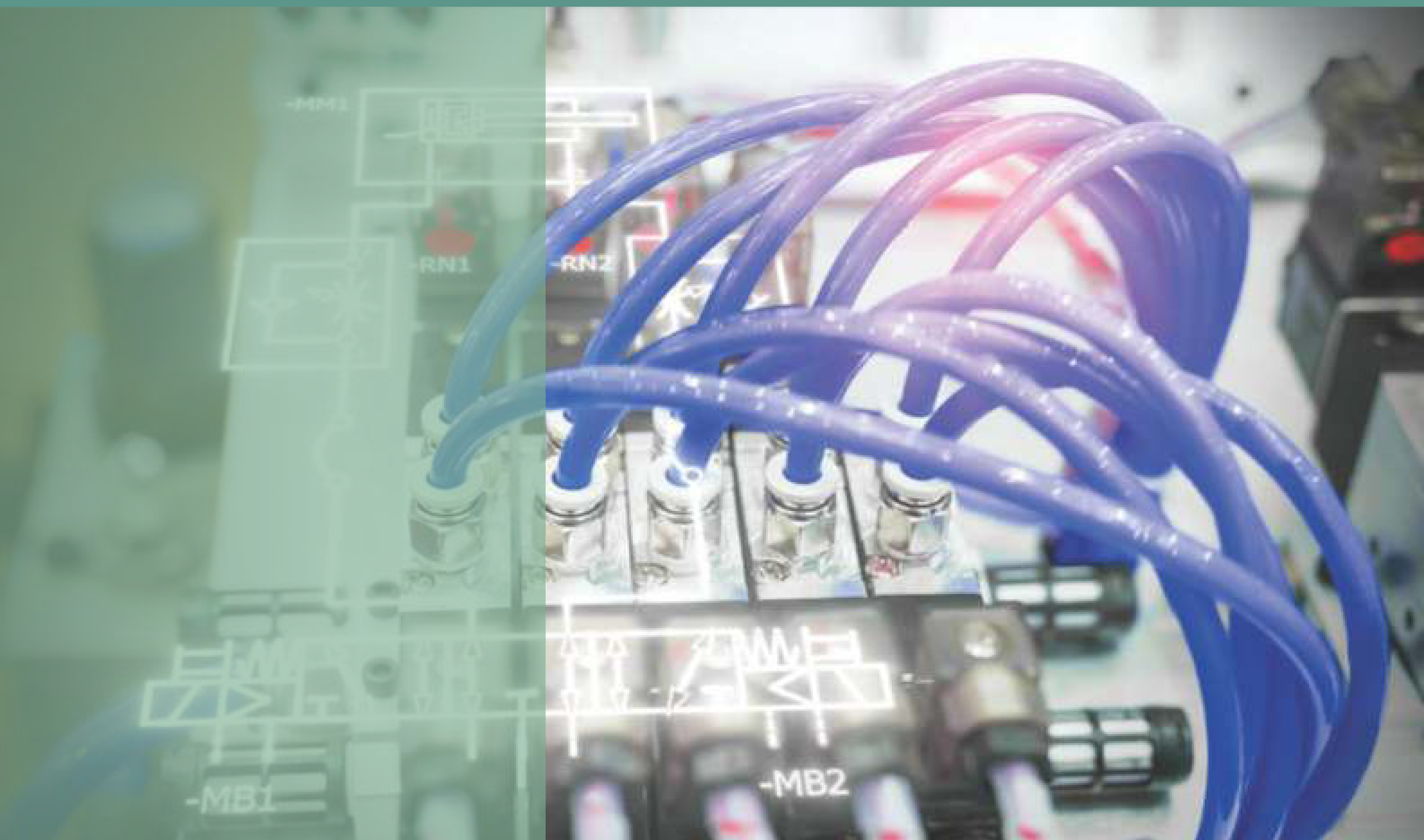

ISSN 1453 - 7303
ISSN-L 1453 - 7303

https://hidraulica.fluidas.ro

CONTENTS

BOARD

Published by:
Hydraulics and Pneumatics Research Institute, Bucharest-Romania
Address: 14 Cuţitul de Argint, district 4, Bucharest, 040558, Romania
Phone: +40 21 336 39 91; Fax: +40 21 337 30 40; e-Mail: ihp@fluidas.ro; Web: www.ihp.ro
with support from:
National Professional Association of Hydraulics and Pneumatics in Romania - FLUIDAS
e-Mail: fluidas@fluidas.ro; Web: www.fluidas.ro

HIDRAULICA Magazine is indexed by international databases

ISSN 1453 – 7303; ISSN – L 1453 – 7303

EDITORIAL

Cum mai stăm cu specialiştii în domeniul hidraulicii şi pneumaticii

Dr. Ing. Petrin DRUMEA
DIRECTOR PUBLICAȚIE

În ultimii câțiva ani dezvoltarea hidraulicii a cunoscut o descreștere treptată pe toate subdomeniile și pe toate direcțiile. Nu prea mai avem concepție și proiectare, nu prea mai avem producție, iar, mai nou, nu mai suntem capabili să întreținem utilajele acționate hidraulic. Ani de zile am avut o asociație profesională care avea și o sectiune a specialiștilor, care constatăm cu surprindere că de câtiva ani este în agonie.

Noua generație de hidraulicieni, extrem de redusă numeric, nu doar că nu mai reușește să se impună pe planul economico-industrial, dar nu mai reușește nici măcar să mai atragă sau să formeze specialiști noi pentru domeniu. Grav este că întreținerea echipamentelor și sistemelor hidropneumatice a trebuit să fie preluată de mecanici sau de electricieni, iar aceștia consideră această activitate, pe bună dreptate, ca pe o muncă suplimentară și, ca urmare, o și tratează în consecință.

Cauzele care au condus la această situație sunt multiple; pe unele am încercat și noi la revistă să le analizăm, dar nu acesta este subiectul discuției de astăzi. Se pare că acum este esențial ca la nivelul pregătirii profesionale să abordăm elementele concrete, să reintroducem ideea proiectării, să reinventăm specialiștii în mentenanță și să analizăm care sunt tendințele de dezvoltare a domeniului. Reamintesc ideea elementară că orice utilaj care implică măcar un element în mișcare trebuie să includă un sistem de acționare care poate fi electric, hidraulic, pneumatic sau pur mecanic. În majoritatea cazurilor sistemul este combinat și, de obicei, comandat electronic cu ajutorul soluțiilor informatice.

Pentru cei care se ocupă de pregătirea profesională a tinerilor, trebuie mare atenție întrucât nu există nici un echipament industrial alcătuit doar din blocul informatic. Trebuie neapărat să existe și specialiști în mecanică, și specialiști în electrică-electronică, și specialiști în hidraulică și pneumatică.

Primul pas care ar trebui făcut în cel mai scurt timp este ca toți lucrătorii din domeniu să urmeze cursuri de perfecționare specifice activităților zilnice. Ca urmare, ar trebui reactivate cursurile de nivelul 1 la nivel de muncitori și tehnicieni și cursurile de nivelul 2 pentru inginerii din mentenanță. Ar fi bine de știut că orice defecțiune cu oprirea unei linii poate produce pagube cu costuri zilnice mai mari decât costurile cu instruirea periodică a tuturor lucrătorilor din unitate.

Nu cred că este foarte greu să ne dezvoltăm o nouă generație de specialiști în domeniul hidraulicii și pneumaticii, acum cât încă mai există oameni cu experiență practică. Succes!

EDITORIAL

What about the specialists in the field of hydraulics and pneumatics nowadays?

Ph.D.Eng. Petrin DRUMEA
MANAGING EDITOR

In the last few years, the development of hydraulics has seen a gradual decline in all sub-domains and in all directions. We don't have much conception and design capabilities, we don't have much production, as well, and, more recently, we are no longer able to maintain hydraulically operated machines. For years we have had a professional association that also had a section of specialists, which we find out with surprise that for several years it has been in agony.

The new generation of fluid power specialists, extremely small in number, not only fails to become prominent on the economic and industrial level, but also fails to fetch or train new specialists in the field. It is serious issue that the maintenance of hydropneumatic equipment and systems had to be taken over by mechanics or electricians, and they rightly regard this activity as extra work and therefore treat it accordingly.

There are many causes for this; we, too, tried to analyse some of them in the magazine, but this is not the topic of today's discussion. Looks like now it is essential to address the concrete elements in terms of professional training, reintroduce the idea of design, reinvent maintenance specialists, and investigate what are the development trends of the field. I remind everyone of the basic fact that any machine that comprises at least one moving part has to include a drive system, which can be an electric, hydraulic, pneumatic or purely mechanical one. In most cases the system is a mixed one, and it is usually controlled electronically using IT solutions.

For those who deal with the professional training of young people, great care must be taken as there is no industrial equipment consisting only of the IT unit. There must necessarily be specialists in mechanics, electrical and electronics specialists, and specialists in hydraulics and pneumatics, as well.

The first step that should be taken as soon as possible is for all workers in the field to take training courses specific to their daily activities. As a result, level 1 courses for operative workers and technicians and level 2 courses for maintenance engineers should be reactivated. It would be good to know that any failure with the shutdown of a production line can cause damage with higher daily costs than the costs of regular training of all employees in the unit.

I do not consider it so difficult for us to develop a new generation of specialists in the field of hydraulics and pneumatics, now while there are still people with practical experience. Best of luck!

Control Performance of an Energy-Efficient Hydrotronic Transmission

PhD. Student Eng. **Alexandru-Polifron CHIRIȚĂ**[1,2*], PhD. Eng. **Radu Iulian RĂDOI**[1],
PhD. Student Eng. **Bogdan Alexandru TUDOR**[1], PhD. Student Eng. **Ștefan-Mihai ȘEFU**[1],
Res. Assist. **Ana-Maria POPESCU**[1]

[1] National Institute of Research & Development for Optoelectronics / INOE 2000 - Subsidiary Hydraulics and Pneumatics Research Institute / IHP, Bucharest, Romania

[2] Technical University of Civil Engineering of Bucharest (UTCB), Faculty of Technological Equipment

* chirita.ihp@fluidas.ro

Abstract: *The article presents the virtual experimentation of a closed circuit hydrotronic transmission that aims at the precise control of an angular displacement with the help of a semi-rotary hydraulic actuator, experimentation performed by using Simcenter Amesim numerical simulation software. Such position control systems are often used in industry; such a system is suitable and can be used to control the pitch angle of the blades of a wind turbine.*
The article deals extensively with the control capabilities of a hydrotronic transmission. Combining high-performance hydraulic components with sensors and a PID controller - components of a hydrotronic transmission - the result is an energy-efficient transmission, with outstanding control capabilities.

Keywords: *Closed circuit, hydrotronic transmission, control performance, energy efficiency, simulation*

1. Introduction

Hydrostatic transmissions can have several methods of transmitting engine power to the actuator by using hydraulic fluid [1, 2]. Mobile machinery use closed - circuit hydrostatic transmissions [3-5] with variable displacement axial piston pumps. Hydraulic fluid leaks that occur at the pump and other system components are compensated by a low-pressure charge pump. Closed - circuit pumps have simple or more efficient and complex servo systems for displacement control. Pump displacement control is done by changing the angle of inclination of the swash plate by means of a piston and levers. The simplest variants have a mechanical control loop with mechanical feedback via levers, and the most advanced ones use PID servo controllers and angular position transducers. Controllers with adaptive feedback are used for certain applications that require high precision, e.g. machine tools or robots.
Some examples of hydraulic drive applications for angular load positioning can be found in Figure 1(a), which shows a servo-hydraulic system that controls rudder movement on tugboats. The rudder operator needs assistance in controlling and moving of it. This system has no feedback for the rudder angle and engaging the propulsion of the boat can take the operator by surprise in certain situations. In figure 1(b) one can see a servo-hydraulic rotary actuator with position control by means of a neurobilogically motivated algorithm [6]. A version of the brain emotional learning based intelligent controller (BELBIC), a bio-inspired algorithm based upon a computational model of emotional learning that occurs in the amygdala, is utilized for position controlling a rotary electro-hydraulic servo system. Figure 1(c) shows a four-way valve controlled motor with position feedback [7]. The hydraulic actuator consists of a rotary hydraulic motor that is controlled with a servo valve and an angular position controller. Figure 1(d) shows a McKibben muscles hydraulic control system for a robotic arm [8]. The authors investigated three different controllers developed for a loaded robotic arm actuated with hydraulic oil. The results of investigations showed that a simple proportional-integral controller has significant phase lag and attenuation at the higher frequencies tested. Inclusion of the feedforward term almost completely eliminates these.
Closed circuit transmissions, compared to open circuit transmissions, have faster response time, are more precise and have a smaller mass because the oil tank has a very small volume.
In the present paper, the authors investigated, through numerical simulation, the control performance of an energy efficient hydrotronic transmission, which controls an oscillating hydraulic motor.

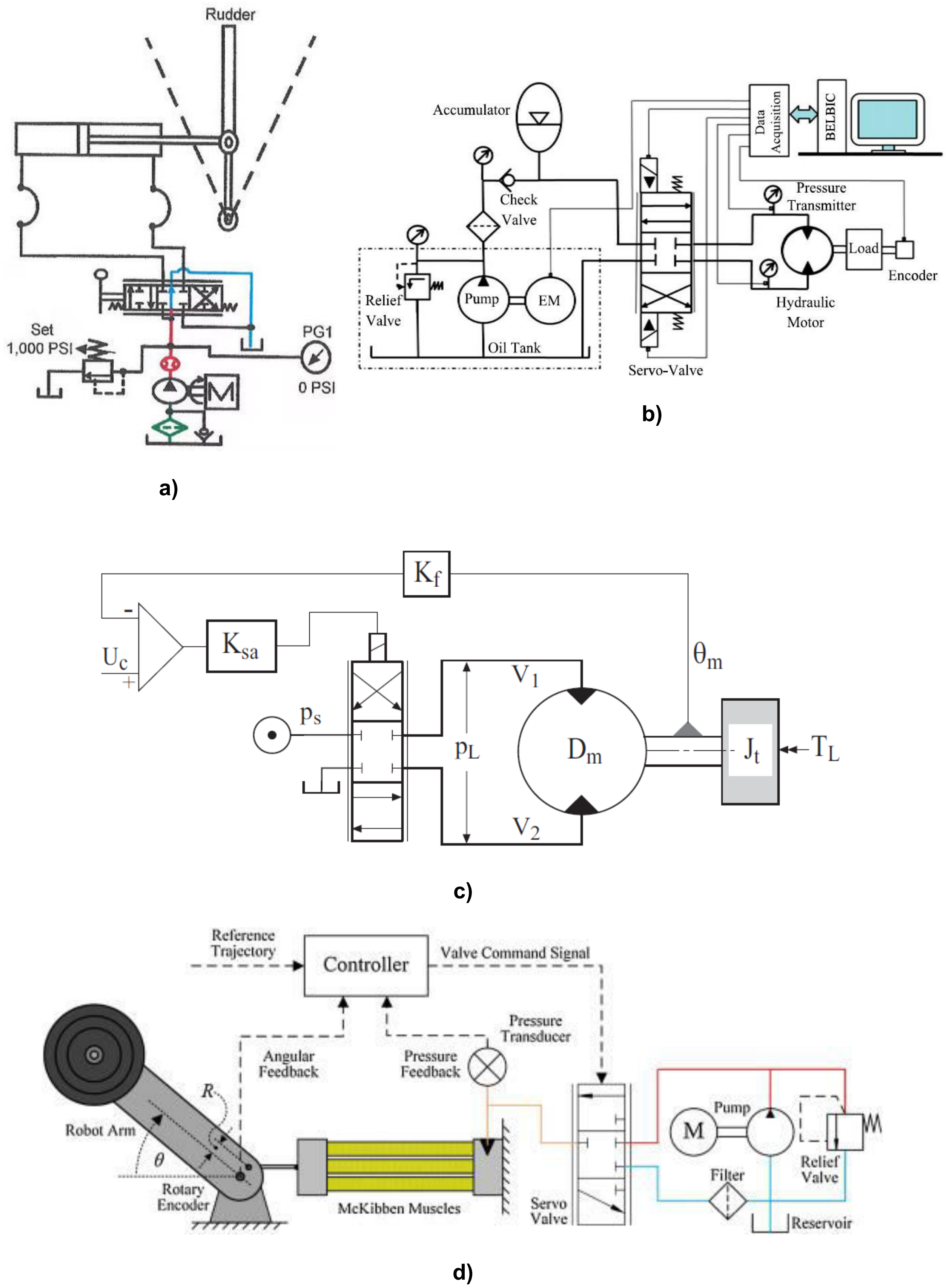

Fig. 1. Angular displacement control systems (a, b, c and d)

2. Material and method

For the analysis of control performances and efficiency of the hydrotronic transmission, the simulation model in **Figure 2** has been developed with the help of Simcenter Amesim numerical simulation software. The simulation network shows a closed circuit transmission, which aims to precisely control an angle in the range of 0.01 - 179.99 degrees.

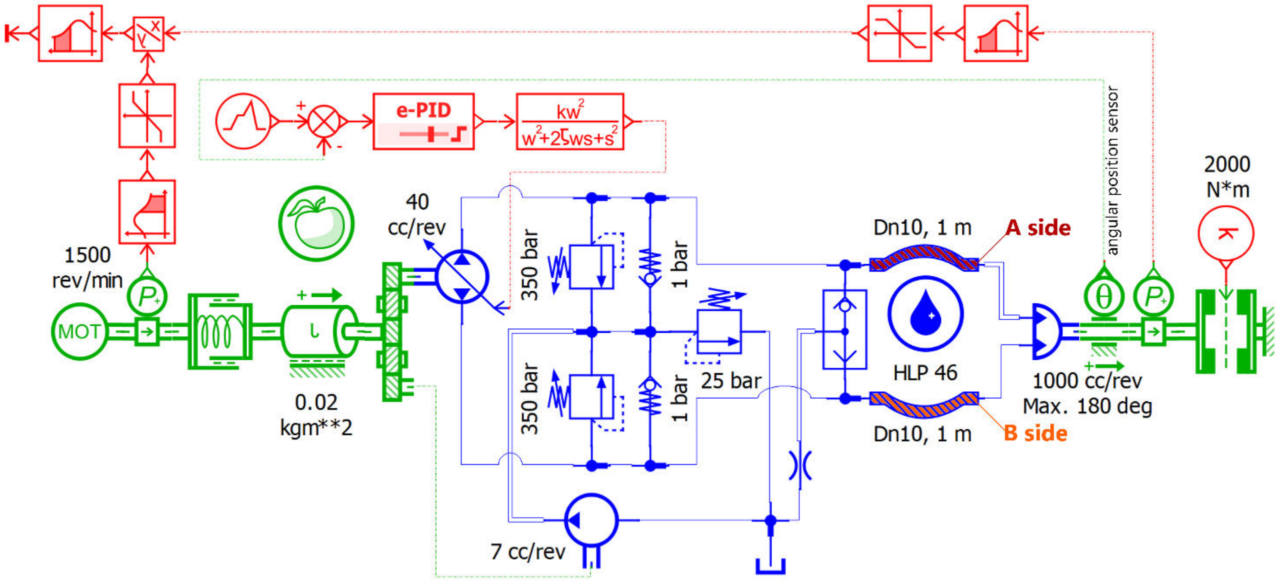

Fig. 2. Simulation network - hydrotronic transmission

Operation and structure of the transmission: an electric motor, with a speed of 1500 rev / min, supplies the two hydraulic pumps, the main one with a variable capacity of 40 cc / rev and the auxiliary one with a capacity of 7 cc / rev. Between the electric motor and the two hydraulic pumps there is a power transducer, a shaft whose model takes into account rigidity, damping, inertia and friction, and a mechanical connector that allows a single motor to operate the two pumps. The hydraulic actuator is a semi-rotary one; it has a capacity of 1000 cc / rev, can achieve an angular displacement between 0.01 - 179.99 degrees, and can develop a large continuous torque. Between the main pump and the semi-rotary actuator there are the specific components of a closed circuit transmission: two pressure valves acting as safety valves set at 350 bar, the check valves that allow for part of the auxiliary pump flow rate to reach the suction port of main pump, a pressure relief valve for the auxiliary pump that discharges the remaining flow to the cooler and tank, two hydraulic hoses Dn16 with a length of 1 m and a group of two components, a selector valve and a throttle that discharges part of the flow rate of the high-pressure side to simulate volumetric losses. Connected to the shaft of the semi-rotary actuator, there are an angle transducer, a power transducer with which the energy efficiency of the transmission is calculated, and a coupling that creates a resistant torque with a constant value of 2000 Nm. The pump capacity is controlled by a PID controller with self-tuning function; between the PID controller and the pump capacity control mechanism there is a filter that limits the frequency and amplitude of the signal; this filter limits the signal frequency with high amplitudes to a maximum of 5.5 Hz, and if the frequency increases, the amplitude of the signal decreases, the maximum frequency for small amplitudes of the signal being 25 Hz. Initial simulation data: start time 0 s – end time 5 s, print interval 0.001 s, tolerance 1e-05 s.

3. Results

Following the experimentation of closed circuit hydrotronic transmission with the help of numerical simulation, a couple of graphs resulted, as presented below.
Figure 3 shows the time variation of flow rates and pressures in the system. This shows the

variation of the main pump flow rate, the volumetric losses of the transmission (3 l/min, at a pressure of 250 bar), the pressures of the two sides with distinct values and variations.

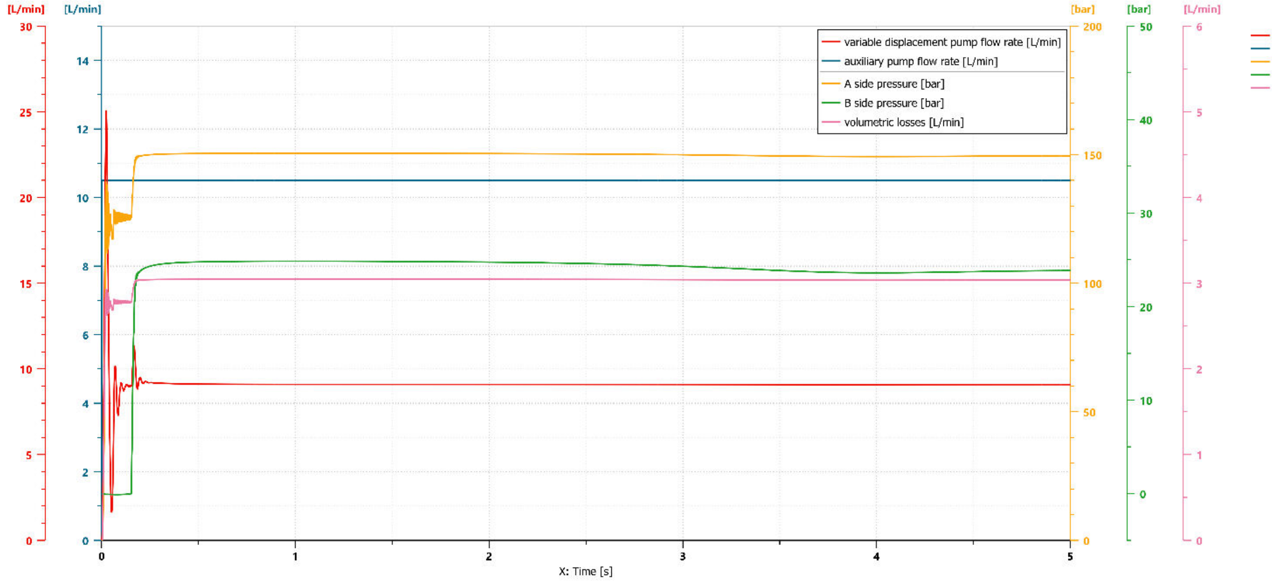

Fig. 3. Time variation of system pressures and flow rates

On the detail in **Figure 4**, one can see that due to the inertia of the hydraulic actuator and the compressibility of the system, a depression occurs (close to the limit of cavitation) on the suction port of the main pump for a short period of time; it is compensated in 0.15 s by the auxiliary pump flow rate passing through the check valve.

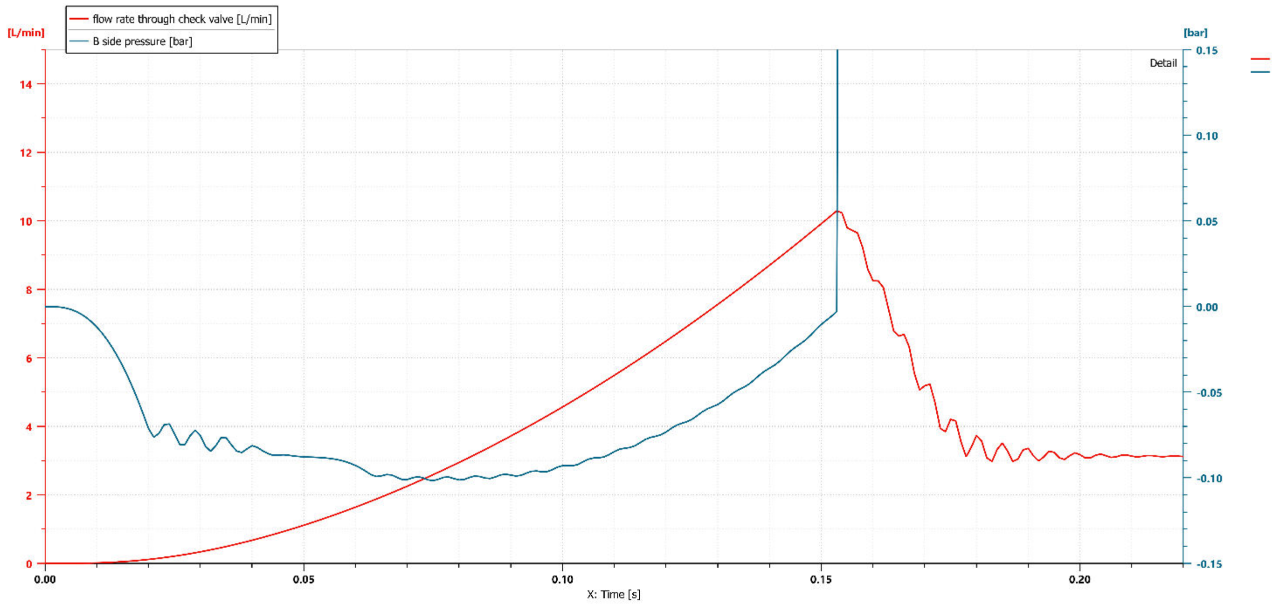

Fig. 4. Detail - Main pump suction port pressure variation and compensation flow rate

Figure 5 shows the PID controller output signal and the pump tilt angle. One can notice that the swash plate position stabilizes in 0.23 s, and the signal from the output of the PID controller is considerably attenuated.
Figure 6 shows the graph with the frequency response of the PID output and the swash plate positioning. The magnitude of swash plate positioning drops sharply over the 25 Hz frequency. The obtained performances are similar to those specified in the catalogs of the manufacturers of closed circuit hydraulic pumps.

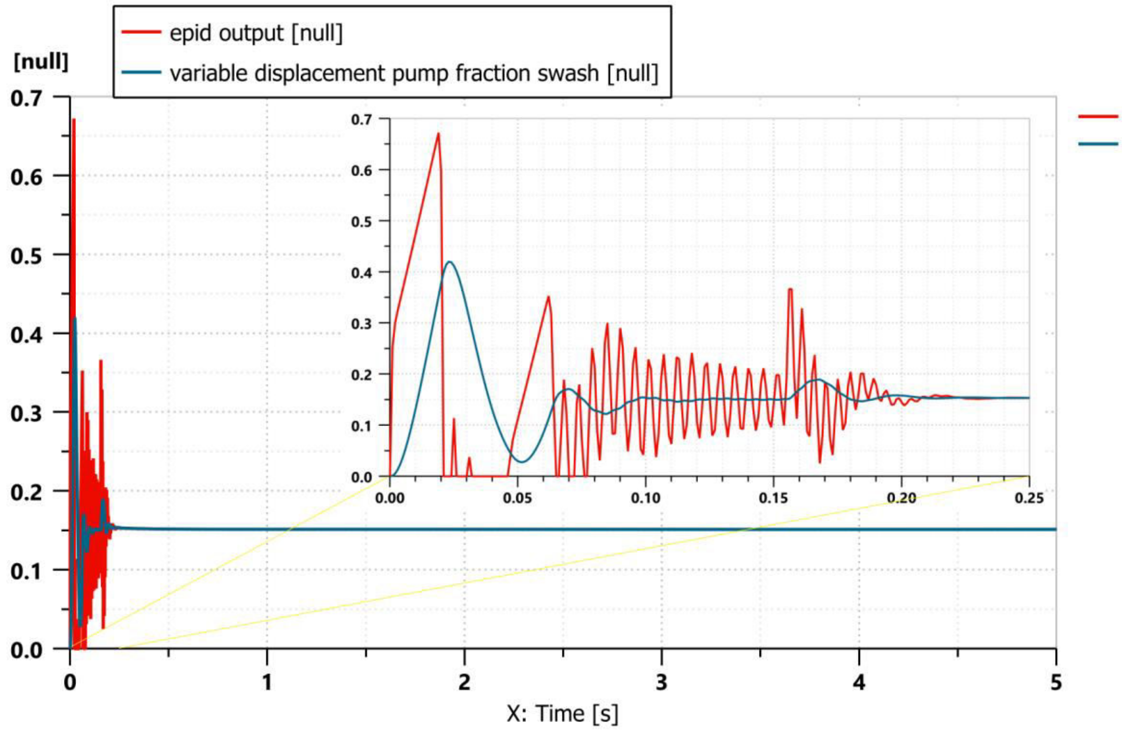

Fig. 5. Time variation of the PID controller output and the pump fraction swash

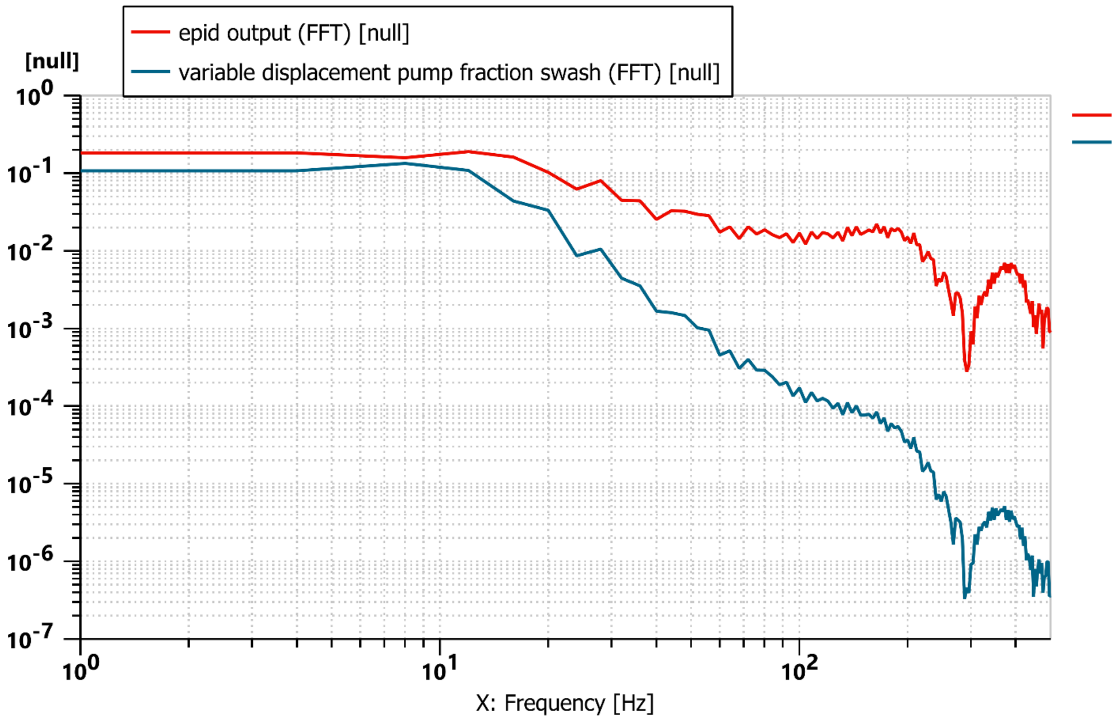

Fig. 6. Frequency spectrum of the PID controller output signal comparative to pump fraction swash

In the graph in **Figure 7**, one can see that the rotation of the hydraulic actuator shaft is opposed by a resistant torque with a constant value. After a while, the actuator speed stabilizes and the actuator achieves the prescribed angular displacement.

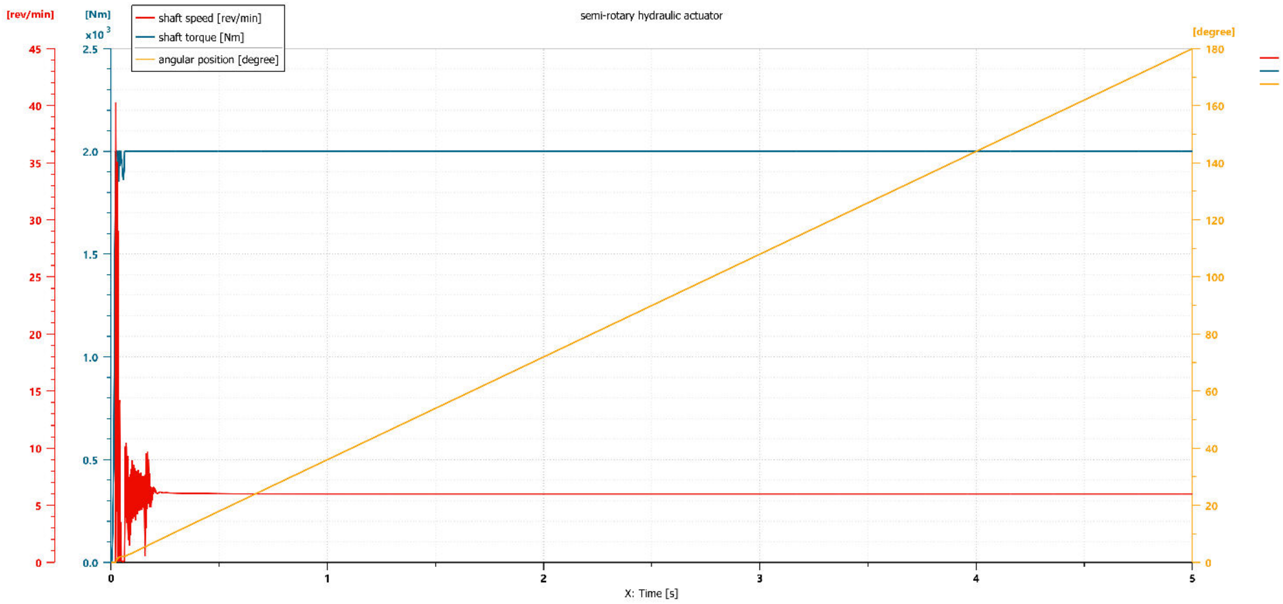

Fig. 7. Time variation of the parameters of the semi-rotary hydraulic actuator

The graph in **Figure 8** shows the external parameters of the PID controller. The graph shows a good tracking of the prescribed value, except for the first second. Moreover, on the same chart one can see the overall control error values.

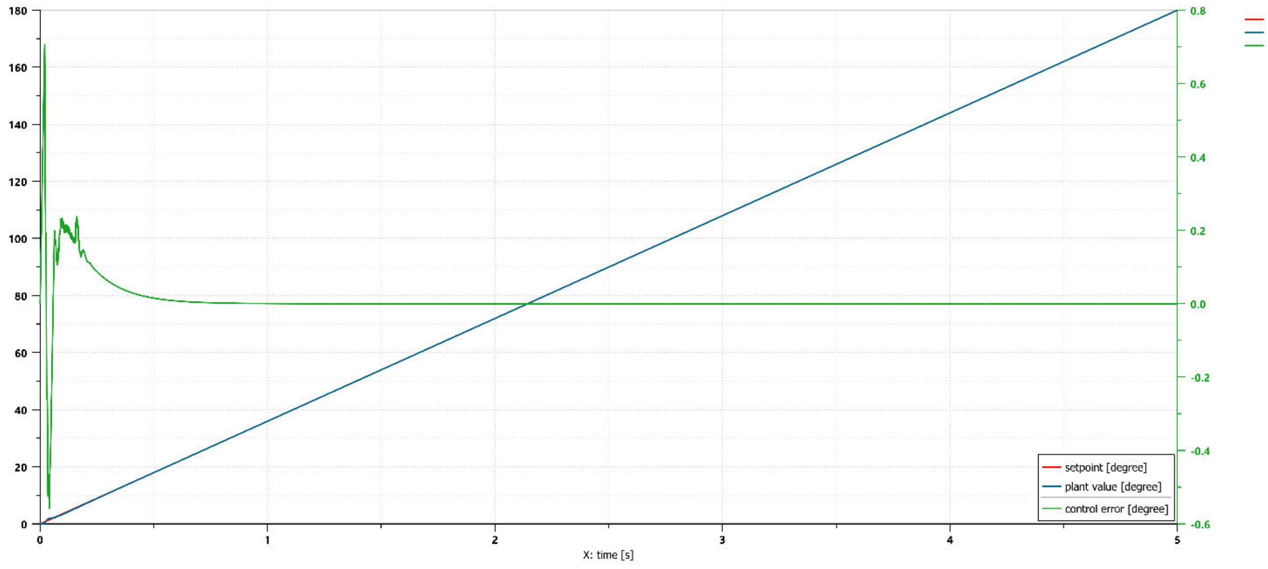

Fig. 8. Time variation of the parameters of the PID controller

Figure 9 shows in detail the variation of the external parameters of the PID controller; in the first quarter of a second of the simulation, the positioning error takes maximum values of 0.7 degrees. The prescribed value is shown in red (setpoint), and the angular displacement in blue (plant value); the large differences between these curves (0.8 degrees) are due to the elasticity of the system, the compressibility of the hydraulic fluid that has a composition of 0.2% gas and the inertia of moving components and fluid. After a very short time, 0.25 s, the value of the positioning error drops below 0.1 degrees and its value continues to decrease.
Figure 10 is intended to show an overview of the angle control error, on which one can see that the error after one second has a value very close to 0.

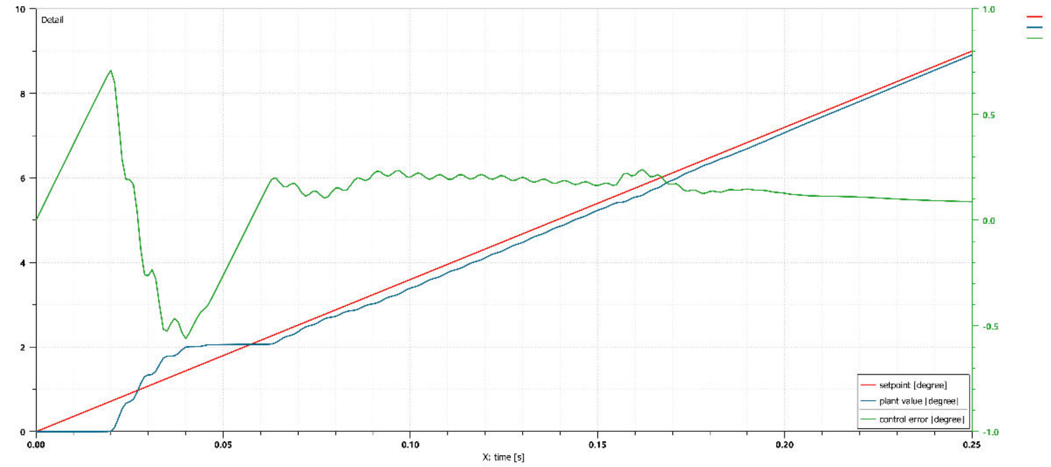

Fig. 9. Detail - Time variation of the parameters of the PID controller

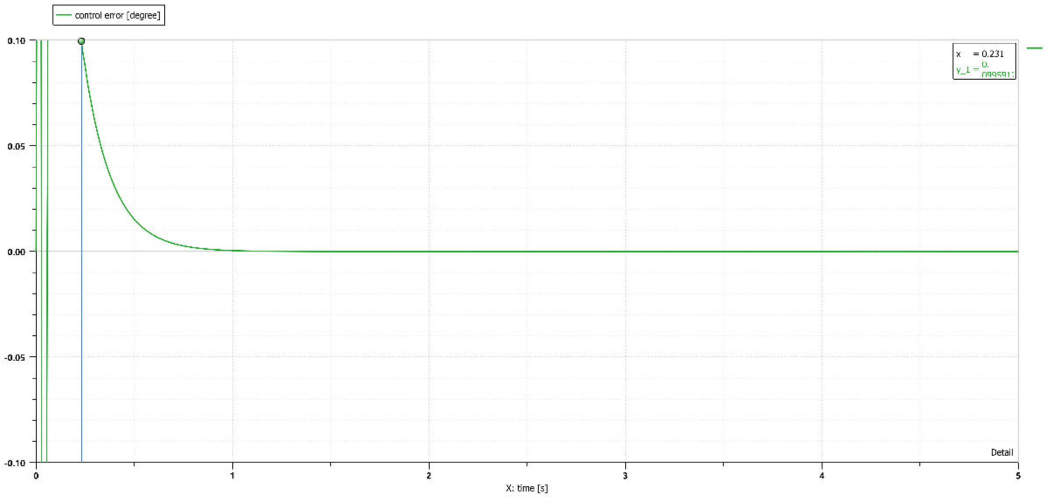

Fig. 10. Detail - Time variation of the control error

The transmission efficiency is shown in **Figure 11**; it has a value of 0.75, which is a very good value for a closed circuit transmission. The 0.2 s delay is caused by the moving average.

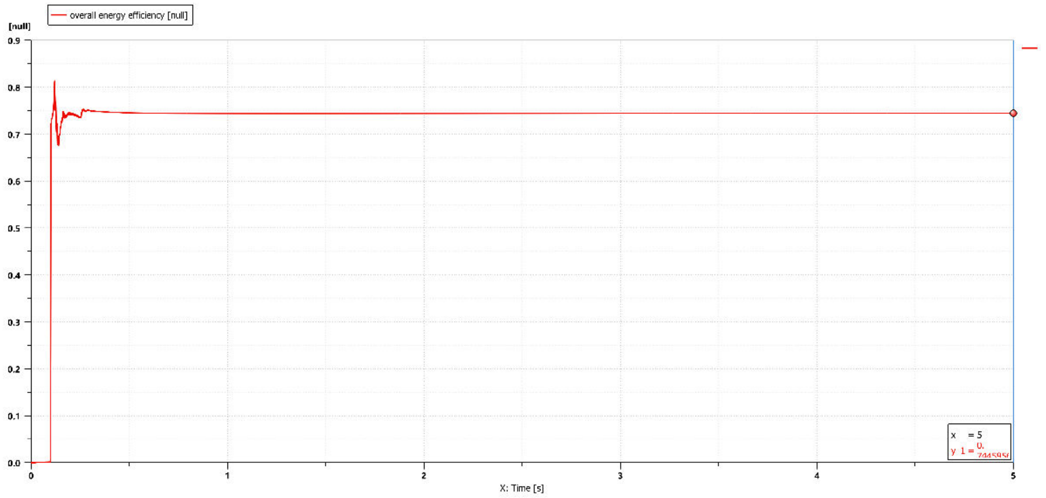

Fig. 11. Time variation of the overall energy efficiency of the closed circuit hydrotronic transmission

4. Conclusions

Using high-performance and energy-efficient hydraulic pumps and motors, in combination with sensors and electronic control systems - components of a hydrotronic system - transmissions with particularly precise control characteristics can be achieved.
Closed circuit transmissions, as opposed to open circuit transmissions, have the following advantages:

- higher control capabilities
- faster response times, especially when changing the direction of displacement
- usually, these transmissions are more compact and are used on mobile machines, because the oil tank capacity is small, consequently, the value of power and mass ratio is higher;

and the following disadvantages:

- if the cooler is not sized / chosen correctly, the transmission will overheat, and after the viscosity of the hydraulic fluid will fall below the permissible limits, the transmission will no longer work as expected by the user
- in the case when the transmission works in difficult conditions (the moment of inertia related to the load and the torque that opposes the displacement have high values or the hydraulic lines have too long lengths), simultaneously with the case when the compensation pump has a too low flow rate, all this leads to the occurrence of cavitation at the suction port of the main pump.

The central topic of this research, that is, closed loop hydrostatic transmissions, is the object of the study of the doctoral thesis of the main author; the simulation model is designed to be scalable so that transmissions with powers between a few hundred watts and a few MW can be simulated.

Acknowledgments

This paper has been funded by the Romanian Ministry of Research and Innovation under NUCLEU Programme, Financial Agreement no. 18N/08.02.2019, Ad. doc. no. 13/14.04.2021, Project code PN19-18.01.01, Project acronym: OPTRONICA VI, Theme 2 - Advanced research on the development of synergistic frontier architectures used in solving global challenges and increasing knowledge-based competitiveness, Phase 3, titled "Developing advanced methods, stands, equipment and teaching materials in order to enlarge specific knowledge in the fields of hydrotronic, pneumotronic and digital hydraulic components and systems". European funding has also been granted, under Competitiveness Operational Programme POC 2014-2020, call POC-A1-A.1.1.3-H-2016, Financial agreement no. 253/02.06.2020, signed between INOE 2000 and the Ministry of Education and Research for the project titled "Horizon 2020 Support Center for European project management and European promotion PREPARE", MYSMIS2014 code 107874.

References

[1] Guo, Xiaofan, and Andrea Vacca. "Advanced design and optimal sizing of hydrostatic transmission systems." *Actuators*, no. 10 (2021): Article ID 243.
[2] Likaj, Ramë, and Ahmet Shala. "Design of automatic system with hydrostatic transmission." *Annals of Faculty Engineering Hunedoara – International Journal of Engineering* XV, fascicule 2 (May 2017): 159-162.
[3] Martelli, Massimo, and Luca G. Zarotti. "Hydrostatic transmission with a traction control." Paper presented at 22nd International Symposium on Automation and Robotics in Construction ISARC 2005, Ferrara, Italy, September 11-14, 2005.
[4] Rossetti, Antonio, and Alarico Macor. "Multi-objective optimization of hydro-mechanical power split transmissions." *Mechanism and Machine Theory* 62 (2013): 112–128.
[5] Wu, Wei, Junlin Luo, Chunhui Wei, Hui Liu, and Shihua Yuan. "Design and control of a hydro-mechanical transmission for all-terrain vehicle." *Mechanism and Machine Theory* 154 (2020): Article ID 104052.
[6] Sadeghieh, Ali, Hadi Sazgar, Kamyar Goodarzi, and Caro Lucas. "Identification and real-time position control of a servo-hydraulic rotary actuator by means of a neurobiologically motivated algorithm." *ISA Transactions* 51 (January 2012): 208-219.
[7] Rydberg, Karl-Erik. *Hydraulic Servo Systems – Theory and Applications*. IEI/Fluid and Mechanical Engineering Systems, Linköpings universitet, 2008.
[8] Meller, Michael, Boris Kogan, Matthew Bryant, and Ephrahim Garcia. "Model-based feedforward and cascade control of hydraulic McKibben muscles." *Sensors and Actuators A: Physical* 275 (June 2018): 88-98.

ISSN 1453 – 7303 "HIDRAULICA" (No. 2/2022)
Magazine *of Hydraulics, Pneumatics, Tribology, Ecology, Sensorics, Mechatronics*

Mathematical Modeling and Simulation of the Operation of Hydraulic Systems with Resistive Adjustment

Prof. PhD Eng. **Anca BUCUREȘTEANU**[1,*]

[1] University POLITEHNICA of Bucharest

* ancabucuresteanu@gmail.com

Abstract: *In this paper, the author presents, based on mathematical models in static and dynamic conditions and with the help of simulation programs, how to achieve the resistive adjustment of the operating speed of the hydraulic cylinders. The described models take into account the characteristics of the cylinders and throttles, but also those of the pressure valve. In all cases it is considered that the drive pump has constant capacity and is actuated by an electric motor whose rotational speed is also constant.*

Keywords: *Resistive adjustment of speed, direct, return, derivation*

1. Introduction. Defining the Elementary Source [1, 2]

The elementary source is formed of the pump P and the pressure valve PV, as shown in Figure 1. The pressure in the hydraulic unit HI is visualized at any moment by means of the pressure gauge M.

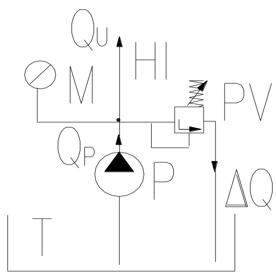

Fig. 1. Hydraulic diagram of the elementary source

The flow rate supplied by the pump is Q_P and is considered constant. The hydraulic unit HI is supplied by the elementary source with useful flow Q_U; the flow ΔQ [1, 3] is discharged through the pressure valve PV.
These flow rates have the following relation:

$$Q_U = Q_P - \Delta Q \tag{1}$$

The discharge of the flow ΔQ is made according to the characteristic shown in Figure 2.

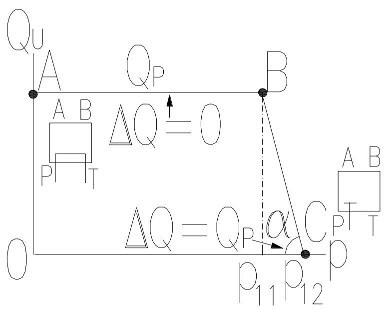

Fig. 2. Operating characteristic of the elementary source

The pressure valve is adjusted so that the first drop of oil passes through it at pressure p_{11}; when the pressure p_{12} is reached, the entire flow of the pump Q_P passes through it. It is considered a linearized characteristic on the segment BC having its angle α very close to 90°. The useful flow can be expressed as follows:

$$Q_U = \begin{cases} Q_P, p \leq p_{11} \\ Q_P \frac{p_{12}-p}{p_{12}-p_{11}}, p_{11} < p \leq p_{12} \\ 0, p_{12} < p \end{cases} \quad (2)$$

As it can be seen in Figure 2, the flow sent by the elementary source to the hydraulic unit depends also on the type of directional control valve used. If this one has a P→T connection, during the "at rest" position, the supplied flow depends on the pressure on the ABC path. If the directional control valve has its P path closed in the "at rest" position [1, 4], the useful flow follows the CBA path when the opening control is actuated. As it will be shown below, depending on the involved cylinder and its load, the operating point will be identified on the characteristic in Figure 2. If the unit is provided with throttling, this one can be used, with real effects, only on the BC segment.

2. Direct Throttling. Stationary Mathematical Models

Let consider the diagram with direct throttling shown in Figure 3.

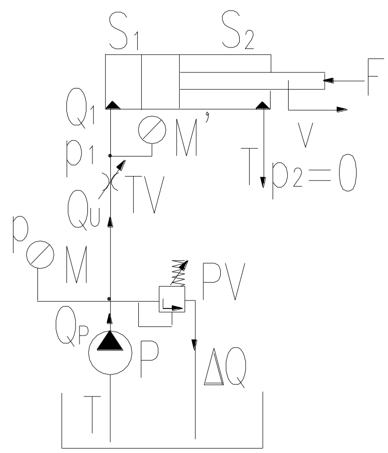

Fig. 3. Flow direct adjustment

The elementary source supplies the cylinder with the active surfaces S_1 and S_2 through the TV throttle. The pressure p_1 is measured by means of the pressure gauge M'. The cylinder rod moves with speed v against force F. It is considered that the entire flow supplied by the elementary source (Q_U) is sent by the throttle (Q_1) to the active surface S_1 and that the return pressure (on surface S_2) is negligible. The coefficient of the surfaces is $k = S_2/S_1$. This one keeps within the range [0, 1] and most often is ~0.5 [5]. If the throttling surface is S_{TV}, the oil density is ρ and the throttling constant is denoted by C_{TV} [5, 6, 7], the following expression is obtained for speed v:

$$v = \frac{C_{TV} S_{TV}}{S_1} \sqrt{\frac{2}{\rho}(p - \frac{F}{S_1})} \quad (3)$$

Starting from the characteristic of the elementary source in Figure 2 and from the relation (3), the Figure 4 shows the way to determine the operating point of the unit (X) and the way to determine the speed for a series of parameters of the unit: Q_P, p_{11}, p_{12} and S_{TV}.
The working pressure must be higher than F/S_1 and the operating point X is obtained by opening (+) or closing the throttle (-) TV, at the intersection of the characteristic of the elementary source with the parabolic characteristic. A certain speed and the pressure p_X correspond to this operating

point. If point X belongs to segment AB, the throttle adjustment is inefficient. If point X belongs to BC segment, the adjustment depends on: Q_P, p_{11}, p_{12} and S_{TV}.

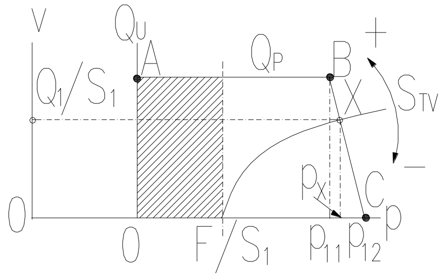

Fig. 4. Determination of the operating point in case of direct throttling

3. Return Throttling. Stationary Mathematical Models

Consider the diagram with return throttling in Figure 5. The TV throttle adjusts the flow rate Q_2 pushed out by the surface S_2 of the cylinder. The pressure p_2 measured by the pressure gauge M' is developed on this surface.

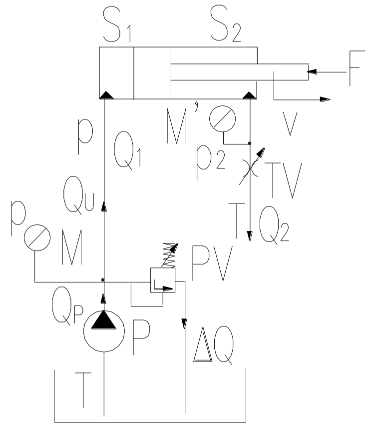

Fig. 5. Adjustment of flow on cylinder return

The pressure of the elementary source acts on the surface S_1 of the cylinder and the useful flow is the flow supplied by the elementary source. The speed obtained in the same conditions as above is:

$$v = \frac{c_{TV} S_{TV}}{k\sqrt{k} S_1} \sqrt{\frac{2}{\rho}(p - \frac{F}{S_1})} \quad (4)$$

It can be noticed that a higher speed is obtained for a same adjustment. Thus, for k = 0.5, the speed obtained by relation (4) is almost three times higher than the one obtained with the help of the relation (3).

The determination of the operating point and speed can be done according to the characteristic in Figure 6.

The operating point X moved to the left related to the position occupied by the characteristic of direct throttling, presented by means of a dotted line. The pressure p_X too moves to the left, approaching the pressure p_{11}.

Therefore, in case of return throttling, the travel can be adjusted more precisely, with higher accuracy.

The presence of the pressures p and p_2 on the surface S_1 and respectively S_2 guarantees a greater stability.

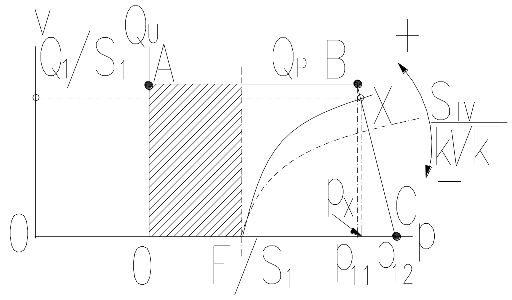

Fig. 6. Determination of the operating point in case of return throttling

4. Derivation Throttling. Stationary Mathematical Models

In this case, the throttle is assembled in front of the consumer, so that the excess flow is discharged directly to the tank, as shown in Figure 7.

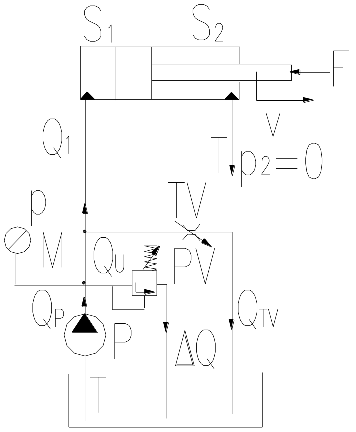

Fig. 7. Flow adjustment by derivation throttling

In such case, the flow rate Q_1 for surface S_1 supply is (keeping the same notations as above):

$$Q_1 = Q_U - Q_{TV} \tag{5}$$

The flow discharged through the TV throttle has the expression below and the characteristic in Figure 8.

$$Q_{TV} = C_{TV} S_{TV} \sqrt{\frac{2}{\rho} p} \tag{6}$$

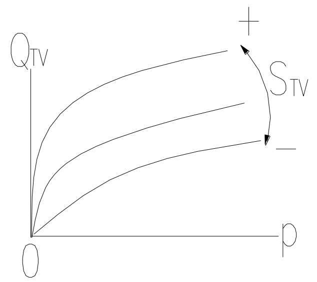

Fig. 8. Characteristic of the throttle assembled in derivation

One can observe that the Q_{TV} flow rate depends parabolic on the pressure. According to the parabola opening, the operating point and implicitly the cylinder speed can be determined by means of the relations (5) and (6) and with the help of the characteristics in Figures 2 and 8.
If the characteristic of Q_{TV} flow has a large opening (large S_{TV}), its intersection with the characteristic of the elementary sources made in the AB segment of this one, thus obtaining the characteristic in Figure 9.

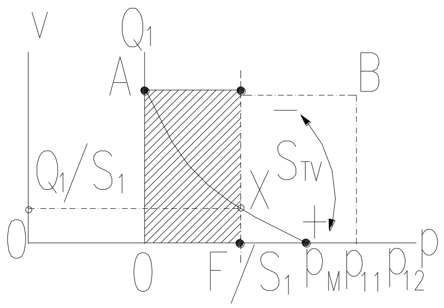

Fig. 9. Determination of the operating point in case of derivation throttling at large opening of the throttle

One can notice that the maximum pressure p_M in the unit is lower than the value p_{11}; the set speed is much reduced.
If the Q_{TV} flow characteristic has a smaller opening (S_{TV} small), its intersection with the characteristic of the elementary source is made on the BC segment of this one, obtaining the characteristic in Figure 10.

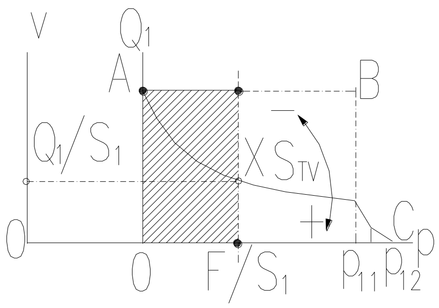

Fig. 10. Determination of the operating point in case of derivation throttling at small opening of the throttle

In this case, it is observed that the pressure can even reach the value p_{12}. In this situation too, the set speed is much reduced.

5. Simulation of Resistive Speed Adjustment Systems for the Hydraulic Cylinders

In order to study the behavior of cylinders in dynamic mode, several methods can be used:

- elaboration of differential equations and their solution by classic methods [8];
- elaboration of differential equations and their solution by specialized programs [6, 9];
- direct use of specialized programs, without the need for specific differential equations [10].

The results of the simulations performed using the AUTOMATION STUDIO programs package are presented below.
The data of the studied elements are: the pump has a flow rate Q_P = 9 l/min, the pressure adjusted at the pump $p_{11} = p_{12}$ = 60 bar, all the equipment is DN6. The TV throttle can be adjusted so that its surface $S_{TV} \in [0, 0.28]$ cm^2; it has an opening of 5% of this value. The hydraulic cylinder has the useful surfaces in the relation $k = S_2/S_1 = 0.7$.
In the direct throttling, if at the moment of the command the pump discharges freely to the tank (P→T), the time necessary for reaching the maximum speed (0.85 m/min) is about 2.7 s according to the characteristic in Figure 11.

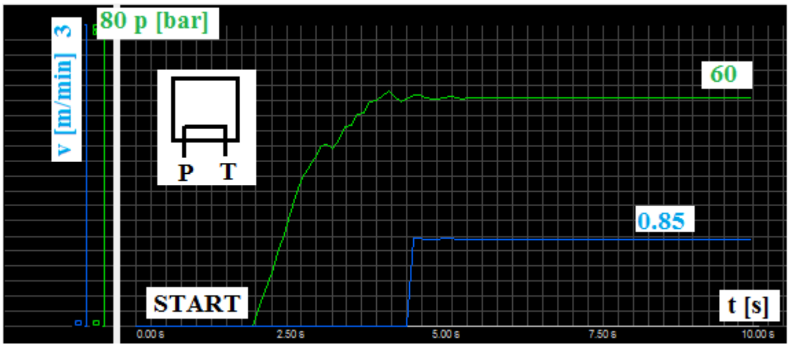

Fig. 11. Characteristic of direct throttling with zero initial pressure

The pressure reaches the maximum value set at the pressure valve PV, namely 60 bar.
If the pressure has its maximum value at the moment of the command, the maximum speed of 0.85 m/min is reached in less than one second. The pressure decreases at the start and then reaches the initial value, as in Figure 12.

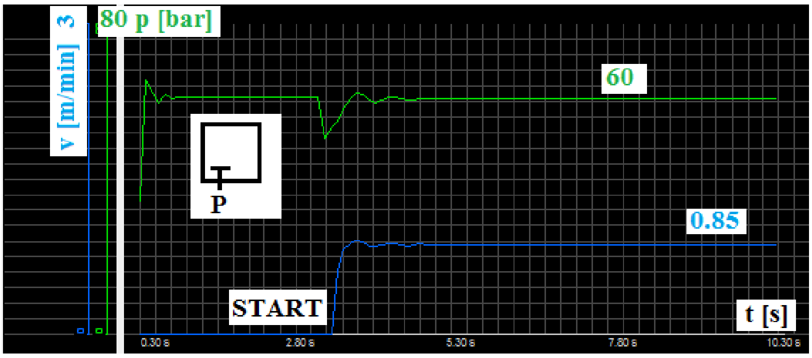

Fig. 12. Characteristic of direct throttling with maximum initial pressure

In this case, the system responds faster to commands, but in the stop phase, a larger amount of electric power is consumed. The unit may heat up for this reason.
By placing the throttle on the return, as it results from the relations (3) and (4), the same parameters make possible a higher speed. Thus, the maximum speed, reached as per the characteristic in Figure 13, is 1.35 m/min.

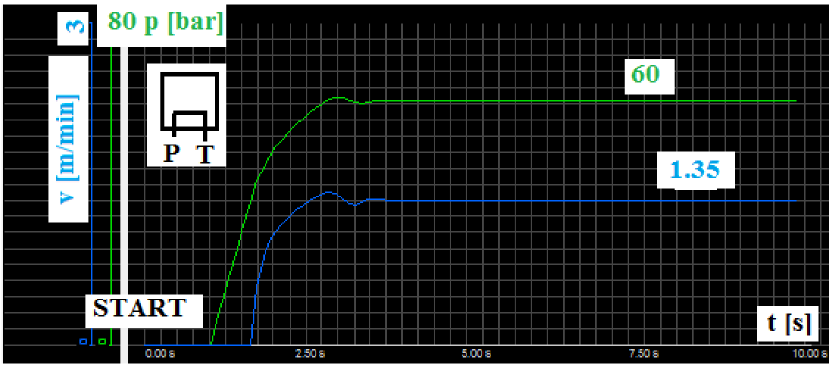

Fig. 13. Characteristic of return throttling with zero initial pressure

Since the initial pressure is zero, the speed stabilization time is approximately 3 s. The pressure is the one set at the pressure valve.
If one chooses a directional control valve that ensures a maximum value of the pressure at the time of the command, the characteristic in Figure 14 is obtained.

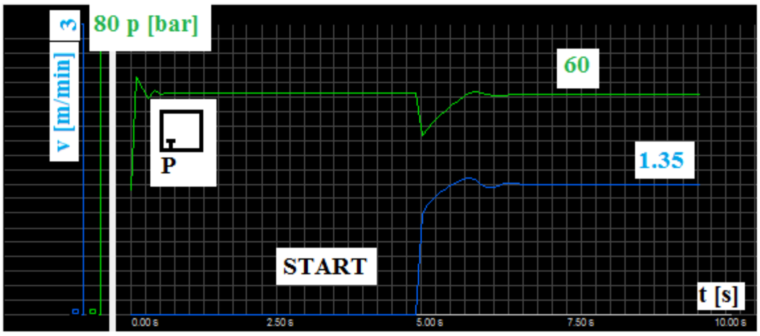

Fig. 14. Characteristic of return throttling with maximum initial pressure

The system is much faster given that the maximum speed is reached in ~0.5 s. The pressure decreases at the moment of the command, which can be explained by the need to compress the column. The major disadvantage of this variant is maintaining the pressure permanently, which can lead to the heating of the system and to an increase in energy consumption.
If the throttling is made in derivation and the pump discharges freely, the characteristic in Figure 15 will be obtained at the moment of the start command.

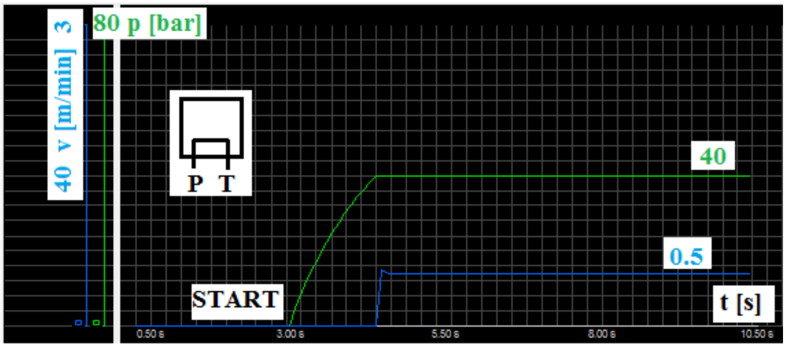

Fig. 15. Characteristic of derivation throttling with zero initial pressure

One can notice that the maximum value of the pressure, adjusted by means of PV valve, is no longer reached. The maximum speed is much reduced, reaching the value of 0.5 m/min. It is the variant with the lowest risk of heating and is also the lowest energy consumer.
If the throttling is made in derivation, but with the maximum pressure at the start-up moment, the characteristic in Figure 16 will be obtained.

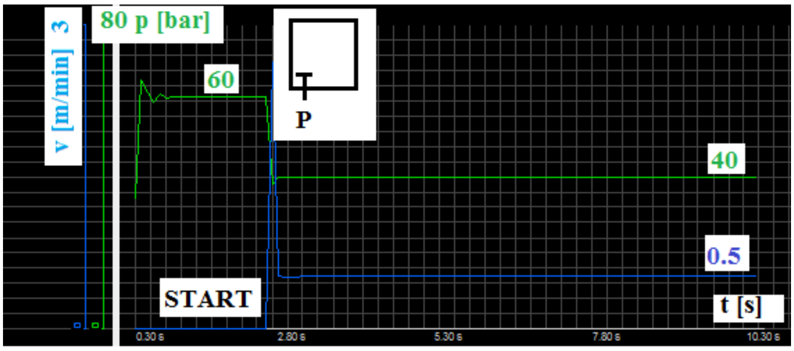

Fig. 16. Characteristic of derivation throttling with maximum initial pressure

One can observe that, even if the start is made with maximum pressure, this one will decrease and get stable when the speed reaches the value of 0.5 m/min. The start-up time is considerably reduced, with a visible pressure drop of ~ 20bar.

6. Conclusions

The resistive adjustment of the speed (flow rate) is usually performed by means of throttles. These ones can be assembled directly (between the pump and the cylinder), on the return (at the outlet from the cylinder towards the tank) or in derivation (after the pump, before the cylinder, but directly connected to the tank). Each of these three variants has its advantages and disadvantages. The return adjustment ensures a higher speed at the same throttle adjustment than the direct adjustment. The ratio of the obtained speeds depends on the ratio of the cylinder surfaces (k) proportional to $k^{3/2}$. The presence of pressures on both sides of the cylinder leads to a much more stable movement.

In the case of derivation throttling, the maximum pressure during operation may be lower than the pressure adjusted at the pressure valve. The speeds in this situation are lower than those in the direct or return adjustment. The energy consumed is lower and the heating level decreases. In some cases, the throttled oil can be used to lubricate some mechanisms.

The characteristics of the throttling are also influenced by the type of directional valve used to drive the cylinders. If the directional valve, in the "at rest" phase, ensures the direct connection P→T, then, after the command, the pressure increases and the cylinder starts only after overcoming the resistance forces.

If the directional valve ensures the maximum pressure at the command moment, the start is much faster, making possible a greater promptness.

Depending on the specifics of each unit, after a thorough analysis and possibly after a simulation with real data, the optimal variant can be determined.

References

[1] Prodan, Dan. *Machine-Tools Hydraulics/Hidraulica Masinilor-Unelte*. Bucharest, Printech Publishing House, 2004.

[2] Prodan, Dan, Emilia Balan, and Sanda Gandila. "The Calculation Method of the Point of Functioning of the Hydraulic System." *Romanian Journal of Technical Sciences Applied Mechanics,* Tome 49 (November 2004): 207-213.

[3] Portelli, Michel. *Industrial Hydraulic Technology/Technologie d'hydraulique industrielle*. Paris, Editions Casteilla, 1995.

[4] Totten, George E., and Victor J. De Negri. *Handbook of Hydraulic Fluid Technology*. Boca Raton, CRC Press Taylor & Francis Group, 2012.

[5] ***. ATOS, PARKER, and BOSCH REXROTH Catalogues and leaflets.

[6] Prodan, Dan. *Machine Tools. Modeling and Simulation of Hydrostatic Elements and Systems/Maşini-Unelte. Modelarea şi Simularea Elementelor şi Sistemelor Hidrostatice*. Bucharest, Printech Publishing House, 2006.

[7] Guibert, Philippe. *Applied Industrial Hydraulics/Hydraulique industrielle appliquée*. Paul Verlaine Université de Metz, 2008.

[8] Mazilu, Ion, and Virgil Marin. *Automatic Hydraulic Systems/Sisteme Hidraulice Automate*. Bucharest, Romanian Academy Publishing House, 1982.

[9] Oprean, Aurel, Constantin Ispas, Emil Ciobanu, Sergiu Medar, Adrian Olaru, and Dan Prodan. *Hydraulic Drives and Automation/Acţionări şi Automatizări Hidraulice.* Bucharest, Technical Publishing House, 1989.

[10] ***. AUTOMATION STUDIO Software package.

ISSN 1453 – 7303 **"HIDRAULICA" (No. 2/2022)**
Magazine *of Hydraulics, Pneumatics, Tribology, Ecology, Sensorics, Mechatronics*

Practical and Simple Laboratory Experiment to Visualize the Correlation among the Hydraulic Flow Parameters in Pipes

Prof. Dr. Eng. **Henrique PIZZO**[1,2,*], Eng. Stud. **Rafaela LIMA**[1],
Prof. Dra. Chem. **Michele RESENDE**[1], Prof. M. Eng. **Ana Flávia CRUZ**[1]

[1] Estácio University of Juiz de Fora, Minas Gerais, Brazil

[2] Municipal Water and Sewage Company of Juiz de Fora, Brazil

* henriquepizzo.estacio@gmail.com

Abstract: *The article presents the development and execution of a simple practical experience, which aims to help students of a civil engineering course, in a better understanding of the theoretical concepts involved in the topic of head loss in pressurized hydraulic conduits. Initially, a literature review is carried out, regarding the importance of practical classes in student training, laboratory practices, and experiments. Afterwards, the methodology used is presented, through measurement tests and the respective impacts on the flow rate, obtained by varying, one at a time, the length of the pipe, its diameters, and height between the water level in the reservoir and the water outlet point. The flow values varied as initially assumed. Finally, through the Fair-Whipple-Hsiao formula for small diameter plastic tubes, calculated flow values were obtained for each of the situations, and contrasted with the respective measured values. The results were considered satisfactory.*

Keywords: *Laboratory experiment, head loss, flow rate, college education, student engagement*

1. Introduction

One of the most challenging, yet crucial, components of good teaching is motivating learners. Student motivation is a key predictor of academic progress, involvement, and progress in higher education, resulting in improved academic performance and increased perseverance in the face of adversity. Despite the fact that there is a richness of motivational theories and lab results on student motivation, inspiring students in the classroom continues to be a difficult task. There is no practical assistance for putting theory into practice, leaving professors with the job of translating the extensive motivational literature into specific course design aspects [1].
It is described in [2] an attempt to understand the attitude of mathematics teachers towards Information Technology as an instructional tool, using the Technology Acceptance Model TAM framework. The results indicated that TAM, as a robust model, could be employed effectively in this context as well, and that a satisfactory match for the proposed model for the data was discovered. The sample consisted of solely high school mathematics instructors, who appeared to agree on the value of computers in mathematics instruction but were not very familiar with using them as teaching aids. This element contributes to the study's result that educators perceived ease of use has a substantial influence on their impression of usefulness and attitude toward the employment of technology in the classroom.
According to [3], some major features of educational apps are ease of access, simplicity, information quality, and a cheaper cost for a functional license. Because traditional commercial software is both costly and sophisticated, free and/or open source code may be a preferable alternative for teaching purposes.
In reference to laboratory activities in education, [4] emphasizes that understanding the events seen and how to interpret the data is a significant problem for students. However, it is apparent that the challenge is beneficial to the students and that they would benefit from the experience in their future studies.
Any laboratory's goal is to help people comprehend theory and practice better [5]. Lab courses may be adapted to include a heterogeneous approach that alters a student's learning experiences and enables a range of approaches in their practice with proper preparation and support. It is proposed that faculty investigate disassembly activities, computer simulation, and other free-form

exercises in addition to the usual instructor activities. Students can get a broader range of abilities and learn in more varied and deeper ways as a result. It is recommended that laboratories depart from regular operating procedures and investigate activity diversification, which can develop alternative modalities of information acquisition, hence enhancing students' interest and learning.
The tasks involved in activities carried out for a laboratory experiment [6], although sometimes relatively simple, are very effective in illustrating the effects of uncertainty on the quality of the results obtained. A pre-test instability assessment can show how inaccuracies in individual measurements might accumulate when utilized to calculate performance parameter values. An understanding of the consequences of mistakes might assist students in learning how to select proper instruments and testing processes. Because the testing is affordable and rapid, students may collect enough repeat measures to complete post-test statistical analysis. This post-test analysis may be contrasted to the pre-test instability assessment to offer a foundation for reflection on elements that were not expected, and thus suggest improvements to the test procedure that will result in improved quality measurements.
After mentioning potential rules that may manage the design and conduct of didactic labs in general, [7] explains how any of those systems could be applied to hydraulic labs. Reference [8] defines hydraulics as the engineering science that pertains to liquid pressure and flow. This study includes the manner in which liquids act in tanks and pipes, dealing with their properties and with ways of utilizing these properties. It includes the laws of floating bodies and the behavior of liquids under various conditions, and ways of directing this flow to useful ends, as well as many other related subjects and applications.
A large effort on learning styles and student involvement is described [5]. Much of the research implies that accomplishing these goals with a diverse student body requires a diversified approach to laboratory sessions. It is cited a study demonstrating that the inclusion of one extra method of learning resulted in better student engagement and performance in the subject of fluid mechanics and hydraulics.

2. Laboratory practices, experiments and the like

It is reported in [9] an experiment to determine the friction factor for a straight tube, with comparative analysis for different types of tubes. Reference [10] introduces a project to design and develop pneumatic laboratory activities for a course on Fluid Power, Mechanical Engineering. Various software packages were available for design, control and simulation of hydraulic, pneumatic, and motion control. The study relates safety rules, objectives, equipment, application, and circuit problems, for each laboratory. At the end, some conceptual questions are presented. It is discussed in [4] an experiment where data was acquired both manually and automatically in a fluid power laboratory.
The goal of the Civil Engineering design students was to illustrate the pneumatic movement of liquid water as it passes through an airtight one-way vessel system known as Heron's Fountain [11]. This study investigates hydraulic and pneumatic concepts often encountered in environmental control systems. Because this was a modest rendition of an ancient Greek fountain, its development required teamwork to carry out its simple function. The criteria involved were diameter, length, height, and density. This study employs Pascal and Bernoulli's equations to emphasize fluid mechanics ideas. The fountain action is represented by flow rate, while head loss is described by Darcy's equation. Reynolds' equation describes friction loss with an angled fitting attached to a fountain head. The research looked at the performance of two kinds of reentrant pipe fittings for head loss: straight and angled. The experiment improved the study team's educational experience by bringing together unique ideas from various academic and cultural contexts.
References [12] presents a fluid mechanics and hydraulics lab manual where, among several experiments, a practice that analyzes the relationship between major head losses and flow velocities for hydraulically smooth tubes, and the relationship between the friction factor and the Reynolds number for hydraulically rough tubes, is described. Similar description happens in [13], reporting an experiment to measure friction losses in pipes.
As illustrated in [14], a hydraulic laboratory course was designed to enhance water engineering students' understanding and knowledge of experimental methods and the basic principle of fluid

mechanics and apply those concepts in practice, while reference [15] describes a then newly implemented and innovative laboratory experience which was centered on a hydraulic position control system.

As expressed in [6], a laboratory exercise based on the performance testing of tiny drinking water pumps is demonstrated. According to the author, it offers a flexible and cost-effective environment for teaching the fundamentals of industrial experimental testing techniques to engineering technology students. Following on from that, this activity would give a practical opportunity for students to learn firsthand about the basic working characteristics of centrifugal pumps and highly associated components such as centrifugal compressors and fans.

A study was carried out to investigate the fluid flow and heat transfer features of microchannels. The hydraulic diameters of rectangular copper microchannels were 1.05 mm, 0.85 mm, and 0.57 mm. Heat transfer and head loss parameters were investigated in the laminar and transitional regimes using water as the work fluid and a constant surface heat flux [16].

Reference [17] describes a work whose major goal is to harmonize the multiplicity of criteria, formulas, tables, graphs, abacuses, images, and so forth in relation to hydraulic resistance coefficients. The study provides an equation that, accordingly, can be utilized to tackle a range of theoretical-practical difficulties that arise in hydraulics in general.

According to [18], understanding head losses in agricultural drainage facilities may be particularly useful both during the design phase to determine the best distance between drains and subsequently during the operating phase to track efficiency. It is presented a study based on the interpretation of data received in the lab and subsequently processed using specialist software engineering drainage system design.

A comparison of the hydraulic parameters, respectively flow rate and pressure, obtained on a physical model and estimated using the automated software for steady flow, RIMIS, is shown in [19]. The researchers developed a physical model to examine motion in a water distribution looping network. The comparative analysis seeks to validate the RIMIS software.

The results of an experiment on head loss and friction factor in small diameter polyethylene pipes are discussed in [20]. Five tubes were employed, with internal diameters of 10.0 mm, 12.9 mm, 16.1 mm, 17.4 mm, and 19.7 mm. The experiment was carried out for Reynolds numbers ranging from 6,000 to 72,000, acquired by varying the flow through the tubes at an average water temperature of 20ºC.

Reference [21] reports the findings of an experimental examination on flow-resistance law in small-diameter plastic pipes. Experiments were conducted over a broad range of Reynolds number values achieved by altering the discharge and water temperature. The experimental results are examined using both a purely empirical and a semitheoretical strategy, both of which are based on the supposition that the velocity profile has a power-law form.

Data on friction loss was obtained for three small diameter plastic tubes [22]. As per the research, a combination of the Blasius and Colebrook-White equations is then offered as an equation for the efficient and accurate prediction of head loss. According to the authors, the combination equation is still dimensionally homogeneous, correctable for viscosity changes, and accurate for small diameter plastic tubes.

3. Methodology

In order to solidify the theoretical foundations transmitted in the classes on the concepts of head loss in pressurized pipes, a laboratory experiment was carried out, with a view to better visualization and understanding of the correlations among the hydraulic parameters involved in the phenomenon of flow resistance.

The elaboration of the practice took place with simple acquisition materials, sometimes even disposable, with a very low assembly cost. Painted plastic paint buckets were used (simulating upstream reservoir) (Figure 1); acrylic groceries box (simulating downstream reservoir) (Figure 2); transparent garden hoses, 11 mm in diameter, 5.0 m and 8.2 m in length (simulating pipes); level hose, 8 mm in diameter, 5.0 m in length (simulating piping) (Figure 3); common garden hose (simulating pipeline to the upstream reservoir); box for material transport (simulating elevation of the upstream reservoir, consequently, of the water level) (Figure 4). The described parts are shown in Figures 1 to 4.

Fig. 1. Upstream reservoir

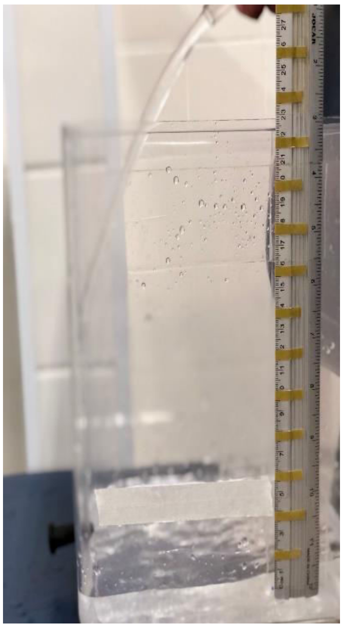

Fig. 2. Downstream reservoir

Fig. 3. Pipes

Fig. 4. Elevated reservoir

It is known that, based on transformations in the Bernoulli equation, one can assimilate the difference between the water level in the upstream reservoir and the water outlet to the atmosphere, at the other end of the pipeline, as the head loss, or part thereof. Equation (1) expresses the universal Darcy-Weisbach formula for head loss in pressurized pipelines.

$$h_f = \frac{8\,f}{g\,\pi^2} \cdot \frac{Q^2\,L}{D^5} \tag{1}$$

Where h_f is the head loss (m), f is the friction factor (dimensionless), g is the gravity acceleration (m/s^2), Q is the flow rate (m^3/s), L is the pipe length (m), and D is the pipe diameter (m).
From an analysis of (1), even though the friction factor f is not constant, it can be verified, in the first instance, that the flow rate Q varies directly with a power of the variation of the head loss h_f and of the diameter D, and that it varies inversely with a power of the change in length L.
Thus, 04 hydraulic combinations (or hydraulic situations) were taken, physically simulated one at a time, consisting of h_f, L and D, and, for each of them, the time to fill the volume of 3.0 L was measured in the downstream reservoir. This resulted in a flow rate for each of the situations. It was then possible to verify that the measured flow rates behaved as expected.
After this step, in order to get around the issue of the variability of the friction factor f of the Darcy-Weisbach formula as a function of the flow velocity, of the diameter itself, of the kinematic viscosity of the fluid and of the internal asperities of the tube wall, it was taken the Fair-Whipple-Hsiao formula for small diameters plastic tubes, also well known, expressed in equation (2).

$$Q = 55.934 \cdot D^{2.714} \cdot J^{0.571} \tag{2}$$

Where J is the head loss gradient, or hydraulic slope (= h_f / L), (m/m). The other quantities have already been defined previously.
At that moment, the flow rate values for each hydraulic situation were calculated using (2), based on the diameter of each situation and the head loss gradient, which consists of the ratio between the head loss and the length, in each situation. It is important to mention that the total energy (levels difference) were relatively small, so that the kinetic energy of the Bernoulli equation could not simply be neglected as a function of the total energy, which could generate inaccuracies. Therefore, the value of the kinetic energy (as a minor head loss) was deducted from the difference in level to result in the major head loss, which is the energy available to generate flow rate.

4. Results and discussion

Table 1 illustrates the combinations of the hydraulic parameters of each situation, as described in the previous section. It presents the flow rate values measured by volumetric process, and calculated by (2). Finally, the modular percentage deviation between the measured and calculated flow rate values is presented.

Table 1: Correlation of hydraulic parameters in pressurized pipes

Case	L (m)	D (mm)	ΔH (cm)	Q_M (10^{-6} m^3/s)	E_k (cm)	J (m/m)	Q_C (10^{-6} m^3/s)	dm (%)
1	5.0	11	56.0	72.9	3.00	0.1060	75.1	2.9
2	8.2	11	56.0	62.5	2.21	0.0656	57.1	9.1
3	5.0	8	56.0	31.0	1.94	0.1081	32.0	3.1
4	5.0	11	83.0	103.0	5.99	0.1540	92.9	10.3

L: length; D: diameter; ΔH: level difference; Q_M: measured flow rate; E_K: kinetic energy; J: head loss gradient; Q_C: calculated flow rate; dm: modular percentage deviation from the mean

As it was a very simple construction experiment, without the use of materials that would give precision to the system, it was understood that the results were quite satisfactory. This resulted, in fact, in a greater engagement of students in the process as a whole, deepening their understanding and apprehension of the concepts presented.

5. Conclusions

The importance of laboratory activities in the training of students in engineering courses and in the technological area in general has been known for a long time. Such activities make it possible to materialize and practice the topics seen in the classroom, testing concepts and hypotheses, modeling situations to be experienced in the future, in professional life.
The practical class, in addition to helping to establish the theoretical content that often requires a certain degree of abstraction, favors the development of critical thinking and the ability to work in a team. In this way, it leads the student closer to the content, bringing him into the process, which ends up learning also through doing, expanding his scientific understanding of the phenomena verified in the classroom.
Along this line, the present article presented a simple laboratory experiment to help students visualize the correlation among hydraulic parameters in pressurized pipes.

References

[1] Ferland, M., C. F. Molinaro, J. J. Kosovich, and J. K. Flake. "Using Motivation Assessment as a Teaching Tool for Large Undergraduate Courses: Reflections from the Teaching Team." *Teaching of Psychology* 0, no. 0 (February 2022): 1–7. https://doi.org/10.1177%2F00986283211066485.

[2] Nair, I., and V. M. Das. "Using Technology Acceptance Model to assess teachers' attitude towards use of technology as teaching tool: A SEM Approach." *International Journal of Computer Applications* 42, no. 2 (March 2012): 1–6. https://doi.org/10.5120/5661-7691.

[3] Drumea, A. "Education in development of electronic modules using free and open source software tools." *HIDRAULICA Magazine*, no. 3-4 (2012): 54–60. https://hidraulica.fluidas.ro/2012/3_4/54_60.pdf.

[4] Jordan, R. L. A., and E. Tisdale. "Using Data Acquisition in the Fluid Power Laboratory." Paper presented at the American Society for Engineering Education Annual Conference, Charlotte, USA, June 20-23, 1999. https://peer.asee.org/80283.

[5] Untener, J. A. "A Multifaceted Approach to a Fluid Power Laboratory Course." Paper presented at the American Society for Engineering Education Annual Conference, Columbus, USA, June 24-28, 2017. https://doi.org/10.18260/1-2--27487.

[6] Tavares, T. S. "Performance Testing of Small Water Pumps: A Versatile and Economical Laboratory Exercise for Engineering Technology Students." Paper presented at the American Society for Engineering Education Annual Conference, Columbus, USA, June 24-28, 2017. https://doi.org/10.18260/1-2--28738.

[7] Addison, H. "Instruction and Research in Hydraulic Laboratories." *Proceedings of the Institution of Mechanical Engineers* 167, no. 1b (June 1953): 401–419. https://doi.org/10.1177%2F002034835316701b25.
[8] University of Colorado Boulder. "Fluid Power Basics". Last modified: May 12, 2022. https://www.teachengineering.org/lessons/view/pur_fluidpower_less1.
[9] Shreyas, H. C., K. Prabhakar, and A. A. P. Thomas. *Hydraulics and Hydraulic Machines Lab: Lab Manual*. Bangalore, Gopalan College of Engineering and Management, 2016-2017.
[10] Verma, M. R., and A. Alavizadeh. "Design and Development of Pneumatic Lab Activities for a Course on Fluid Power." Paper presented at the American Society for Engineering Education Annual Conference, Columbus, USA, June 24-28, 2017.
[11] Abcarian, G., Z. Algharib, O. Hussain, A. Martin, A. Villa, F. Villalobos, T. Zirakian, and D. Boyajian. "Discharge Coefficient Measurements Using Heron's Fountain." *Journal of Civil Engineering and Architecture* 13, no. 3 (March 2019): 195–203. https://doi.org/10.17265/1934-7359/2019.03.004.
[12] Alastal, K. M., and M. Y. Mousa. *Fluid Mechanics and Hydraulics Lab Manual*. Gaza: Islamic University of Gaza, 2015.
[13] Jorhat Engineering College. *Hydraulics Laboratory Manual*. Jorhat, Assam Science and Technology University.
[14] Ayalkie, B., L. Matusal, S. Miheretu, and K. O. A. Askari. "Hydraulics Lab Manual for Water Engineering Students." (submitted manuscript).
[15] Widmann, J., C. Birdsong, J. Ridgely, and F. Owen. "Integrating Experiment, Modeling And Design Using A Hands On Hydraulic Positioning Laboratory For Mechanical Control Systems Education." Paper presented at the American Society for Engineering Education Annual Conference, Pittsburgh, USA, June 22-25, 2008. https://doi.org/10.18260/1-2--4036.
[16] Garach, D. V. "Heat transfer and pressure drop in microchannels with different Inlet geometries for laminar and transitional flow of water." Master's thesis, University of Pretoria, 2014. http://hdl.handle.net/2263/40831.
[17] Medina, O. J. "General formula for the evaluation of linear load losses." *International Journal of Hydrology* 2, no. 6 (December 2018): 726–735. https://doi.org/10.15406/ijh.2018.02.00150.
[18] Rares, H. C. Z. "The Study of Head Losses for Land Drainage Pipes with and without Filtering Materials." In *Recent Advances in Energy and Environmental Management*, edited by V. Mladenov, T. Tashev, H. Wang, I. Kralov, S. Stankevich, P. Yildiz, and J. Burley, 33–38. Rhodes Island, WSEAS Press, 2013.
[19] Stănescu, M., A. Constantin, C. Şt. Nițescu, L. Roşu, and A. M. Dobre. "Comparative analysis of the hydraulic parameters of steady water flow in a looped pipe network." *International Journal of Mathematical Models and Methods in Applied Sciences* 5, no. 8 (2011): 1301–1309. https://www.naun.org/main/NAUN/ijmmas/2011.html.
[20] Cardoso, G. G. G., J. A. Frizzone, and R. Rezende. "Friction factor in small diameter polyethylene pipes (Fator de atrito em tubos de polietileno de pequenos diâmetros)." *Acta Scientiarum. Agronomy* 30, no. 3 (2008): 299–305. https://doi.org/10.4025/actasciagron.v30i3.3497.
[21] Bagarello, V., V. Ferro, G. Provenzano, and D. Pumo. "Experimental Study on Flow-Resistance Law for Small-Diameter Plastic Pipes." *Journal of Irrigation and Drainage Engineering* 121, no. 5 (September 1995): 313–316. https://doi.org/10.1061/(ASCE)0733-9437(1995)121:5(313).
[22] Bernuth, R. D., and T. Wilson. "Friction Factors for Small Diameter Plastic Pipes." *Journal of Hydraulic Engineering* 115, no. 2 (February 1989): 183–192. https://doi.org/10.1061/(ASCE)0733-9429(1989)115:2(183).

Criteria and Instruments for Choosing a Wind Turbine

Prof. PhD. Eng. **Fănel-Viorel PANAITESCU**[1], Prof. PhD. Eng. **Mariana PANAITESCU**[1,*], PhD. student Eng. **Paula PANAIT**[2]

[1] Constanta Maritime University, Romania

[2] Doctoral School of Constanta Maritime University, Romania

* Panaitescu Mariana, panaitescumariana1@gmail.com

Abstract: *Wind energy is becoming one of the most widely used renewable energy sources in Romania as well. In order for production to be efficient and implicitly profitable, wind turbines are usually arranged in wind farms. The main purpose of the paper is to present intelligent criteria and tools for designing wind turbines. In the present study, the following are pointed out as topics of interest: the shading of the wind given by an obstacle, the height of the turbine hub, the distance between the obstacle and the turbine, the roughness class of the turbine location, the height and width of the obstacle and the porosity of the obstacle. These elements help to determine the variation of the wind front, the power of the wind captured by the turbines and the calculation of the energy captured. The results obtained using calculation programs are: wind speeds are in the range of 5-10 m / s in the predominant direction S-SE (between 270^0-330^0) and V-NV (between 150^0-210^0); power density function; Weibull distribution for wind speed; turbine power curve; Wind turbulence in the turbine area; power coefficient depending on wind speed; The amount of energy that the wind transfers to the rotor; Wind frequency curve; speed insurance curve. Finally, by using the modelling tools in Math Lab Simulink, the random speed distributions were obtained, which can be analyzed and then provided to obtain a maximum power, and consequently a maximum amount of energy.*

Keywords: *Tool, wind, turbine, parameter, shade, obstacle, power, energy*

1. Introduction

Wind energy is becoming one of the most widely used renewable energy sources in Romania as well. In order for production to be efficient and implicitly profitable, wind turbines are usually arranged in wind farms. It should be noted that a wind speed of a minimum of 3m/s and a maximum of 25 m/s is required for the operation of a wind turbine. In addition, at start-up, a wind turbine consumes about 750 kW. The service life of a turbine is 20 years [1].
In order for a wind turbine to be installed in a particular location, certain conditions must be met:

• the intensity of the wind during a year to allow a constant production;

• signalling the presence of access roads in the area;

• signalling the presence in the area of high voltage transmission lines;

• no environmental restrictions (protected areas);

• the location of the wind turbine to support its mass;

• the site should be free of loads.

From wind studies [2] it can view wind intensity maps depending on the chosen location. These points clearly show the points where the wind intensity is maximum, points where the wind turbines will be installed later. Because wind turbines have a considerable height (¬150 m with a blade) and must withstand the maximum wind speeds recorded at the site, buried concrete foundations are built to fix them.
Turbines do not require a human operator. They are monitored from a dispatcher through internet connections and SCADA programs - Supervisory Control And Data Acquisition - Surveillance, control and data acquisition program.

2. Material and methods

2.1. The influence of obstacles on the speed picked up by the turbine

In the present study are pointed out as topics of interest: the shading of the wind given by an obstacle, the height of the turbine hub, the distance between the obstacle and the turbine, the roughness class of the turbine location, the height and width of the obstacle and the porosity of the obstacle. These elements help to determine the variation of the wind front, the power of the wind captured by the turbines and the calculation of the energy captured.

2.2. Assumptions and calculation elements

2.2.1. Calculation hypotheses

- the presence of the obstacle on the wind can extend up to 2..3 times the height of the obstacle at a certain distance.
-- distance between obstacle and turbine- On very rough terrain the effect of obstacles can be measurable up to 20 km distance from the obstacle.

- roughness of the terrain between the obstacle and the wind turbine - The terrain with low roughness will allow the wind that passes outside the obstacle to mix more easily after the obstacle, so that the shade of the wind is relatively less important.

- obstacle height-The higher the obstacle, the greater its influence on the wind front.

- obstacle width - The obstacle calculation model works on the assumption that the obstacles are infinitely long and that they are placed at right angles (perpendicular) to the wind direction. For practical reasons, we assume that we are investigating the horizon around the wind turbine in twelve 30-degree sections (in 10 percent steps).

- the porosity of an obstacle is a percentage indication of how open an obstacle is, i.e. how easily the wind can pass through it (A building obviously has zero porosity. A group of buildings with a certain space between them and have a porosity equal to (open space area) divided by (total area of both buildings and the open space between them, seen from the wind turbine).

2.2.2. Experimental research

2.2.2.1. Input data

- the location of the turbine and the height of the turbine tower (Figure 1);

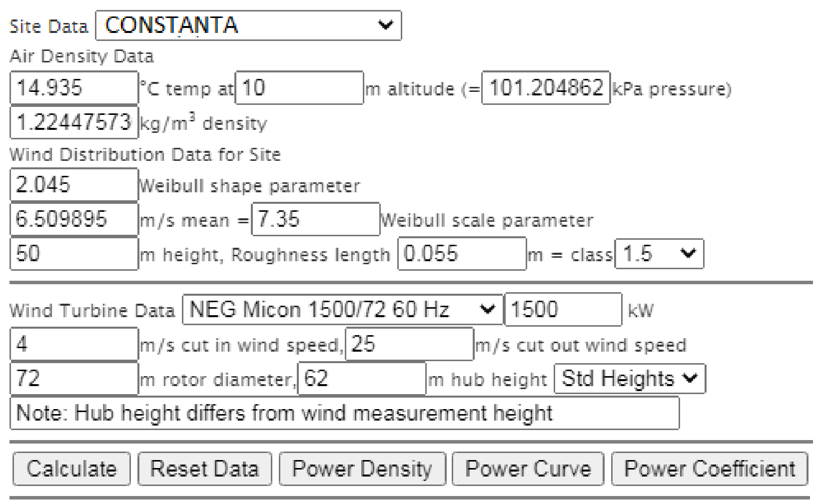

Fig. 1. Chosen study location

- wind speed in the given location (wind rose) [3] (Figure 2, Figure 3);

- obstacles in the area (height, width, roughness, porosity).

Therefore, using a virtual computer to simulate the case study, we introduce the option for the study location and data related to altitude, temperature, air density, pressure, turbine type, wind speed and we will get information about power, energy, power curve of the turbine depending on the wattage speed, power coefficient (Figure 1).

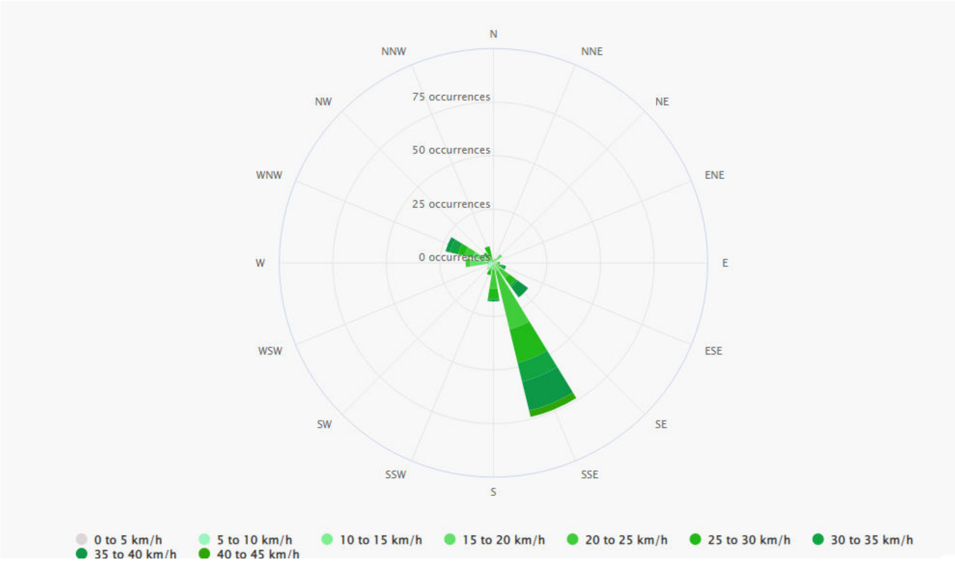

Fig. 2. Wind rose for the study location

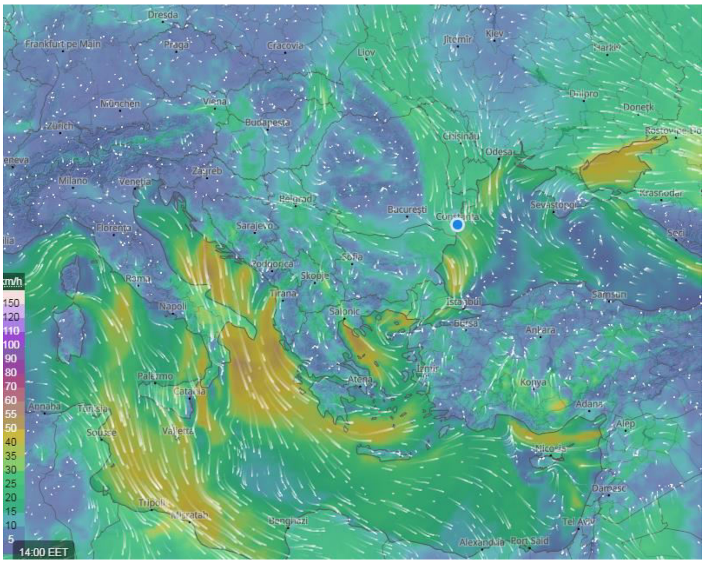

Fig. 3. Wind map for the study location

It is observed that most values for wind speed are in the range of 5-10 m / s in the predominant direction S-SE (between 270^0-330^0) and V-NV (between 150^0-210^0).

2.2.2.2. Results

The results were obtained using a virtual computer [2]:

- *porosity of obstacles*;

Using a calculation program [2], results are obtained for the porosity of the obstacles [4] (Figure 4) depending on the height of the turbine tower (Figure 5):

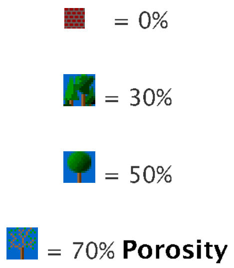

Fig. 4. Obstacle porosity representation code [4]

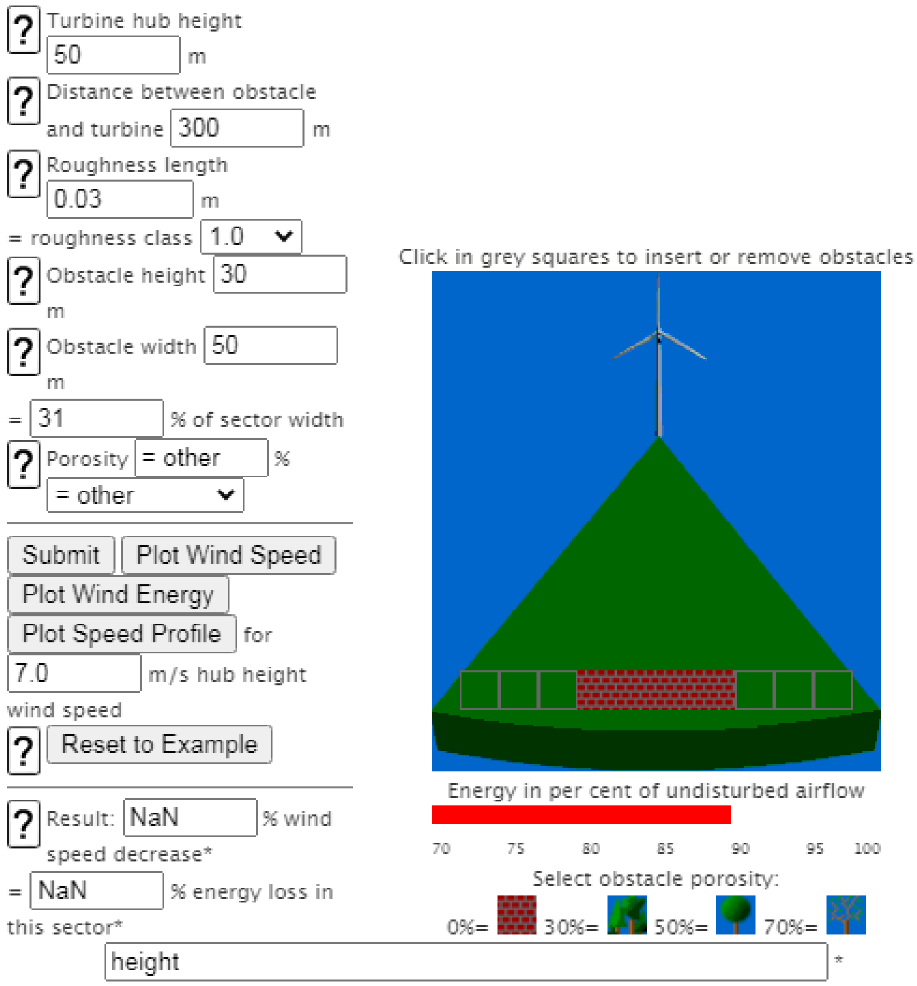

Fig. 5. Obstacle porosity [4]

To estimate the potential in the study location, measurements were made by purchasing 2000 data for wind speed and direction for the reference elevation of 10 m and using the Simulink MathLab program. The speed variations that were later used to assess the turbine power were estimated.

- *wind power*

Wind power– it can be calculated the power density function (Figure 6) [5]:

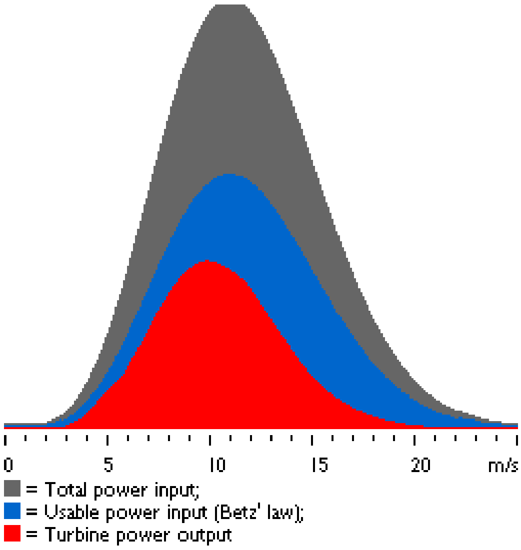

Fig. 6. Wind power variation [5]

- *Weibull wind speed distribution* (Figure 7) [6]

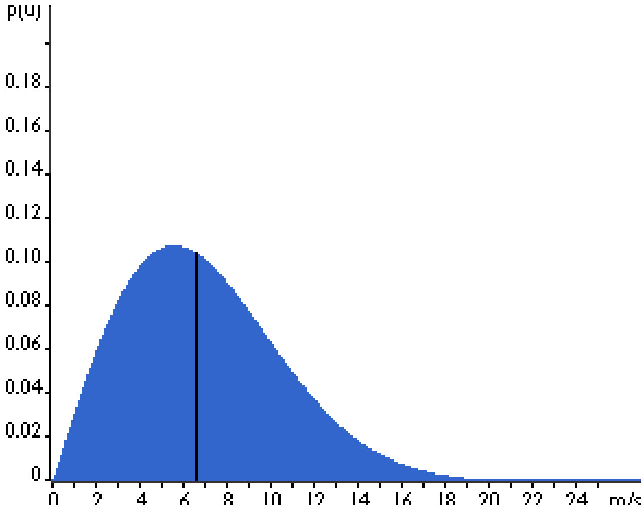

Fig. 7. Weibull distribution for wind speed [6]

- *turbine power curve* (Figure 8, Figure 9)

We can calculate the turbine power using the formula:

$$P = \frac{1}{2}\rho \cdot \mathrm{v}^3 \cdot \pi r^2 \quad (1)$$

Where

P - the power of the wind measured in W;

ρ - the density of dry air = 1.225 [kg/m^3], at p_0- atmospheric pressure at sea level at 15° C;

v = the velocity of the wind [m/s];

π = 3.1415926535...;

r = the radius (a half of the diameter of the rotor [m]).

Site Power Input Results
Power input* 347 W/m2 rotor area
Max. power input at* 10.6 m/s
Mean hub ht wind speed* 6.7 m/s

Turbine Power output Results
Power output* 110 W/m2 rotor area
Energy output* 964 kWh/m2/year
Energy output* 3925989 kWh/year
Capacity factor* 30 per cent

Wind Turbine Power Curve

m/s	kW	m/s	kW	m/s	kW
1	0	11	1285	21	1500
2	0	12	1426	22	1500
3	0	13	1451	23	1500
4	0	14	1483	24	1500
5	74	15	1500	25	1500
6	202	16	1500	26	0
7	356	17	1500	27	0
8	576	18	1500	28	0
9	808	19	1500	29	0
10	1058	20	1500	30	0

Fig. 8. Numerical values for wind turbine power curve

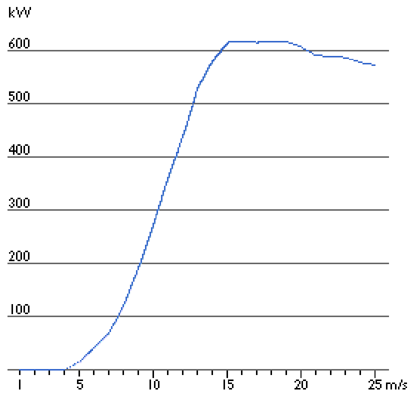

Fig. 9. Wind turbine power curve [7]

- *turbulence* (Figure 10) - decreases the possibility of efficiently using wind energy for a wind turbine. It also requires more wind turbine rupture and wear voltage:

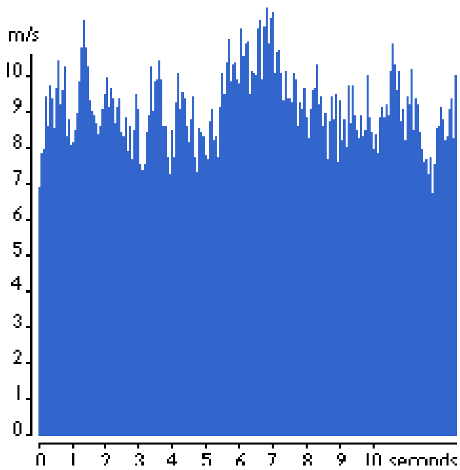

Fig. 10. Wind turbine power curve in the turbine area

- *the power coefficient* depending on the wind speed has the value 44 (Figure 11):

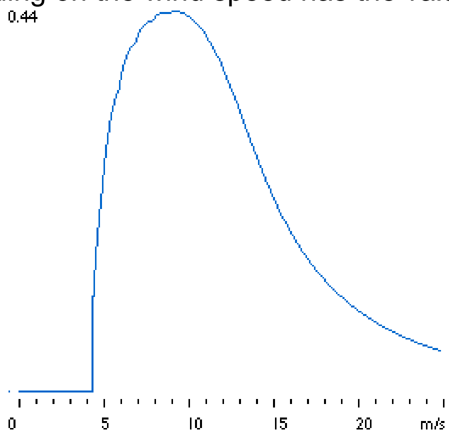

Fig. 11. Power coefficient

- *wind energy (*Figure 12)

The amount of energy that the wind transfers to the rotor depends on the air density, the rotor area and the wind speed. Wind energy in an air stream can be viewed depending on:
- the height of the obstacles on the direction of the wind turbine (maximum 30m);
- width of obstacles (maximum 50 m)
- height at the axis of the platform (maximum 50 m);
- roughness / porosity (NaN) (figure 3.5).

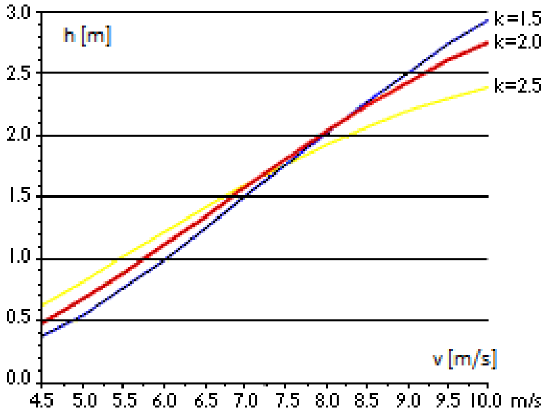

Fig. 12. Wind energy

Where
h- height of obstacles [m]; v-wind speed [m / s]; k-shape parameter; k-shape parameter [8]; k = 1.05 ... 0.73; average = 0.94. For average = 5.58 ... 9.98 [m / s] we take k = 0.915 ... 0.900
From the results from the literature, for the case study at an average value of wind speeds, v_{med} = 7.37 m / s, the wind class according to IEC is class III (true = 37.5 m / s). Thus, you can choose a turbine with a nominal power that varies between 1285 ... 1500 kW.
The type of turbine chosen may vary as a model (Table 1):

Table 1: Technical parameters on types of wind turbines

Wind turbine type	Wind class	Rotor Diameter [m]	Tower height [m]	P_{nom} [kW}	V_s [m/s]	v_0 [m/s]
VESTAS	IA	100	80	3600	4	25
SIEMENS	IA	90	80	3000	4	25
JIANSGHU NAIR	III	72	62	1500	6.7	25

Where
P_{nom}-nominal power [kW]; v_s- start speed [m/s]; v_0- Stop speed [m / s].
Using the data obtained for wind speeds recorded over short and equal intervals, two types of curves can be drawn:
- frequency curve (Figure 13), in which time intervals are associated depending on the frequency of occurrence of the speed

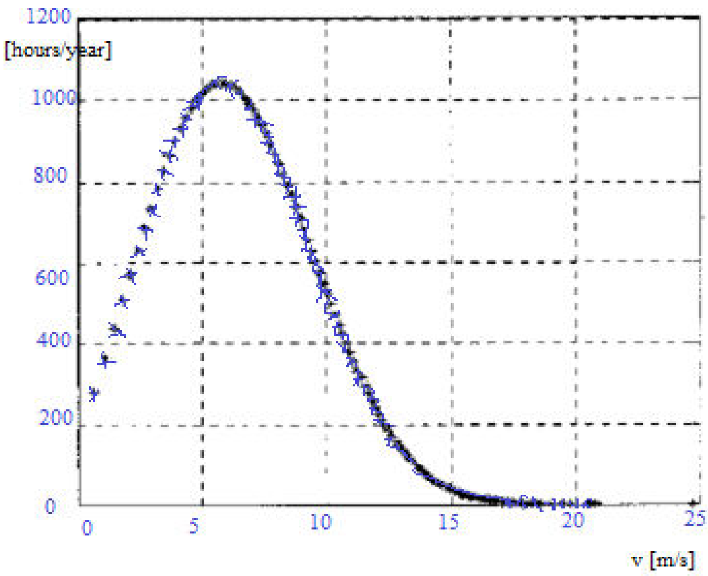

Fig. 13. Wind frequency curve

-- the speed assurance curve (Figure 14) in which the dependence between the frequency of occurrence of the speed and the speed threshold is visualized.

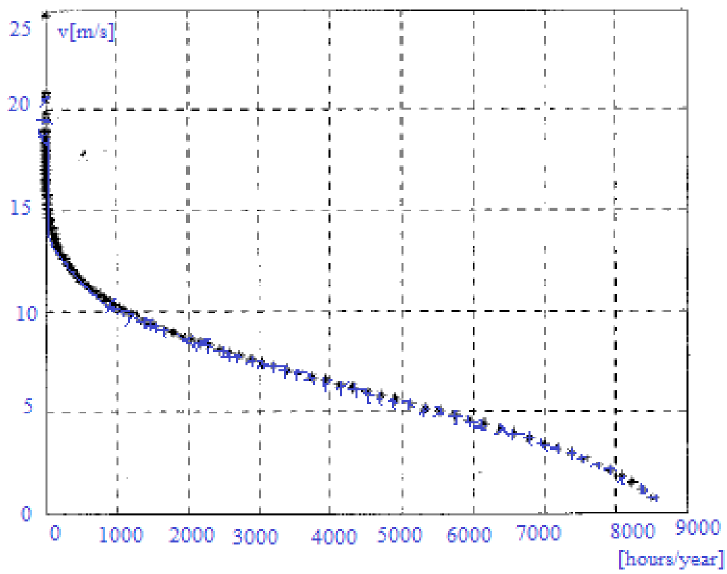

Fig. 14. Wind Speed insurance curve

If the speeds and the safety curve are taken into account, it is observed that the wind turbine cannot work at speeds lower than the minimum speed or at speeds higher than the maximum speed. Then it is established what is the optimal speed at which the turbine starts to produce electricity, v_{min}, the speed at which it has a maximum energy, v_{max} and what is the installation speed vi, that is, we will make an assessment of the speeds characteristic of the wind turbine location by a simulation in Math Lab.

The results before the revaluation obtained are:

- average speed v_m = 7.389786 m / s; where

$$v_m = \sum_{i=1}^{2000} \frac{v_i}{2000} \quad (2)$$

-maximum speed v_{max} = 24.753 m / s.

Now, after the re-evaluation of the speeds depending on the characteristics of the terrain, the final results are obtained:

- v_{min} = 6.37 m / s;
- v_{max} = 23.5 m / s.

3. Conclusions

Wind patterns, turbulence, wind rose, velocity distributions and their frequency were simulated in the context of a chosen location, and the random speed distributions that can be analyzed were finally obtained by using Math Lab Simulink modeling tools, then provided to obtain a maximum power, and consequently a maximum amount of energy.
Thus, it was realized:

- Establishing the wind turbine framing class
- Wind speed variation and turbulence
- Power characteristic and energy produced by turbines.

References

[1] "Wind Farm"/ "Parc eolian". Accessed April 6, 2022. https://ro.wikipedia.org/wiki/Parc_eolian.
[2] "Wind Turbine Power Calculator". Accessed April 6, 2022. http://xn--drmstrre-64ad.dk/wp-content/wind/miller/windpower%20web/en/tour/wres/pow/index.htm.
[3] "The Wind Rose". Accessed April 6, 2022. http://www.xn--drmstrre-64ad.dk/wp-content/wind/miller/windpower%20web/en/tour/wres/rose.htm.
[4] "Wind Shade Calculator". Accessed April 6, 2022. http://xn--drmstrre-64ad.dk/wp-content/wind/miller/windpower%20web/en/tour/wres/shelter/index.htm.
[5] "Power Density Function" Accessed April 6, 2022. http://xn--drmstrre-64ad.dk/wp-content/wind/miller/windpower%20web/en/tour/wres/powdensi.htm.
[6] "Describing Wind Variations: Weibull Distribution". Accessed April 6, 2022. http://www.xn--drmstrre-64ad.dk/wp-content/wind/miller/windpower%20web/en/tour/wres/weibull.htm.
[7] "The Power Curve of a Wind Turbine". Accessed April 6, 2022. http://xn--drmstrre-64ad.dk/wp-content/wind/miller/windpower%20web/en/tour/wres/pwr.htm.
[8] Safta, Carmen Anca, Teodor Zabet, and Ion Antonescu. *Wind Energy. Guide for practical activities. / Energie eoliană: îndrumar pentru activităţi practice*. Bucharest, Printech Publishing House, 2013.

ISSN 1453 – 7303 **"HIDRAULICA" (No. 2/2022)**
Magazine *of Hydraulics, Pneumatics, Tribology, Ecology, Sensorics, Mechatronics*

Researches on Water Aeration Flowing through Pipes

PhD Std. **Marilena Monica BOLTINESCU (ROZA)**[1], Prof. Dr. Eng. **Nicolae BĂRAN**[1],
PhD Std. **Alexandru Iulian GRIGORE**[1], PhD Std. **Remus VOICU**[1],
Ș.l. Dr. Eng. **Mihaela CONSTANTIN**[1,*]

[1] University Politehnica of Bucharest

* i.mihaelaconstantin@gmail.com

Abstract: *The paper proposes that the water aeration to be carried out by introducing compressed air into the wastewater transport pipelines. For this purpose, a system for dispersing the air in the water flowing through the pipes was designed and built; the air coming out through a series of orifices drilled in a spiral mounted inside the pipe moves equidistantly with the water. An experimental installation for the study of the biphasic air + water flow is presented, an installation that also serves to measure the concentration of dissolved oxygen in water.*

Keywords: *Water aeration, dissolved oxygen, oxygenometer, oxygen transfer.*

1. Introduction

Water aeration is a process of increasing the amount of dissolved oxygen in water, to ensure proper water quality.
Oxygen in water comes in two forms:
• O_2 bound to H_2.
• Free O_2, called dissolved oxygen in water.
Free oxygen is represented by oxygen that is not bound to any other element. Dissolved oxygen is represented by these free oxygen molecules in the water. The water-bound oxygen molecule (H_2O) is a compound and is not considered in determining the level of dissolved oxygen.
Dissolved oxygen is an important parameter in the evaluation of water quality due to its influence on living organisms in a water volume, a level of dissolved oxygen too high or too low can affect aquatic life and water quality.
An optimal level of dissolved oxygen must be maintained in the water.
The amount of dissolved oxygen in water differs from one life form to another; crabs and oysters need minimal amounts of oxygen (1 ÷ 6 mg / dm^3), while shallow water fish need a higher level (4 ÷ 15 mg / dm^3) [1] [2].
Water aeration is used in the following areas [3] [4]:
- in water treatment processes by removing dissolved inorganic substances, or chemical elements such as: arsenic, cadmium, cobalt, chromium, iron, manganese, nickel, zinc, lead.
- biological treatment of wastewater.
- in water disinfection processes by ozonation.
-in the separation and collection of existing fats in wastewater.

It is known from the literature [5] [6] that the process of aeration of water can be achieved by:
a. mechanical aeration.
b. pneumatic aeration.
c. mixed aeration.

Pneumatic aeration is clearly superior to mechanical aeration systems [7] and is achieved by introducing compressed air into the water, below the free surface of the liquid.
The aerating equipment consists of:
I. drilled pipes located on the water tank base.
II. porous diffusers of ceramic, glass, perforated membranes.
III. fine bubble generators (FBG) at which ø <1 mm.
In the case of stationary water, any of the three variants may be used: I, II, III.

For water flowing through pipes, the placement inside the pipe, in a flow section, of one of the constructive solutions I, II, III, would reduce the area of the flow section, which would lead to large pressure losses.
As a result of the researches, the authors found an original solution for dispersing air into water flowing through pipes, a solution presented in paragraph 3.

2. Analysis of the biphasic fluid (water + air) flow through pipes.

In the study of biphasic fluid flow, there may be different types of flows, of which three cases may occur:
a) Bubble flow (figure 1)
- in this case, the air is dispersed in the water in the form of bubbles.

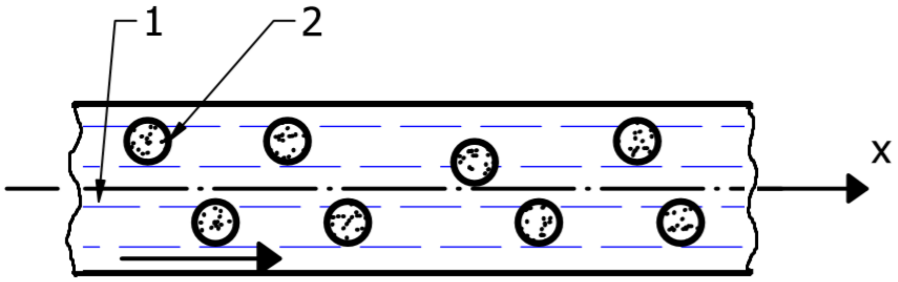

Fig. 1. Bubble flow
1- water; 2- air bubbles

b) Flow with gas plugs (figure 2)

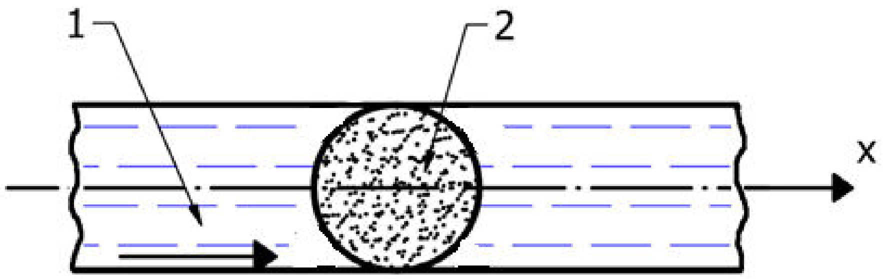

Fig. 2. Flow with gas plugs
1- water; 2- air bubble

The air bubbles form a plug that will move at a speed equal to the speed of the water.
c) Layered flow (figure 3)

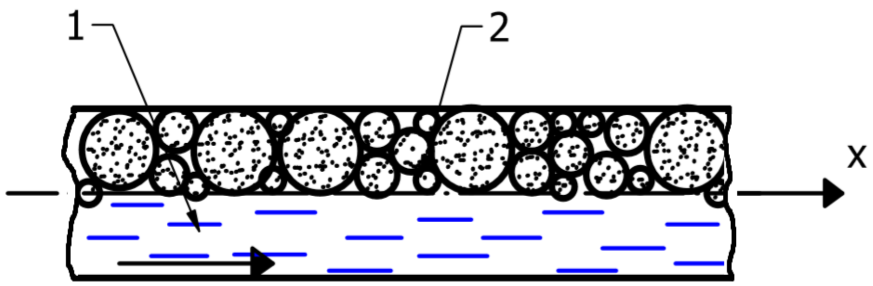

Fig. 3. Layered flow
1- water; 2- air bubbles

Since the density of the air is lower than the water density, the air bubbles rise in the upper part of the pipe, thus appearing the separation surface between liquid and gas.

To determine the flow regime, it is considered that the water volume to be aerated in time (τ) of 2 hours, is V = 0.125 m^3.
This volume will flow through a pipe with an inner diameter of 44 mm, as a result the flow rate and water speed will be [8]:

$$\dot{V} = \frac{V}{\tau} = \frac{0.125}{2\cdot 3600} = 0.01736\cdot 10^{-3}\ m^3/s \tag{1}$$

$$w = \frac{\dot{V}}{\frac{\pi}{4}d^2} = \frac{0.01736\cdot 10^{-3}}{0.786\cdot(0.044)^2} = 0.0115\, m/s \tag{2}$$

For water at 20 °C, the kinematic viscosity is [8]:
$\nu = 1\cdot 10^{-6}\ m^2/s$
so, Reynolds number will be:

$$\mathrm{Re} = \frac{w\cdot d}{\nu} = \frac{0.0115\cdot 0.044}{1\cdot 10^{-6}} = 506 \tag{3}$$

Since Re <2320, the water flow regime is laminar.
The air flow rate in water:

$$\dot{V} = \frac{0.6}{3600} = 0.0001666\ m^3/s \tag{4}$$

The area of the air outlet section in the water, considering previous researches [9] [10] [11] is chosen A = 1,2 · 10^{-6} m^2; the number of air orifices in the water is:

$$n = \frac{A}{\frac{\pi d^2}{4}} = \frac{1.2\cdot 10^{-6}}{\frac{\pi}{4}\cdot(0.3\cdot 10^{-3})} = 17 \tag{5}$$

3. Presentation of the constructive solution for the air dispersion in the water flowing through a pipe

For the controlled and uniform introduction of compressed air into the water, a flat spiral was constructed; the spiral is made of a copper capillary tube with an outer diameter of 3 mm and an inner diameter of 1 mm.
In the spiral, 17 orifices were made with ø = 0.3 mm.
The spiral contains three circles (figure 4) with diameters of 16 mm, 26 mm, 36 mm and lengths of 50.24 mm, 81.64 mm, 113.24 mm.
The total length (L) of the spiral is 244.92 mm.

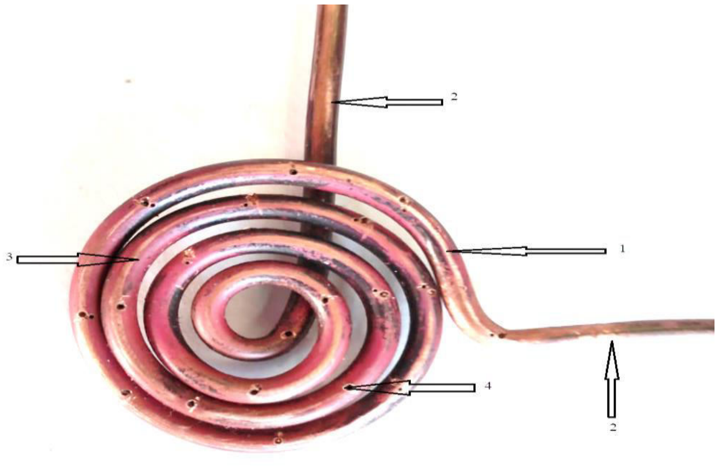

Fig. 4. Spiral with 17 orifices with ø = 0.3 mm
1– pipe Ø - 50 x 3 mm; 2 - compressed air inlet connections;
3 - spiral; 4 - orifices

The distance between two orifices will be:

$$l = \frac{L}{n} = \frac{244.92}{17} = 14.4\ mm \tag{6}$$

Several orifices will be made in each circle:

$$n_1 = \frac{L_1}{l} = \frac{50.24}{14.4} = 3 \tag{7}$$

$$n_2 = \frac{L_2}{l} = \frac{81,64}{14.4} = 6 \tag{8}$$

$$n_3 = \frac{L_3}{l} = \frac{113.24}{14.4} = 8 \tag{9}$$

There are a total of 17 orifices with ø = 0.3 mm (figure 5).

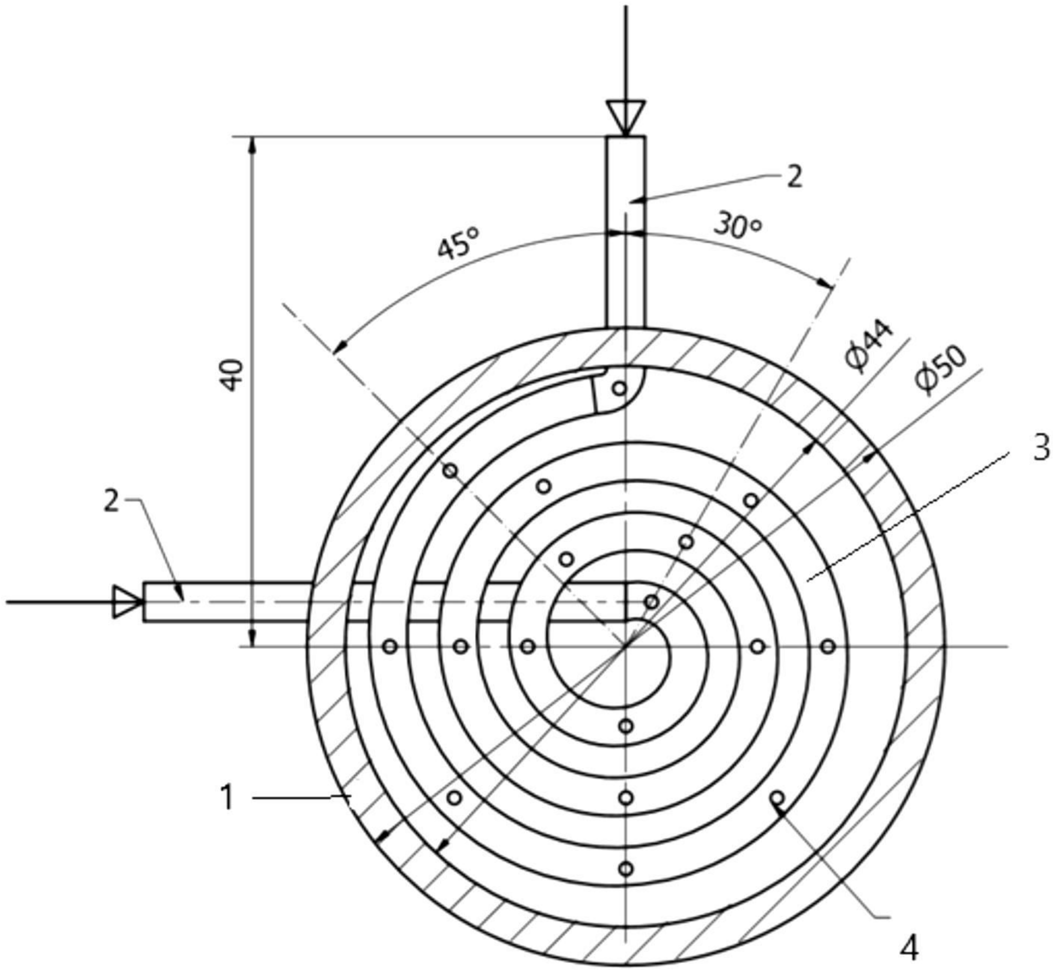

Fig. 5. Cross section through the pipe where the spiral is located.
1-pipe Ø 50x3 mm; 2- compressed air inlet connections; 3- spiral; 4- orifices Ø 0.3 mm

Compressed air enters the spiral through the two connections (2).

4. Presentation of the experimental installation for water aeration flowing through pipes

Pipes that carry water can be placed in a horizontal or vertical position. Only the case of horizontal pipes will be analyzed (figure 6).

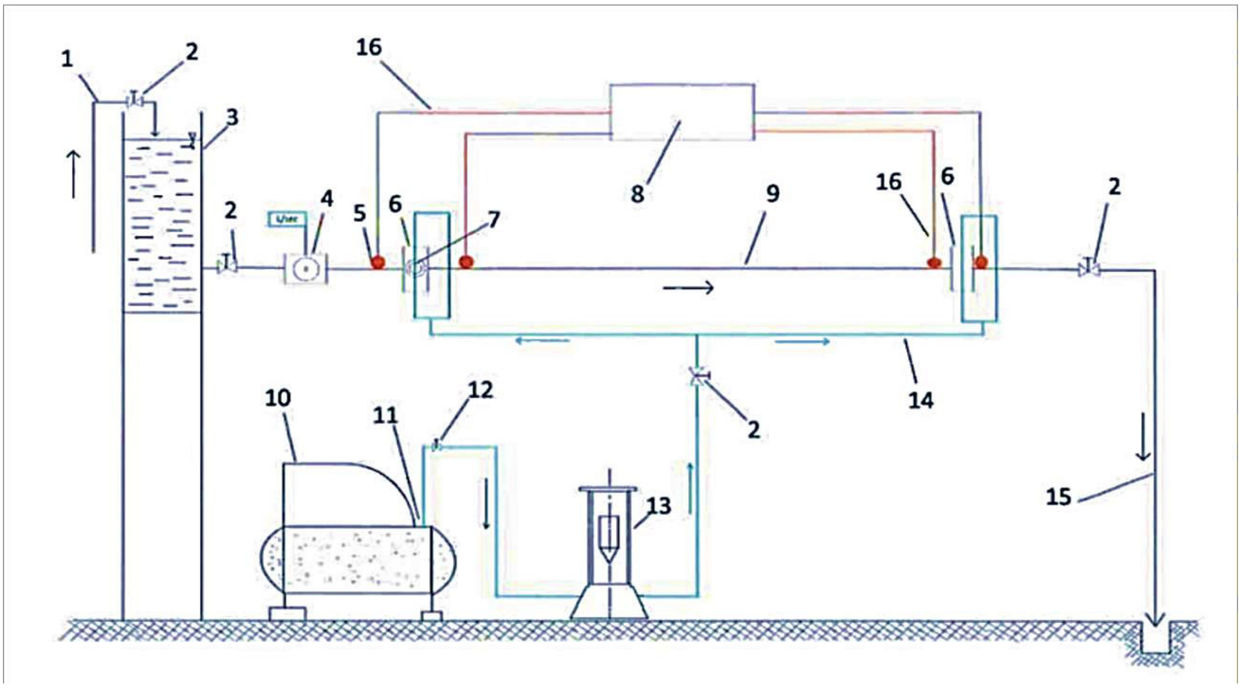

Fig. 6. Scheme of the experimental installation
1– water supply pipe; 2 - tap; 3 - water tank; 4 - flow meter; 5 - light insulating spot; 6- flanges; 7 - spiral; 8 - oxygenometer; 9 - transparent plexiglass pipe; 10 - electrocompressor; 11 - compressed air tank; 12 - pressure reducer; 13 - rotameter; 14 - compressed air pipes; 15 - water drainage pipe to the sewer network; 16 - optical fiber.

Figure 7 shows that a spiral (1) is mounted inside the transparent plexiglass pipe. Through the two connections (2), the compressed air enters the spiral and then, through the 17 orifices, exits and moves concurrently with the water.

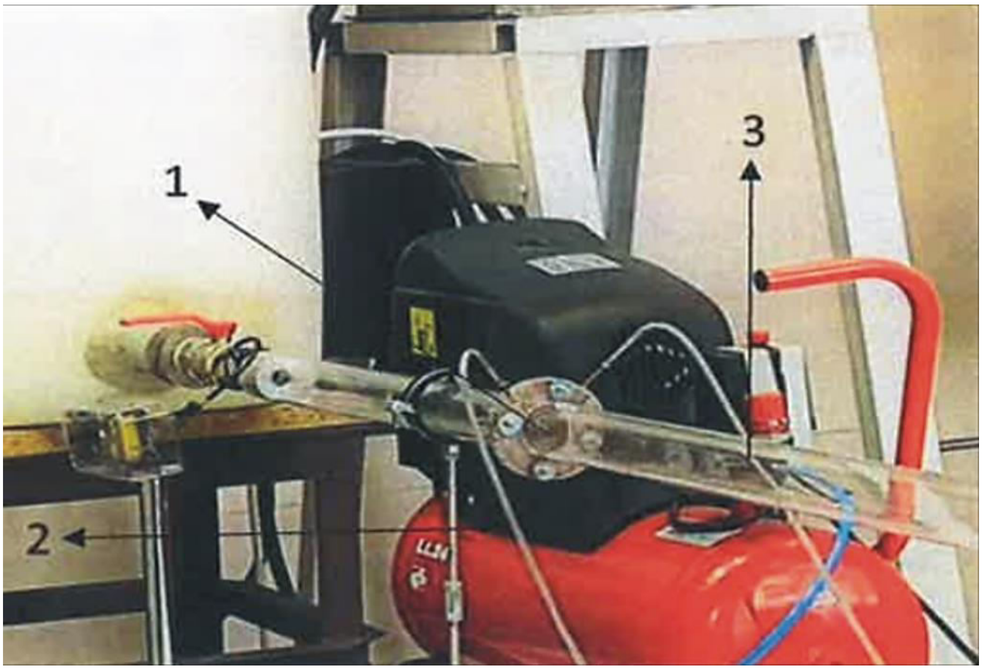

Fig. 7. The spiral placed between the flanges
1– spiral; 2 - compressed air connections; 3 - transparent plexiglass pipe.

The dissolved oxygen concentration in water can be measured by one of three methods: chemical, electrical, optical [12] [13].

The transparent plexiglass pipe (3) allows the measurement of the dissolved oxygen concentration in water by the optical method, namely by a non-invasive process.
The signal from the sensor (5) is transmitted to the oxygenometer via the optical fiber (16).
In Figure (8), an overview of the experimental installation can be seen.

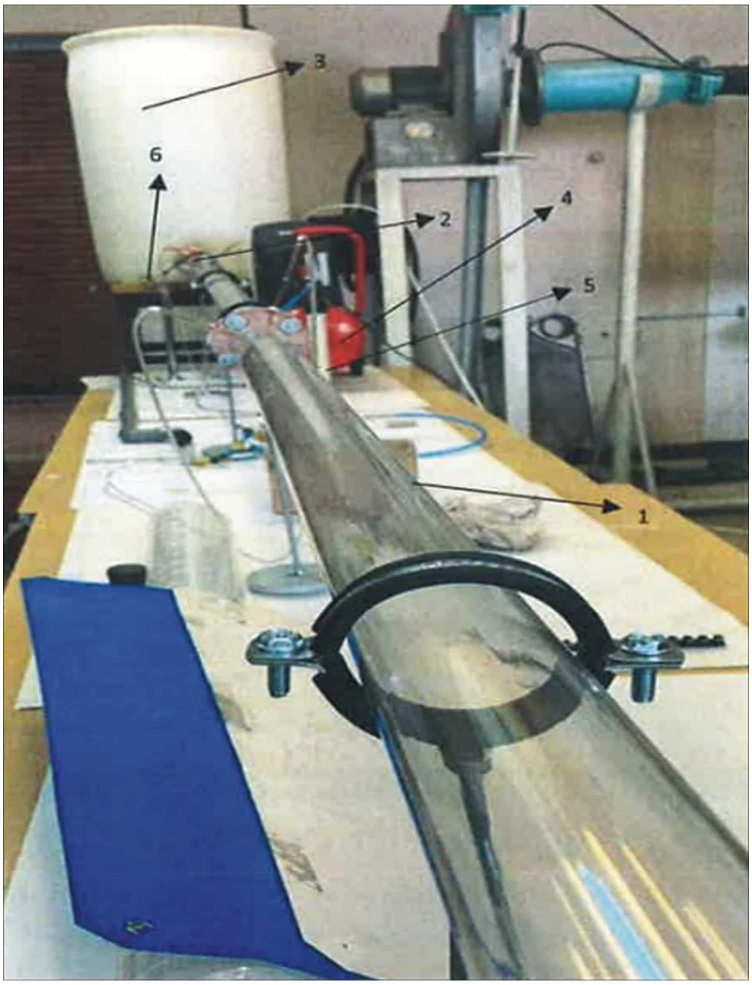

Fig. 8. Overview of the experimental installation
1-pipe ø 50 x 2; 2- spiral; 3- water tank; 4- compressor; 5- rotameter; 6 - electronic flow meter.

The experimental installation designed and built in the laboratory of the Faculty of Mechanical and Mechatronics Engineering is useful for the study of increasing the dissolved oxygen concentration in water flowing through horizontal pipes.

5. Conclusions

1. An air dispersion system in cross-section of the pipe carrying the aerated fluid is an efficient and original solution.
2. The shape and number of orifices in the spiral depend on the air flow rate to be introduced into the water at one or two successive points.
3. By introducing air into the horizontal pipes at several successive points, until the dissolved oxygen concentration at saturation is reached, those enormous basins can be removed from the water treatment plants, thus reducing the value of the investments.
4. If the pipe carrying the aerated fluid is metallic, a short tube of transparent plexiglass shall be fitted along its path so that it is possible to measure the dissolved oxygen concentration in the water by a non-invasive method.
5. The aeration of the water flowing through vertical pipes will be studied later and will be compared with the solution proposed in this paper.

References

[1] Tănase, E. Beatrice. *The influence of the instilled gas composition in water on the dissolved oxygen content / Influența compoziției gazului insuflat în apă asupra conținutului de oxigen dizolvat*. Doctoral thesis, Politehnica University of Bucharest, Faculty of Mechanics and Mechatronics, Bucharest, 2017.
[2] Oprina, G., I. Pincovschi, and Gh. Băran. *Hydro-Gas-Dynamics Aeration systems equipped with bubble generators* / *Hidro-Gazo-Dinamica Sistemelor de aerare echipate cu generatoare de bule*. Bucharest, Politehnica Press, 2009.
[3] Pătulea, Al. S. *The influence of functional parameters and the architecture of fine bubble generators on the efficiency of aeration installations* / *Influenţa parametrilor funcţionali şi a arhitecturii generatoarelor de bule fine asupra eficienţei instalaţiilor de aerare*. Doctoral thesis, Politehnica University of Bucharest, 2012.
[4] Crittenden, J.C., R.R. Trussell, D.W. Hand, K.J. Howe, and G. Tchobanoglous. *MWH's Water Treatment: Principles and Design*. Third Edition. Chapter 4 - *Air stipping and aeration*. John Wiley & Sons, Inc., 2012.
[5] Rajendren, R. ”Water treatment aeration.” *Kirk-Othmer Encyclopedia of Chemical Technology*. John Wiley & Sons, Inc., Published Online: 2000.
[6] Schierholz, E.L., J.S. Gulliver, S.C. Wilhelms, and H.E. Henneman. ”Gas transfer from air diffusers.” *Water Res*. 40, no. 5 (2006): 1018–1026.
[7] Căluşaru, I. M. *The influence of the physical properties of the liquid on the efficiency of the oxygenation processes* / *Influenţa proprietăţilor fizice ale lichidului asupra eficienţei proceselor de oxigenare*. Doctoral thesis, Politehnica University of Bucharest, 2014.
[8] Dobrovicescu, Al., N. Băran, Al. Chisacof, S. Petrescu, E. Vasilescu, D. Isvoranu, M. Costea, C. Petre, and A. Motorg. *The basics of technical thermodynamics* / *Bazele termodinamicii tehnice*. Vol. I: ”Elements of Technical Thermodynamics / Elemente de Termodinamică Tehnică.” Bucharest, Politehnica Press, 2009.
[9] Băran, N., Gh. Băran, G. Mateescu, and Al. S. Pătulea. ”Water Oxigenation.” *Buletinul Institutului Politehnic din Iaşi* LVI (LX), fasc. 3b (2010): 77-84.
[10] Căluşaru, I.M., N. Băran, and Al. Pătulea. ”Researches regarding the transfer of oxygen in water.” Paper presented at the 3rd International Conference on Mechanic Automation and Control Engineering (MACE 2012), Baotou, China, July 27 -29, 2012.
[11] Căluşaru-Constantin, M., E.B. Tănase, N. Băran, and R. Mlisan-Cusma. ”Researches Regarding the Modification of Dissolved Oxygen Concentration in Water.” *IJISET - International Journal of Innovative Science, Engineering & Technology* 1, no. 6 (August 2014): 228-231.
[12] Pătulea, Al., N. Băran, and I.M. Căluşaru. ”Measurements of Dissolved Oxygen Concentration in Stationary Water.” *World Environment* 2, no. 5 (2012): 104-109.
[13] Pătulea, Al., I.M. Căluşaru, and N. Băran. ”Reasearches regarding the measurements of the dissolved concentration in water.” *Advanced Materials Research* 550-553 (2012): 3388-3394.

Numerical Simulation of Water Flow through an Ecological River Intake

Lect. **Ștefan-Mugur SIMIONESCU[1,*]**, Assoc. Prof. **Daniela-Elena GOGOAȘE[1]**,
Sci. Res. **Gabriela CÎRCIUMARU[2]**, Sci. Res. **Rareș-Andrei CHIHAIA[2]**

[1] University Politehnica of Bucharest, Faculty of Energy Engineering, Department of Hydraulics, Hydraulic Machines and Environmental Engineering, 060042 Bucharest, Romania

[2] National Institute for R&D in Electrical Engineering ICPE-CA, 030138 Bucharest, Romania

* s.simionescu@upb.ro

Abstract: *The present study uses the CFD numerical approach to analyse the flow of water through the model of an ecological water intake structure located on the bank of a river. It aims to obtain and validate qualitative and quantitative hydrodynamic parameters, by comparing the numerical results with experimental data obtained previously on a small-scale model built in the laboratory. For this purpose, several numerical flow geometries with corresponding discretizations are specially built, under two simplifying assumptions: a 2D model, solved with HEC-RAS software and a 3D model, solved with the ANSYS Fluent code. Following the validation of the numerical results, the numerical model can be extended to a prototype of this ecological intake, which is to be built and located on a river in nature.*

Keywords: *River water intake, CFD simulation, HEC-RAS, ANSYS Fluent*

1. Introduction

Fish population and aquatic fauna decline represent indicators of environment degradation and alarms for human health. A negative impact on fish is related to the operation of river constructions for diversion, bypass, or intake of water. These constructions may be part of different complex facilities, such as: micro-hydropower developments – considered as a green energy source [1], irrigation pumping stations, water supply for household or industrial consumers, navigation, fish or touristic developments etc. If not properly designed, they may have a negative impact on the ecological flow, channel stability and survival of biota.

During operation of water intakes fish may pass through screens, into the feeder pipes or canals towards the turbines or other mechanical devices, or may remain on a river reach with insufficient water flow under improper surviving conditions. Protecting fish habitat around intakes or diversion constructions along the rivers represents a main interest for the engineers and scientific community [2], which have developed various physical or behavioural guiding systems to reduce entrainment of fish, such as: screens, bubble injection systems, noise, light, etc. Flow characteristics, such as temperature, velocity field or direction may attract or reject fish. However, few experimental investigations of the efficiency and impact of such systems exist.

Therefore, the main objective of the current study is to investigate through numerical simulations the flow through a previously designed ecological water intake, in order to obtain qualitative and quantitative information on the variation of characteristic hydrodynamic variables, important for the fish population. The validation of the numerical results is based on the experimental ones obtained on a laboratory model [3]. The results arising from the present numerical modelling can be applied in the case of a prototype of this ecological intake, which is to be built and located on a river in nature.

Numerical models based on Reynolds Averaged Navier-Stokes (RANS) equations compute the flow field by integrating the equations for conservation of mass (continuity) and conservation of momentum, the local equations of conservation of turbulent energy and, in case of two-phase systems, the equation of mass conservation for immiscible fluids [4]. As open channel flows through canals and rivers are turbulent, numerical simulations have been performed for this flow regime. Thus, the Navier-Stokes equation for laminar motion were averaged over time and added a turbulence closure, leading to the Reynolds averaged equations for turbulent motion (Reynolds Averaged Navier-Stokes equations - RANS, [5]).

2. Intake geometry

The ecological water intake model consists of a rectangular canal reach with a 1:1 H:V inclined bank and an another vertical one, with a smaller depth than the river channel, placed onto a river. In this bank are performed multiple orifices to collect the water (without suspended sediments) in a separate lateral chamber from which it is conducted into another canal or into a pipe [2]. Larger bedload sediments may be transported underneath this intake, on the riverbed. A variant of this intake may have a horizontal slit instead of orifices through which water can flow. This variant will be used in the present paper for the numerical simulations.

3. Methodology

The equation of conservation of mass for liquids, in differential form for 2 dimensions, is written:

$$\frac{\partial h}{\partial t} + \nabla \cdot (h\mathbf{v}) = q \tag{1}$$

where t - time, h - local water depth (from the free surface to the bed of the bed, vertical), q - lateral flowrate (may be positive in case of a lateral input/tributary or negative in case of an outlet).

The equation of conservation of momentum (motion) can be written (neglecting the Coriolis force effect) as follows:

$$\frac{\partial \mathbf{v}}{\partial t} + (\mathbf{v} \cdot \nabla)\mathbf{v} = -g\nabla z_s + \frac{1}{h}\nabla \cdot (\boldsymbol{\nu_t}\, h\, \nabla \mathbf{v}) - \frac{\boldsymbol{\tau_b}}{\rho R} + \frac{\boldsymbol{\tau_s}}{\rho h}, \tag{2}$$

where g is the gravitational acceleration, z_s is the free surface level with respect to an arbitrary reference level, $\boldsymbol{\nu_t}$ is the turbulent viscosity tensor with $\nu_{t,xx}$ and $\nu_{t,yy}$ being the coefficients of turbulent viscosity in the horizontal directions x and y, $\boldsymbol{\tau_b}$ is the tangential frictional force vector on the riverbed with its components $\tau_{b,x}$ and $\tau_{b,y}$, $\boldsymbol{\tau_s}$ is the tangential frictional force vector at the free surface due to wind, with its horizontal components $\tau_{s,x}$ and $\tau_{s,y}$ (usually neglected), R is the hydraulic radius. These equations are obtained from Reynolds equations for turbulent motion, which are mediated by depth.

The tangential viscous frictional force depends on the square of the velocity and on the coefficient of friction with the riverbed, C_f, which in turn can be expressed as a function of Manning's roughness coefficient, n, as follows [6-8]:

$$\boldsymbol{\tau_b} = \rho C_f |\mathbf{v}|\mathbf{v} = \rho \frac{n^2 g}{R^{1/3}} |\mathbf{v}|\mathbf{v}. \tag{3}$$

Since the Manning coefficient depends on the size of the bedrock sediment, vegetation, temperature, etc., it is usually initially estimated and then used as a calibration parameter for the numerical model.
The friction force due to the air is calculated with the relation:

$$\boldsymbol{\tau_s} = \rho_a C_D |\mathbf{w_{10}}|\mathbf{w_{10}}\,, \tag{4}$$

where is the density of air at sea level (≈ 1.29 kg/m^3), is the coefficient of friction at the surface of water with air and $\mathbf{w_{10}}$ is the air velocity at 10 m above the water.

The turbulent viscosity is calculated by the relation:

$$\boldsymbol{\nu_t} = \mathbf{D}\, u_*\, h + (C_s\Delta)^2|\overline{S}|, \tag{5}$$

where $\mathbf{D}$ is the diffusion tensor (due to turbulence and dispersion), $u_* = \sqrt{\frac{\tau_b}{\rho}}$ is the rate of friction with the riverbed, C_s is the Smagorinsky coefficient (with values between 0.05 and 0.2), Δ is the size of the calculation mesh and $|\overline{S}|$ is the shear rate.

The system (1) - (5) has more unknowns than equations, so it must be completed with two more equations to quantify the turbulent efforts. As in the case of the RANS equations (from 3D modeling), several "closing" models are available for this, of which the most used are the $k - \varepsilon$ and $k - \omega$ models.
In the context of free surface flow on rivers, where the depth of the current is much smaller than the width of the river or the length of the computation reach, it is possible to simplify the equations of flow in 3 dimensions, by reducing them to two or even one dimension. Thus, the Shallow Waters Equations allow the following simplifying hypotheses [9], [10]:

- the fluid is incompressible (liquid), of uniform density;
- Reynolds equations are time-averaged so that the turbulent flow is approximated by the turbulent viscosity;
- the vertical scale is much smaller than the horizontal one, therefore, the vertical velocity is negligible and the vertical pressure distribution is hydrostatic.

Thus, the velocity vector $\mathbf{v}$ and the stresses in the mass and momentum conservation equations can only be written as a function of 2 components along the directions Ox (along the flow) and Oy (normal to it, in the direction of the banks), neglecting the component along Oz (of depth). The 2 components can be mediated in depth, on each calculation vertical, as follows [11-13]:

$$\begin{aligned} \mathbf{v} &= u \cdot \vec{i} + \mathrm{v} \cdot \vec{j}\,; \\ u &= \frac{1}{h}\int_0^h u_s \, dz\,; \\ \mathrm{v} &= \frac{1}{h}\int_0^h \mathrm{v}_s \, dz\,, \end{aligned} \tag{6}$$

where u_s, v_s and h are the two local horizontal velocity components and depth, respectively.

3.1 Numerical simulation of the river intake model in 2D, with HEC-RAS

The HEC-RAS program solves the 2D equations of shallow water, especially for river flow, through a combination of methods of differences and finite volumes, on a computing unstructured polygonal network based on the finer topo-bathymetric subnetwork of the channel bottom below. Thus, the computational mesh consists in prismatic elements of vertical local depth. Each element volume is given by a relationship between the depth and base area. Since only one depth is calculated in the centre of each cell, it is important that the slope of the free surface and the velocity components do not vary greatly from one cell to another. Therefore, for the stability of the numerical models, computational networks with spatial steps as small as possible must be used. Hence the mesh is finer in the flow areas where there are large variations of the hydraulic parameters.

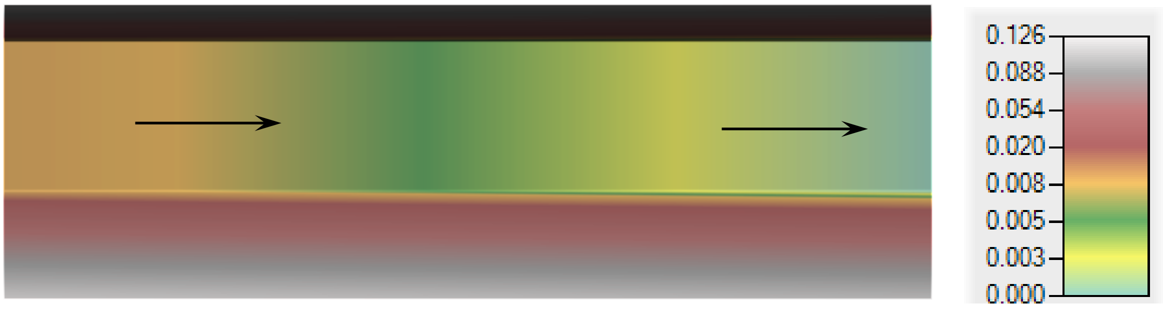

Fig. 1. Plane view of the canal with the elevations of the surface of the invert and the banks. The bank has a 1:1 H:V slope, on which the intake is located, is the lower one

For the 2D numerical study, the geometry characteristics are: main channel length L = 1 m and maximum width B = 0.3 m, was diagrammed in section with the left bank having the slope of H:V = 1:1 - as the experimental model, and the right bank at a slope H:V = 1:3 - unlike the experimental model which has a vertical wall. Then, starting from the cross-sections upstream and downstream, the 3D surface of the main channel was created, with an invert slope of 1%, i.e. 1 cm drop at 1 m length (Fig. 1).

It was not sought to reproduce the geometry of the experimental model identically, as the purpose of the 2D simulations was to obtain stable and fast results, only for preliminary qualitative field investigations.

For the 2D case, two more channel geometries were made (Fig. 2), as follows:

• G_1 - for the simple channel, without intake - for the initial verification of the hydraulic parameters;

• G_2 - for the intake channel, including a side sample with evenly distributed flow. It has been placed in the downstream part of the channel so that there is a sufficient length to stabilize the upstream profile.

a)
b)
c)

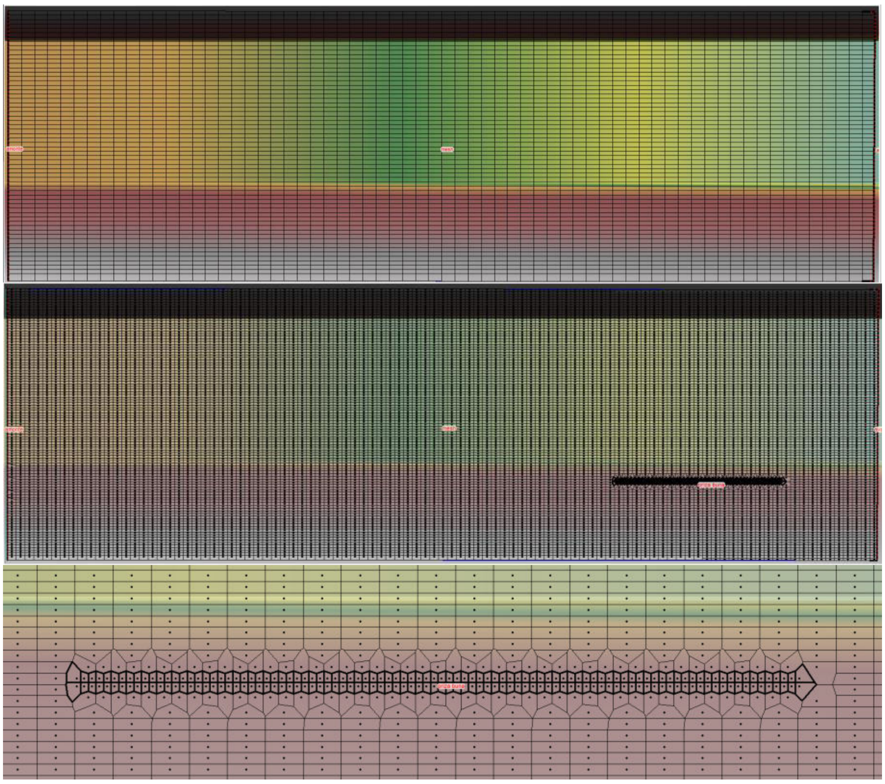

Fig. 2. Examples of 2D computational meshes for: (a) G_1 geometry with 4026 cells, b) G_2 geometry with 10296 cells, and c) detail at the intake of the calculation network for the schematization of the water sampling area at the outlet

For the G_1 geometry, the rectangular computation network (with regular-shaped cells) was created with several dimensions of the rectangular cell in the range 0.002 m - 0.01m, keeping the ratio between length and width the same as that of the channel ($L:B \approx \Delta x/\Delta y \approx 1:3$). This resulted in various discretization networks with a number of elements from 1000 to 15000. In the case of G_2 geometry, an irregular and finer network was created in the area of the intake. For the 2D case, the calculations were performed in an unsteady regime, but at a constant flow, and the imposed boundary conditions were:

- Upstream cross-section: flow rate of 5 l/s, corresponding to the experimentally measured velocity;

- Downstream cross-section: uniform regime condition with a slope equal to the slope of the main anal canal 1%;
- Laterally, at the intake - the flow taken through the intake, of 2 l/s (introduced as a negative input).

The simulations were performed with very small calculation steps, in the range of 0.1 ÷ 0.5 s over a period of 5 seconds, so as to stabilize the flow. Care was taken to comply with the Courant - Friedrich - Levy stability criterion (C <1, where C = v_calculation / v_flow) by either reducing the time step or the spatial step of the network to an acceptable limit.

3.2. Numerical simulation of the 3D Eco-WIBB experimental model with ANSYS Fluent

The numerical modelling of the free surface flow in the water intake was performed using the VOF method. In order to perform the numerical calculation with the help of the ANSYS Fluent code, geometries are constructed that reproduce the real flow domain. These domains are then discretized into finite elements of hexahedral volumes (quadrilateral prisms) and/or tetrahedrals/pentahedrals (triangular/quadrilateral pyramids), through a network of spatial discretization (mesh).

The construction of a geometry and the discretization of the flow field have a great influence on the obtained results. For the present study, the construction of the flow domain and its discretization were performed with the help of the ANSYS Gambit pre-processor. It offers a common set of CAD functions for domain creation, as well as specially implemented functions for creating complex, structured or unstructured discretization networks [15].

The geometry used to model the free surface flow corresponds to the actual geometry of the experimental laboratory installation: the upstream portion of the channel includes a long sector of l = 500 mm in the area where the main channel connection ramp is located. The length of the horizontal main channel is L = 1000 mm, of which l_p = 400 mm is the length of the water intake. The distance from the upstream section of the horizontal channel to the outlet was chosen so that the water speed could be stabilized, l_1 = 260 mm. The maximum height and the maximum width of the main channel were considered equal to those on the model, H_{max} = 117 mm, B = 280 mm, and the height of the lower tank h_{max} = 110 mm.

In order to obtain as clear results as possible on the studied flow, 3 three-dimensional flow geometries were built together with the related discretizations (Fig. 3):

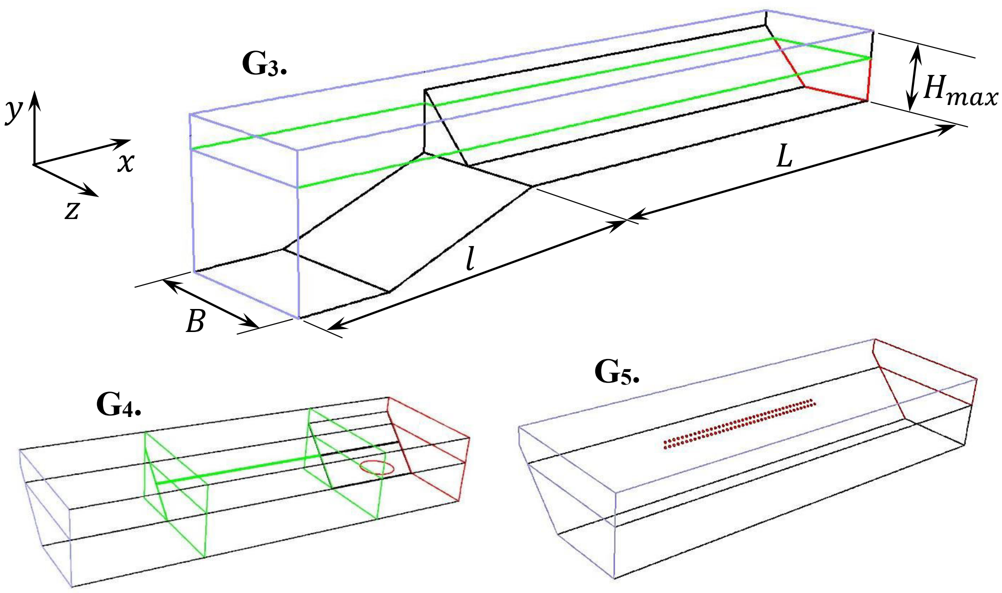

Fig. 3. Flow geometries built for 3D simulations; the definition of the coordinate system

- G_3 - preliminary, without water intake, for testing the flow parameters in the main channel. For this geometry, the upstream portion of the channel (l = 500 mm) was also considered, including the connecting ramp;
- G_4 - with simplified water intake in the form of a longitudinal slot, with an area equal to the area of the holes in the experimental model. To this geometry was added the lower tank for collecting water from the water intake;
- G_5 - complex, water intake with holes, similar to the experimental model.

The mesh dimensions for the geometries G_3, G_4 and G_5 are presented in Table 1.

Table 1: The characteristics of the discretization meshes for the 3 calculation geometries used

Geometry type	Nr. of cells	Nr. of faces	Nr. of nodes	Nr. of viscous layers at the walls	Mesh type	Type of mesh cells
G_3	1927748	5851616	1996632	3	unstructured	hexahedral
G_4	1297004	3715323	1158115	2	unstructured	hexahedral/pentahedral/ tetrahedral
G_5	2539809	5410914	680900	2	unstructured	hexahedral/pentahedral/ tetrahedral

The boundary conditions imposed for the 3D study are (Fig. 4): upstream main channel: water inlet speed (normal at the inlet surface) and constant water level (as the upstream section is far enough from the outlet, the speed distribution was imposed uniform [13]); downstream the main channel – atmospheric pressure; downstream – lateral to the water outlet of the intake chamber (G_4 and G_5) – atmospheric pressure.

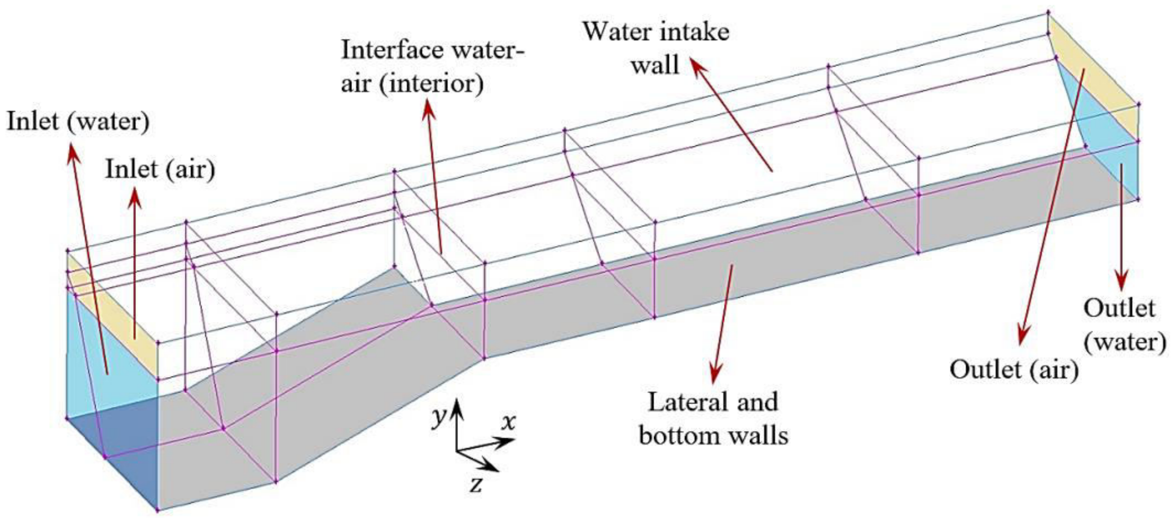

Fig. 4. Numerical calculation domain for G_3 geometry; boundary conditions imposed at the borders

4. Results and discussion

Figures 5 ÷ 8 show some qualitative results of the 2D simulations performed with the HEC-RAS program.

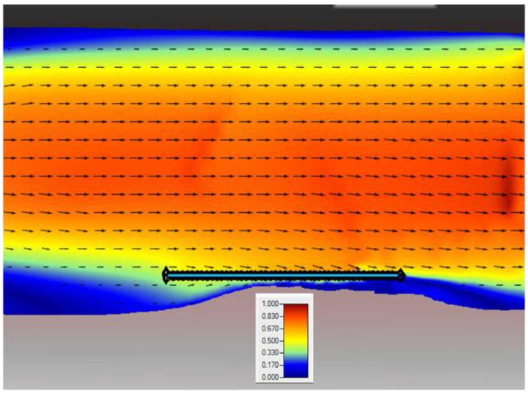

Fig. 5. Direction of velocity vectors for G_2 geometry near the intake

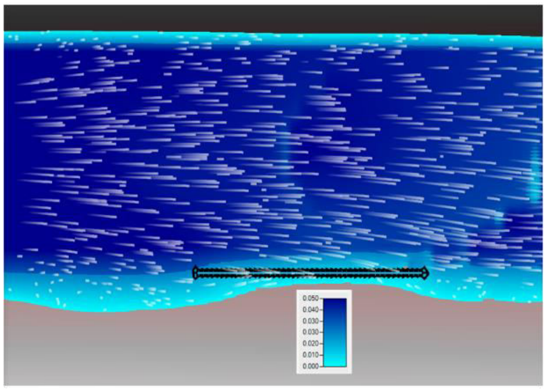

Fig. 6. Direction of streamlines for G_2 geometry in the intake area, superimposed over the water depth

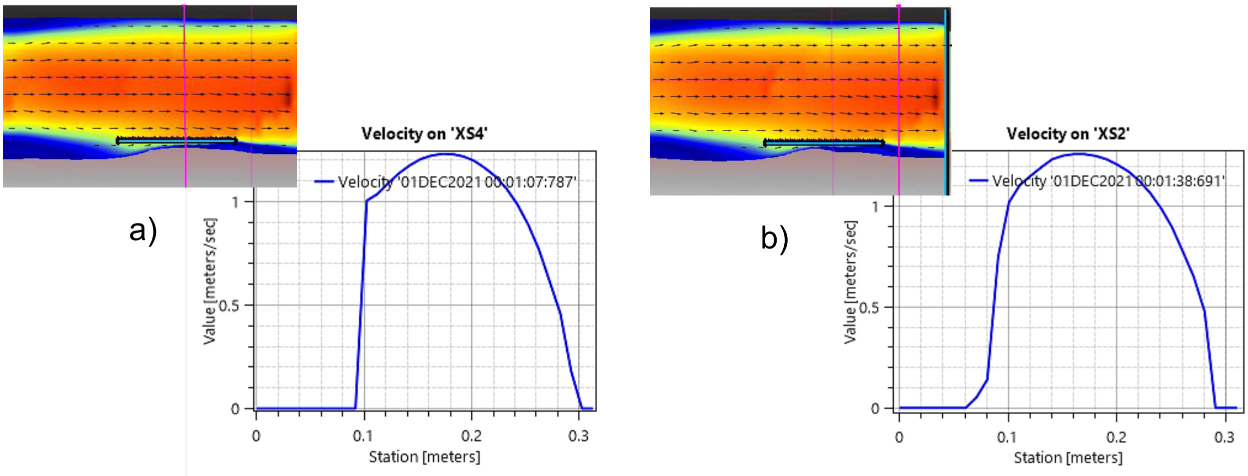

Fig. 7. The change in the shape of the velocity distribution for the G_2 geometry, in a cross section next to the intake (a) and downstream of it (b) (flow from the right)

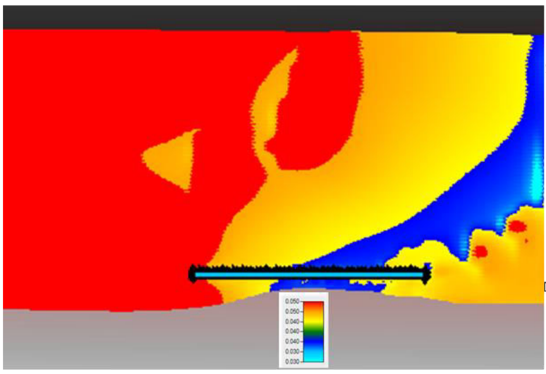

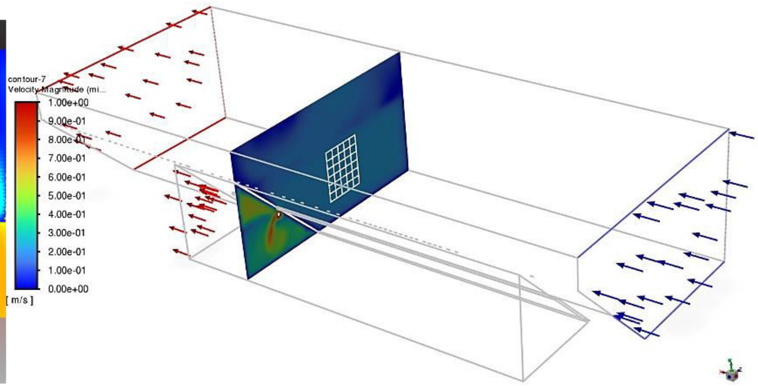

Fig. 8. The change (decrease) in the free surface area of the water near the intake for G_2 geometry

Fig. 9. Velocity distributions in a transversal measurement plane; position of the measurement lines for velocity distributions (G_4 geometry)

The results obtained from the 3D simulations are validated qualitatively and quantitatively based on the experimental results, for the average speeds of 0.22 m/s and 0.33 m/s. In this respect, in the numerical flow domain (geometry G_4) 6 vertical lines and 7 horizontal lines are created (Fig. 9) positioned similarly to the matrix for the experimental measurements with the Pitot-Prandtl tube. Figure 10 a) and b) show comparisons for validation between the numerical and experimental results, for the average velocity v = 0.22 m/s and, respectively, v = 0.33 m/s, on some of the vertical and horizontal lines of the test matrix. A good agreement was identified between the experimental and numerical results, both in terms of the value of the velocity and its trend.

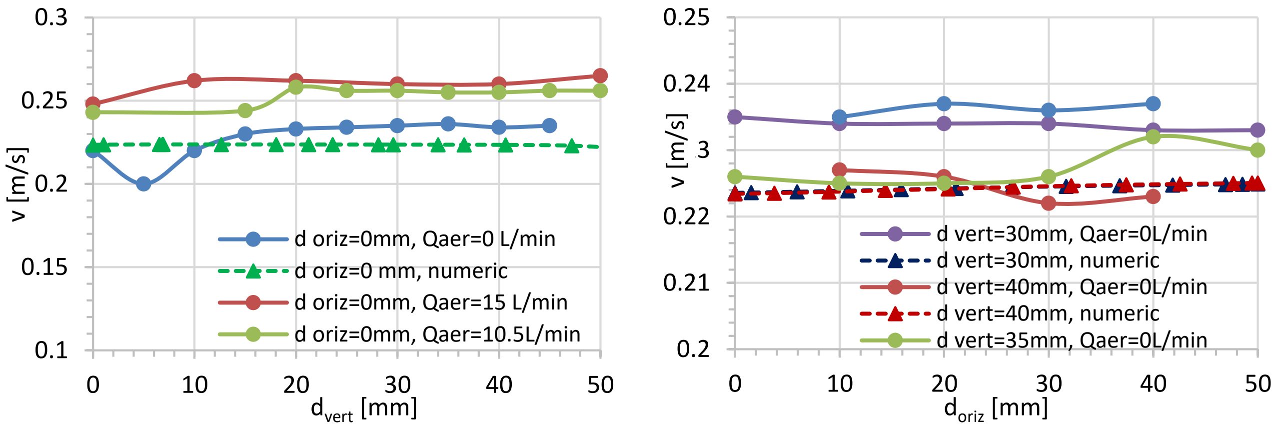

Fig. 10. Comparison of numerical and experimental results, on vertical (a) horizontal (b) lines

Figure 11 shows velocity distributions in cross-section planes, for G_4 geometry. For better visibility of the flow area in the main channel, the velocity value scale has been adjusted so that areas with values between 0 and 1 m/s are visible. Figure 12 presents the velocity vectors in a horizontal plane at the water intake slot. They are dimensioned and coloured according to the value of the velocity and the area of water entry in the slot of the side outlet is observed.

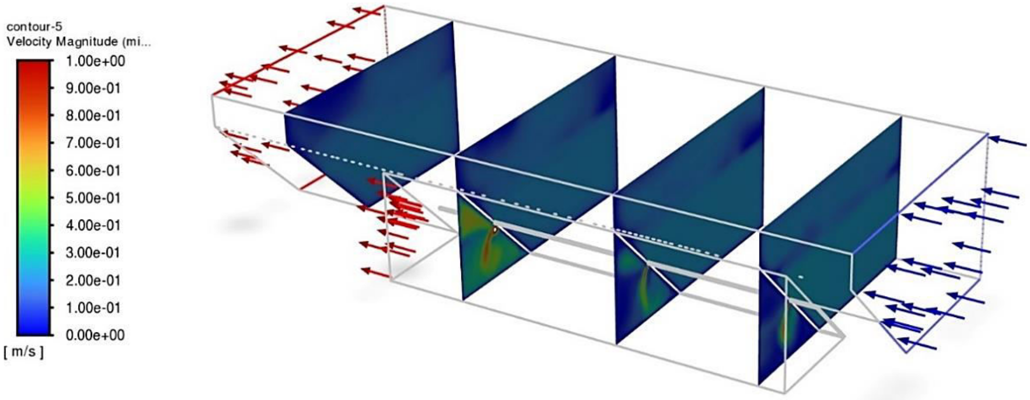

Fig. 11. Transversal velocity distributions for G_4 geometry

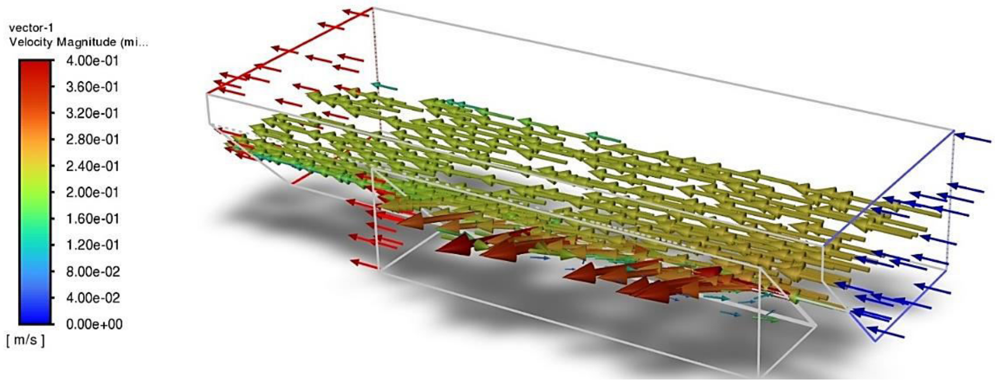

Fig. 12. Velocity vector distributions in a horizontal plane through the slit, colored by velocity, for G_4 geometry

The velocity distribution in a cross-section plane of the channel is shown in Figure 13. For better clarity in the flow area in the main channel, the velocity scale has been adjusted so that areas with values between 0 and 0.5 m/s are visible. At the median level of the water intake, the velocity distribution was extracted from the graph.

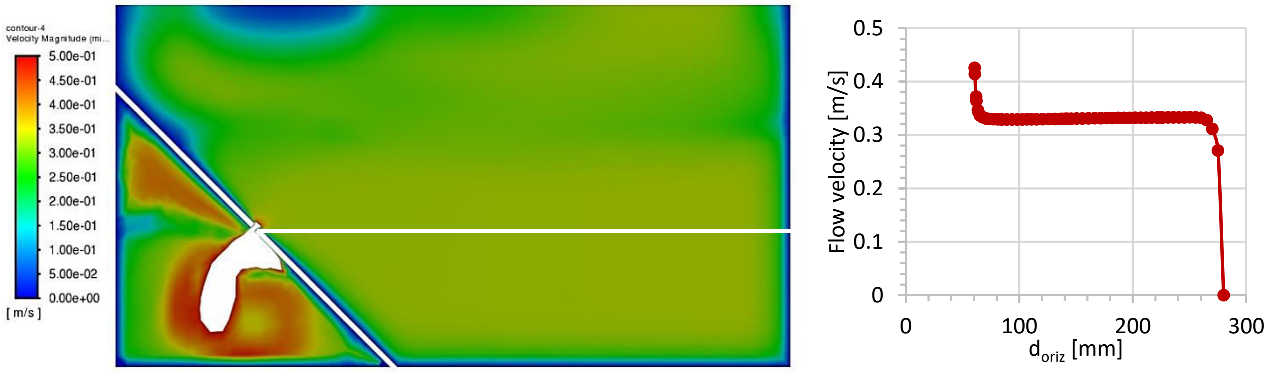

Fig. 13. Cross-section velocity distribution through channel and plot with velocity distribution at the water intake (horizontal line marked in white): horizontal distance is measured from left wall

Another quantitative criterion for comparing the numerical and experimental results is the balance of the inlet/outlet flows from the main channel, respectively from the water intake. The measured and numerically determined values are centralized in Table 2. For the first velocity at which experimental measurements and numerical simulations were made (v = 0.22 m/s), differences of 10.23% were obtained regarding the channel inlet flowrate, 7.61% for the outlet flowrate and 35.64% for the flow discharged through the water intake. For the second velocity at which experimental and numerical results were obtained (v = 0.33 m/s), there were differences of 5.2% in terms of channel input flowrate, 3.23% for channel output flowrate and 21.7% for the outlet discharged through the water intake. The differences in the main channel flowrates are fairly small, the higher relative errors for the water intake may be due to the constructive differences between the water intake holes on the physical model and the slot with equivalent area on the G_4 geometry in the simulations. In this sense, the numerical results on the G_5 geometry, which better reproduces the holes in the water intake, will be able to show an approximation of the experimental results.

Table 2: Balance of inlet / outlet flows in the water channel

Case	Water flowrate at the channel inlet (*l*/s)	Water flowrate at the channel outlet (*l*/s)	Water flowrate at the channel (*l*/s)	Inlet/outlet flowrate balance (*l*/s)
Exp., v = 0.22 m/s	4.23	-3.666	-0.564	–
Num., v = 0.22 m/s, G_4	4.663	-3.945	-0.765	-0.047
Exp., v = 0.33 m/s	6.345	-5.778	-0.567	–
Num., v = 0.33 m/s, G_4	6.676	-5.965	-0.690	0.021
Exp., v = 0.535 m/s	10.287	-9.72	-0.567	–

5. Conclusion

In the numerical simulations from this study, the calculation procedure was used to simulate the flow of water through an open channel with a water intake. Several sets of numerical simulations were performed on 2D and 3D geometries, in conditions similar to those tested experimentally on a laboratory model. The 2D simulations results offered a qualitative set of hydrodynamic variables of the flow field, whereas the 3D simulations were validated quantitatively based on the experimental results in the laboratory. Thus, the 3D simulations, could extend the experimental results to other points in the domain and other discharge value in the same range.

A challenge of the present study was the creation of 3D discretizations, taking into account the large dimensional differences of the working areas - for example, length 1000 mm, circular holes 4 mm. This has been overcome by the proper sizing of discretization meshes and the use of size functions. However, very fine discretizations led to very long computation time (> 24 h).

The velocity distribution resulting from the simulations shows a slight change in the intake area for the case of airless simulations. The longitudinal component of the velocity decreases to the detriment of the transversal one, which ensures the supply of water in the intake. For this reason, the level of the free surface also suffers a slight decrease in this area (a phenomenon qualitatively observed especially from the 2D simulations, performed at a ratio captured flow/transit flow ratio of 2/5, much higher than the one measured experimentally, 0.7/5).

Experimental measurements also showed a slight decrease in velocity towards the free surface near the outlet, but they could not detect the change in the local water depth, as the water flow captured by the intake was reintroduced into the channel, upstream. As the flow rate in the main channel was small, this disturbance has spread upstream, smoothing the level in the channel along its entire length.

In the future, an extension of the simulations on the G5 geometry is desired, as it reproduces best the water intake model tested in the laboratory, and also to perform the simulations in a biphasic system, including an air bubble curtain.

Acknowledgments

This work was funded by a grant of the Romanian National Authority for Scientific Research, CNCS, UEFISCDI, through the project PN-III-P2-2.1-PED-2019-1444, "Eco-hybrid water intake, with behavioural barrier to reduce the impact on fish fauna and river morphology – Eco-WIBB".

References

[1] Cowx, I. G., and M. Portocarrero Aya. "Paradigm shifts in fish conservation: moving to the ecosystem services concept." *Journal of Fish Biology* 79, no. 6 (December 2011): 1663-1680. https://doi.org/10.1111/j.1095-8649.2011.03144.x.

[2] Poletto, J. B., D. E. Cocherell, T. D. Mussen, A. Ercan, H. Bandeh, M. Levent Kavvas, J. J. Cech, and N. A. Fangue. "Fish-protection devices at unscreened water diversions can reduce entrainment: Evidence from behavioural laboratory investigations." *Conservation Physiology* 3, no. 1 (2015): 1–12. https://doi.org/10.1093/conphys/cov040.

[3] Cîrciumaru, G., R.-A. Chihaia, A. Voina, D.-E. Gogoașe Nistoran, Ș.-M. Simionescu, L.-A. El-Leathey, and L. Mândrea. "Experimental analysis of a fish guidance system for a river water intake." *Water* 14, no. 3 (2022): 370. https://doi.org/10.3390/w14030370.

[4] Versteeg, H. K., and W. Malalasekera. *An introduction to computational fluid dynamics. The finite volume method*. 1st edition. London, Longman Scie.&Tech., 1995.

[5] Shen, L., and E. S. Chan. "Numerical simulation of fluid–structure interaction using a combined volume of fluid and immersed boundary method." *Ocean Engineering* 35, no. 8 (June 2008): 939-952.

[6] Bălan, C. *Lectures in fluid mechanics / Lecţii de mecanica fluidelor*. Bucharest, Technical Publishing House, 2003.

[7] Jasak, H. *Turbulence Modelling for CFD*. Report for the NUMAP-FOAM Summer School, Zagreb, September 2-15, 2009.

[8] Pozrikidis, C. *Fluid dynamics: Theory, computation and numerical simulation*. 2nd edition. Springer, 2009.

[9] Moukalled, F., L. Mangani, and M. Darwish. *The Finite volume method in computational fluid dynamics. An Advanced Introduction with OpenFOAM® and Matlab*. Springer, 2016.

[10] Anderson, J.D. Jr., J. Degroote, G. Degrez, E. Dick, R. Grundmann, and J. Vierendeels. John F. Wendt (Ed.) *Computational Fluid Dynamics. An introduction*. 3rd edition. Springer, 2009.

[11] Rodriguez, S. *Applied Computational Fluid Dynamics and Turbulence Modeling. Practical tools, tips and techniques*. Springer, 2019.

[12] Blazek, J. *Computational Fluid Dynamics: Principles and Applications*. 3rd ed. Kidlington; Waltham, Elsevier, 2007.

[13] Bates, P., S. Lane, and R.I. Ferguson. *Computational fluid dynamics. Applications in Environmental Hydraulics*. John Wiley & Sons, 2005.

[14] ***. HEC-RAS 6.0 (2020), US Army Corps of Engineers, Hydraulic Engineering Center, River Analysis System, User's Manual.

[15] ***. Ansys Fluent 12 (2009) Tutorial 18. "Using the VOF Model".

GASDP Hybrid Model to Optimize the Minimum and Maximum Extractions of a Cascade Reservoir System

Dr. **Maritza ARGANIS**[1,2,*], Dr. **Ramón DOMÍNGUEZ**[1], Eng. **Rosa VALENCIA**[1], M.Eng. **Eduardo JUAN**[1], M.Eng. **Javier OSNAYA**[1], M.C. Rosalva **MENDOZA**[1], M.Eng. **Eliseo CARRIZOSA**[1]

[1] Universidad Nacional Autónoma de México. Instituto de Ingeniería

[2] Universidad Nacional Autónoma de México. Facultad de Ingeniería

* Corresponding author's e-mail address: MArganisJ@iingen.unam.mx

Abstract: *The determination of operating policies of a system of cascade dams for the purpose of electricity generation is a widely studied problem; the approach of the minimum and maximum extraction volumes between which the extraction policy must oscillate, taking into account the installed and physical capacity in the reservoirs, are data that are commonly set in the analysis. In the case of a cascading dam system, stochastic dynamic programming (SDP) has turned out to be an optimization algorithm that, with relatively little computational cost, solves the problem of obtaining an extraction policy for the filling state of the reservoir and for each stage of the year in which the problem is divided. The optimization process ends by the number of iterations or by meeting an established tolerance value, requiring approximately two hours to obtain an optimal policy. In this research, it was proposed to jointly use a simple genetic algorithm GA to obtain the values of the minimum (kmin) and maximum (kmax) extractions that can be used by stochastic dynamic programming to obtain an optimal operating policy, with the aim of minimizing the differences between the total benefits obtained between two successive years of application of the SDP. The one obtained with SDP was taken as the comparison policy and five tests were made with the GASDP hybrid algorithm; in four of the cases the algorithm was able to reduce the range of kmin and kmax values to initialize the SDP algorithm; in the fifth case, the kmin values were set and the kmax values were obtained. Despite achieving the objective of reducing the errors between the total accumulated benefits determined by the SPD, the policies found in tests 1 to 4 cause deficits in the system, a situation that does not happen with the policy obtained in test 5 in which there are no more spills or deficits as happens with the SDP policy and the calculation time with it is 59 minutes, the total maximum storage, sum of the two reservoirs, decreases by 0.4% with respect to the PDE policy, the average energy generated fortnightly drops 1.89 GWh. An inconvenience found in the GASPD hybridization was the calculation times, which grow from hours to days as the number of individuals and generations increases.*

Keywords: *Objective function; deficit; hybrid optimization; computational cost; Grijalva river dams; hybrid optimization; computational cost; Grijalva river dams*

1. Introduction

The application of optimization tools to solve resource allocation problems in engineering issues has increased in importance to the extent that computer equipment continues to evolve; specifically, the issue of hydraulic exploitation and the determination of extraction policies in reservoirs and reservoir systems with different uses has been the subject of numerous investigations in recent decades [1,2,3,4,5,6].
The calculation times used by the different optimization algorithms are a criterion that helps to identify its efficiency; but sometimes it is worth the computational effort to obtain results in the simulations of the systems that are reflected in the reconciliation between the expected benefits and the occurrence of undesired events.
Stochastic dynamic programming is an algorithm that is applied with relative simplicity to reservoir operation problems to obtain optimal policies, exponentially decreasing operations as it is a sequential process, although it can be affected by the so-called curse of dimensionality in the case of a growth in the number of states, stages and decision or search variables that the problem has. [7,8,9,10,11].

Recently, research aims to hybridize optimization methods, seeking to highlight the benefits of each method involved [12,13,14].
In this study, it was proposed to combine a simple genetic algorithm (GA) and the stochastic dynamic programming (SDP) algorithm, calling it the SGASDP algorithm, to determine the values of maximum and minimum extractions, and obtain the optimal policies of an equivalent system of two dams. that work in cascade; the methodology was applied in the Grijalva river dam system.
The article is organized in the following parts, the introduction indicated above, the methodology used, the results and discussion, as well as the conclusions derived from the analysis.

2. Methodology

GA

Simple genetic algorithms [15,16], were among the first bioinspired random algorithms, stand out for being robust and having convergence towards global optima. The algorithm begins with the random generation of an initial population of n individuals (chromosomes) containing the search variables, the performance of the best individual is tested through the evaluation of the objective function consisting of the maximization or minimization of a function preset, depending on the problem analysed; relative and population fitness are identified to use a method for selection of the best individuals; later some of said best individuals are selected for the cross with the roulette, universal stochastic or tournament method; the random cross can be at a single point or multipoint; the new individuals generated with the cross can mutate in one or more points; the population resulting from this last operator passes to the next generation and the process is repeated until reaching the number of generations given in the problem. The best individual in the last generation represents the optimal solution sought.

SDP

Dynamic programming [8] solves the problem of obtaining the decision variables and trajectories that manage to optimize a process by considering a finite number of states, stages and sequential decisions that are applied in a large number of iterations or horizon. planning; when the decision variables are random, the transition probabilities of passing from an initial state to a final state intervene; the objective function that is solved with SDP may or may not be linear and considers the expected value of a benefit, in the case of the analysis of a system of hydroelectric dams that work in cascade, in addition to the fact that it is desired to maximize the expected benefit for electricity generation , terms that reduce said benefit can be included in the same objective function by imposing penalties in the event of undesired events of spills in the system or in the event of deficits (that is, the promise is not fulfilled). The SDP algorithm can be divided into two parts to avoid repetitive calculations and reduce process times [17,18]. In the case of a system of two dams that work in cascade, the algorithm can be separated into the following parts:

$$\emptyset_{n,k1,k2}(i_1,i_2) = \sum_{j_1=1}^{NS_1} q_{n,k1}(i_1,j_1) b_{n,k1}(i_1,j_1) + \sum_{j_2=1}^{NS_2} q_{n,k2}(i_2,j_2) b_{n,k1,k2}(i_1,j_{1,}i_2,j_2) \tag{1}$$

$$B_{n,k1,k2}(i_1,i_2) = \emptyset_{n,k1,k2} + \sum_{j_1=1}^{NS_J} \sum_{j_2=1}^{NS_J} q_{n,k1}(i_1,j_1)\, q_{n,k2}(i_2,j_2) B^*_{n+1(j_1,j_2)} \tag{2}$$

Where:
$\emptyset_{n,k1,k2}(i_1,i_2)$ is the expected value of the immediate total benefit in stage n, given the initial conditions i1, i2 and the extractions k_1, k_2, of dams 1 and 2. These values are first calculated for all stages
$q_{n,k1}(i_1,j_1)$ transition probabilities from state i to state j of dam 1, at stage n and given extraction k1 .

$b_{n,k1}(i_1, j_1)$ benefit at stage n, given a draw k of moving from an initial state i to a final state j1 of dam 1.
$q_{n,k2}(i_2, j_2)$ transition probabilities from state i to state j of dam 2, at stage n and given extraction k2 .
$b_{n,k1,k2}(i_1, j_{1,} i_2, j_2)$ benefit in stage n, given extraction k_1 and k_2, to go from initial state i1 to final state j_1 in dam 1 and from state initial i_2 to the final state j_2 of dam 2.

$B_{n,k1,k2}(i_1, i_1)$ total benefit in stage n, given the extraction k_1 and k_2 in dams 1 and 2, in the final state j_1 and j_2 of dams 1 and 2, respectively. These values are calculated in a second part of the algorithm.
$B^*_{n+1(j_1,j_2)}$ optimal benefit at stage n+1, corresponding to the final state j_1 and j_2 of dams 1 and 2, respectively corresponding to the optimal extractions k_1* and k_2* in the dams 1 and 2.
The algorithm delivers in matrix form, for each stage n of the year, an extraction policy consisting of a matrix arrangement in whose rows the states of dam 1 are indicated and in the columns the states of dam 2 and in the intersection are established by unit of volume in the stage the extractions that will be made in the reservoir in the stage, depending on the filling levels of each reservoir at the beginning of the stage, Table 1 illustrates an example of said operating policy matrix.

Table 1: Example of extraction policy table. La Angostura and Malpaso Dams

S T A G E 2: OCT ΔV_{Stage2}=100 hm^3																
MALPASO STATES																
	ID	**1**	**2**	**3**	**4**	**5**	**6**	**7**	**8**	**9**	**10**	**11**	**12**	**13**	**…**	**46**
LA ANGOSTURA STATES	**1**	**304**	**304**	**304**	**304**	**304**	**304**	**304**	**304**	**304**	**304**	**304**	**304**	**304**	**…**	**318**
	2	**304**	**304**	**304**	**304**	**304**	**304**	**304**	**304**	**304**	**304**	**304**	**304**	**304**	**…**	**318**
	3	**304**	**304**	**304**	**304**	**304**	**304**	**304**	**304**	**304**	**304**	**304**	**304**	**304**	**…**	**318**
	4	**304**	**304**	**304**	**304**	**304**	**304**	**304**	**304**	**304**	**304**	**304**	**304**	**304**	**…**	**318**
	5	**304**	**304**	**304**	**304**	**304**	**304**	**304**	**304**	**304**	**304**	**304**	**304**	**304**	**…**	**318**
	6	**304**	**304**	**304**	**304**	**304**	**304**	**304**	**304**	**304**	**304**	**304**	**304**	**304**	**…**	**318**
	7	**304**	**304**	**304**	**304**	**304**	**304**	**304**	**304**	**304**	**304**	**304**	**304**	**304**	**…**	**318**
	8	**304**	**304**	**304**	**304**	**304**	**304**	**304**	**304**	**304**	**304**	**304**	**304**	**304**	**…**	**318**
	9	**304**	**304**	**304**	**304**	**304**	**304**	**304**	**304**	**304**	**304**	**304**	**304**	**304**	**…**	**318**
	10	**304**	**304**	**304**	**304**	**304**	**304**	**304**	**304**	**304**	**304**	**304**	**304**	**304**	**…**	**318**
	-	**-**	**-**	**-**	**-**	**-**	**-**	**-**	**-**	**-**	**-**	**-**	**-**	**-**	**-**	**-**
	-	**-**	**-**	**-**	**-**	**-**	**-**	**-**	**-**	**-**	**-**	**-**	**-**	**-**	**-**	**-**
	-	**-**	**-**	**-**	**-**	**-**	**-**	**-**	**-**	**-**	**-**	**-**	**-**	**-**	**-**	**-**
	22	**304**	**304**	**304**	**304**	**304**	**304**	**304**	**304**	**304**	**304**	**304**	**304**	**304**	**…**	**318**
	23	**304**	**304**	**304**	**304**	**304**	**304**	**304**	**304**	**304**	**304**	**304**	**304**	**304**	**…**	**318**
	24	**304**	**304**	**304**	**304**	**304**	**304**	**304**	**304**	**304**	**304**	**304**	**304**	**304**	**…**	**318**
	25	**304**	**304**	**304**	**304**	**304**	**304**	**304**	**304**	**304**	**304**	**304**	**304**	**304**	**…**	**318**

S T A G E 2: OCT ΔV_{Stage2}=100 hm^3																
MALPASO STATES																
	ID	1	2	3	4	5	6	7	8	9	10	11	12	13	…	46
	26	304	304	304	304	304	304	304	304	304	304	304	304	304	…	318
	27	304	304	304	304	304	304	304	304	304	304	304	304	304	…	318
	28	304	304	304	304	304	304	304	304	304	304	304	304	304	…	318
	29	304	304	304	304	304	304	304	304	304	304	304	304	304	…	318
	30	304	304	304	304	304	304	304	304	304	304	304	304	304	…	318
	31	304	304	304	304	304	304	304	304	304	304	304	304	304	…	318
	32	304	304	304	304	304	304	304	304	304	304	304	304	304	…	318
	.	.	.	.	.	.	.	.	.	.	.	.	.	.	…	.
	.	.	.	.	.	.	.	.	.	.	.	.	.	.	…	.
	.	.	.	.	.	.	.	.	.	.	.	.	.	.	…	.
	65	1204	1204	1204	1205	1206	1207	1208	1209	1210	1213	1213	1213	1213	…	1218

2.1 GASDP algorithm

A hybrid model is proposed that takes advantage of the random nature of the simple genetic algorithm to obtain the maximum and minimum extractions in each stage of analysis using a stochastic dynamic programming algorithm applied in a system of two cascade dams, using minimization as objective function. of the differences of the total accumulated benefits found by the stochastic dynamic programming divided into two parts, the calculation of the immediate benefit in the stage and the calculation of the total benefit; the steps of the SGASDP are expressed below and in the flowchart given in Figure 1.
Start
Give the input data: Number of individuals: minimum and maximum extraction proposals (kmin and kmax).
Give the number of generations.
Randomly generates the initial population from the search intervals (based on SDP test 7).
Start the iterations.
Evaluates the performance of individuals with the objective function.
OF= Minimize the difference of the sum of the total benefits between one year and another obtained with the SDP (executes the Cafitb and opdin optimization programs).
Select the best individuals with the roulette method.
Crossing processes are carried out, mutate individuals.
A new population is generated and passed on to the next generation.
The process is repeated until the number of generations is reached.
It saves the individual with the best performance in the last generation that contains the values of the minimum and maximum extractions of the optimal policy, the optimal policy is saved in files for each time interval that is being worked on (month, fortnight) and the policy in matrix form for each defined stage.
The optimal policy is simulated with the joint vessel operation simulation program.
Ends the process.

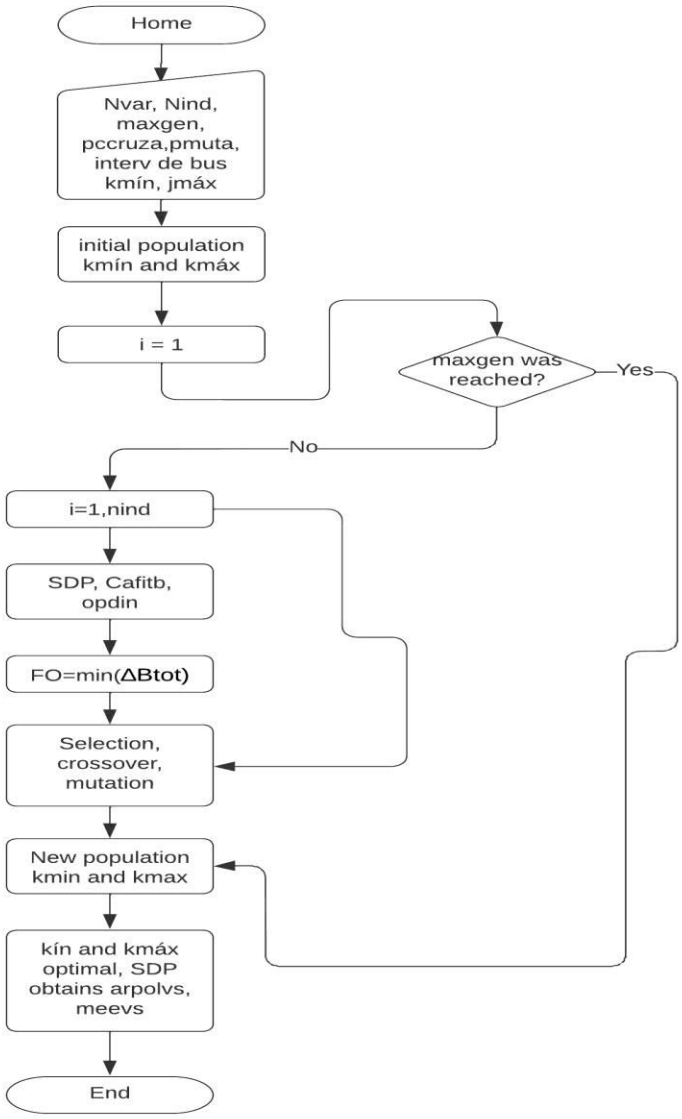

Fig. 1. SGASDP method flowchart

2.1 Study site and data considered

In this investigation, the system of hydroelectric dams of the Grijalva River, Chiapas, was considered, which are arranged in a cascade (Figure 2), from upstream to downstream, said dams are: La Angostura, Chicoasén, Malpaso and Peñitas. Together they generate approximately 40% of hydroelectricity in Mexico, although in 2021 a generation of about 21% of the total annual hydroelectric energy generated was reported [19]. Due to the low regulation capacity of the Chicoasén and Peñitas dams, in order to obtain the optimal extraction policies, the system is analyzed in a simplified way as if there were only two dams: La Angostura and Malpaso, considering the contributions of potential energy that from Chicoasén to La Angostura and Peñitas to Malpaso; The total income from the La Angostura dam to Malpaso is also considered to take Chicoasén into account.

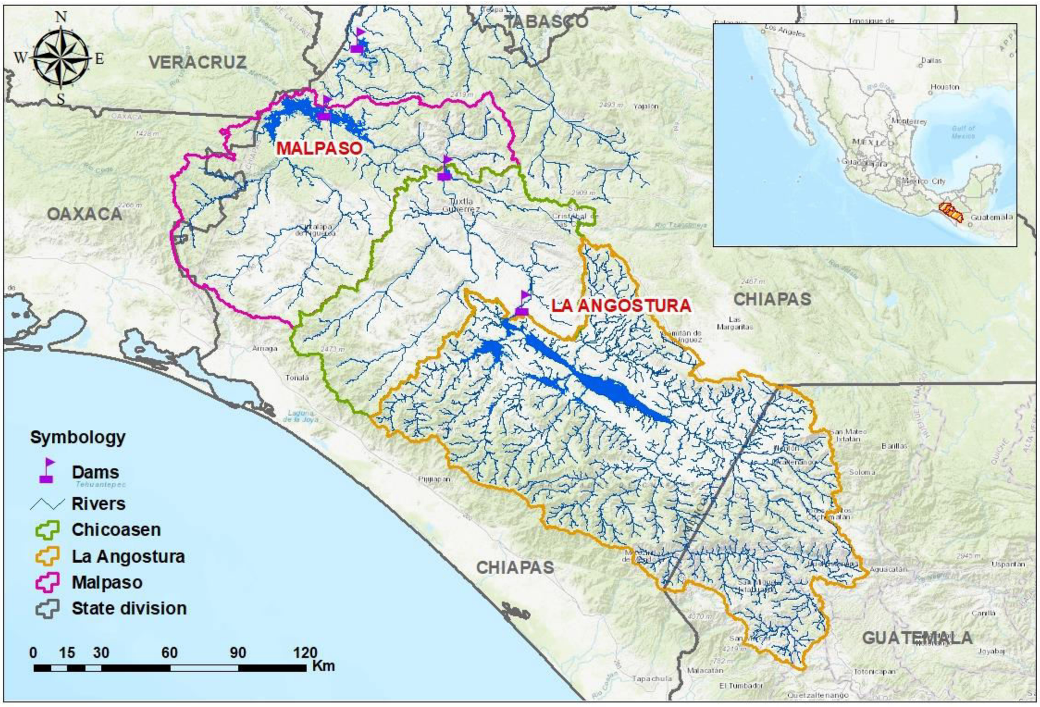

Fig. 2. Grijalva River Dams, Chis., Mexico. Source: Own design

For the purposes of using the SDP for each dam, ∆V units of their useful capacity were considered as states of the problem, divided between the Minimum Water Level (mWL) that corresponds to state 1 and the Maximum Ordinary Water Level (MOWL) that corresponds to state NSi, with i=1, 2 (counter number of dams), ∆V=200 hm^3 was assumed, which resulted in NS1=65 states for La Angostura and NS2=46 states for Malpaso. Groups of fortnights of the year were considered as stages of the problem according to the average values of fortnightly income, with which a total of 7 stages were defined: stage 1: the 2 fortnights of the months of November and December, stages 2, 3, 4 and 5: the 2 fortnights of the months of October, September, August and July, respectively, stage 6: the 2nd fortnight of May and the two fortnights of June, and stage 7: the 2 fortnights of the months of January, February , March and April, and the first half of May. For the use of the GA together with the SDP, the search intervals of the values of the minimum extractions (kmin) and maximum extractions (kmax) were proposed, taking into account the drinking water requirements in the populations downstream of the dam and the capacities installed in them for purposes of maximum available monthly generation. Different proposals for years of analysis of the SDP and also different number of generations used by the GA were defined, the selection method used was the roulette and with crossover probabilities of 0.7 and mutation of 0.7/length of the individual defined by the size of the binary string [20].

3. Results

This section presents the results obtained by applying the GASDP algorithm considering five tests called GA1SDP, GA3SDP, GA4SDP to GA5SDP that consider the conditions for optimization highlighted in columns 4 and 6 of Table 2, in addition to considering the kmin variable. in the GASDP search interval and the GA5SDP test in which kmin is fixed in the GASDP search interval, these policies were simulated, and the results compared against the values of test 7 using only SDP and was taken as a point of comparison because it is a policy that does not report spills or deficits when simulating with the historical record.
Table 2 summarizes the value reported by the objective function (OF) with the different GASDP policies tested, in addition to indicating the sum of differences in total benefits (Difan) and the number of years of iterations carried out by the SDP (Max iter) within the GASDP with said best policy.

Table 2: Comparison of results. Total benefitis differences (Difan), iterations (iter), tolerance (Tol). SDP and GASDP

Operation rule	OF GASDP	Difan	Max iter	Final iter	Tol≤
Test 7 SDP		22.05756	100	100	1.00E-05
GA1SDP	26.0702	26.07019	50	50	1.00E-01
GA3SDP	3.0897	3.089722	50	36	5
GA4SDP	0.0000	0.00E+00	100	82	1.00E-03
GA5SDP	0.0000	0.00E+00	100	100	1.00E-03
GA6SDP	20.6640	20.664	100	100	1.00E-03

From Table 2 it is observed that the GA4SDP and GA5SDP tests achieve values equal to zero in the objective function, and in particular test 4 decreases the number of years simulated with SDP within the GASDP algorithm, the GAS6DP test has a slightly lower value. than the GA1SDP test and with double the number of iterations, but the tolerance used was smaller compared to the GA1SDP and GA3SDP tests.
Table 3 reports the calculation times that were taken in each test with the GASDP, based on the number of individuals proposed and the number of generations with which the GASDP was fed.

Table 3: Calculation times according to number of individuals and generations. GASDP

(h)	Number of individuals	Max number of generations	Calculation time, h, min	Calculation time, h
GA1SDP	4	5	10 hours ,16 min	10.3
GA3SDP	4	5	8 hours ,38 min	8.6
GA4SDP	8	10	40 hours, 31 min	40.5
GA5SDP	10	20	145 hours, 29 min	145.48
GA6SDP	10	20	102 hours, 23 min	102.33

Table 3 shows that doubling the number of individuals and generations almost quadruples the calculation time (GA1SDP test vs. GA4SDP test), and for 2.5 times the number of individuals and 4 times more the number of generations and doubling the maximum number of years in the SDP the calculation time is 14 times higher (GA5SDP vs. GA1SDP test). The foregoing is to be expected since with each pair of kmin and kmax values for each stage in which the analysis is considered, the GASDP performs the dynamic programming process to evaluate the performance of the individuals. When the value of kmin is fixed and with the same number of individuals and generations as the GA5SDP, it is observed that the calculation time grows approximately 10 times.
Table 4 contains a summary of the simulation of the operation of the joint basin of the system of two cascade dams, highlighting the information on the total spills and deficits in the period of simulated years, for La Angostura, Malpaso and the sum of both; The values of the minimum and maximum initial storage of each dam, of the sum of both and the average fortnightly energy obtained in the simulation are also highlighted. In this case, the GA1SDP to GA5SDP tests were simulated both with the fortnightly volume data of the kmin and kmax extractions from base test 7, as well as with the kmin and kmax values obtained by the GASDP, the GA6SDP test was simulated only with the kmin and kmax values of the GASDP.

Table 4: Summary of results of the joint reservoir operation simulation

La Angostura						
Alternative		Spill	Deficit	Initial storage (hm³)		Average energy/fortnight
		hm³		Minimum	Maximum	GWh
SDP	**Test 7**	0	0	1824.27	10308.70	279.97
GASDP	**GA1SDP**	0	10577.9	0	9386.97	279.47
	GA1SDP *	**0**	**47033.21**	**0**	**8270.85**	**277.69**
	GA3SDP	0	123454.75	0	9386.97	275.58
	GA3SDP*	**0**	**185336.90**	**0**	**6766.22**	**275.19**
	GA4SDP	0	39440.46	0	9032.84	276.74
	GA4SDP *	**0**	**91514.92**	**0**	**7796.62**	**275.85**
	GA5SDP	0	59606.80	0	8513.75	276.91
	GA5SDP *	**0**	**113846.86**	**0**	**7204.58**	**276.14**
	AG6SDP*	**0**	**0**	**802.56**	**10067.97**	**279.78**
Malpaso						
Alternative		Spill	Deficit	Initial storage (hm³)		Average energy/fortnight
		hm³		Minimum	Maximum	GWh
SDP	**Test 7**	0	0	1533.58	7824.95	197.59
GASDP	**GA1SDP**	0	1021.51	0	8081.82	194.68
	GA1SDP *	**0**	**9842.21**	**0**	**8203.34**	**194.33**
	GA3SDP	0	2075.82	0	8581.56	196.97
	GA3SDP*	**0**	**4686.19**	**0**	**8494.11**	**197.08**
	GA4SDP	0	8907.42	0	7702	191.94
	GA4SDP *	**0**	**27745.64**	**0**	**7309.89**	**192.09**
	GA5SDP	0	12622.15	0	7587.82	193.52
	GA5SDP *	**0**	**34198.67**	**0.00**	**7564.22**	**192.94**
	GA6SDP*	**0**	**0**	**1422.35**	**7992.24**	**195.89**
Totals						
Alternative		Spill	Deficit	Total initial storage (hm³)		Average total energy/fortnight
		hm³		Minimum	Maximum	GWh
SDP	**Test 7**	0.00	0.00	3357.85	18133.65	477.56
GASDP	**GA1SDP**	0.00	11599.41	0.00	17468.79	474.15
	GA1SDP *	**0.00**	**56875.42**	**0.00**	**16474.19**	**472.02**
	GA3SDP	0.00	125530.57	0.00	17968.53	472.55
	GA3SDP*	**0.00**	**190023.09**	**0.00**	**15260.33**	**472.27**
	GA4SDP	0.00	48347.88	0.00	16734.84	468.68
	GA4SDP *	**0.00**	**119260.56**	**0.00**	**15106.51**	**467.94**
	GA5SDP	0.00	72228.95	0.00	16101.57	470.43
	GA5SDP *	**0.00**	**148045.53**	**0.00**	**14768.80**	**469.08**
	GA6SDP*	**0**	**0**	**2224.91**	**18060.21**	**475.67**
Notes:						
* It was obtained from the maximum of the total initial storage fortnightly sum of both dams						
** The total fortnightly sum of both dams was obtained from the minimum of the initial storage. *** The averages La Angostura + Malpaso were added						

The policies highlighted in Table 4 were obtained using the kmin and kmax passed to volume in the simulation program in each case and those indicated with white used in the simulation the kmin and kmax from the data file of policy 7. That is to say that the highlights are correct, and the whites have that combination of information when simulating

From Table 4 it stands out that the results GA1SDP to GA5SDP are policies that give extremely high spill and deficit conditions, and that condition worsens when the kmin and kmax values optimized with the GASDP are used in the simulation, so these policies are discarded. as an option to operate the analyzed dam system; On the contrary, with the GA6SDP policy, by fixing the kmin values in order to ensure the conditions of test 7 in minimum guaranteed volume, it is possible to obtain an operation policy without spills or deficits in the system's dams, it decreases a little the total minimum initial storage with respect to test 7 (by 33.74%), but also the maximum total initial storage with respect to test 7 (by 0.4%), and the total annual fortnightly energy decreases by about 2 GWh/fortnight. Therefore, the GA6SDP policy can be considered a policy that competes with that of test 7, in addition to the fact that, if the kmin and kmax data given by the GA6SDP policy are used and SDP is used to obtain said policy, the calculation decrease with respect to test 7 in about one hour.

This is that the time taken for hybridizing the optimization using GA and SDP does not seem to give an optimal policy with a slight improvement in the total maximum initial storage issue, but in return with lower minimum storages, less energy generated, but without spills and without deficit using lower maximum extraction values.

Figures 3 and 4 summarize the optimized values of kmin and kmáx, for each stage and each dam, using the GASDP algorithm, contrasting them with test 7. Figures 5 and 6 show the differences between the values of kmin and kmax of each test with respect to test 7, for each reservoir.

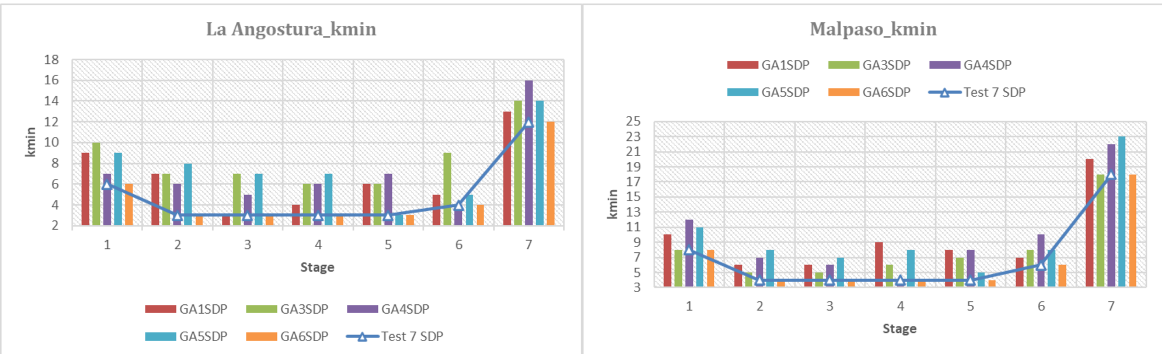

Fig. 3. Comparison of kmin used PDE and GASDP for both dams

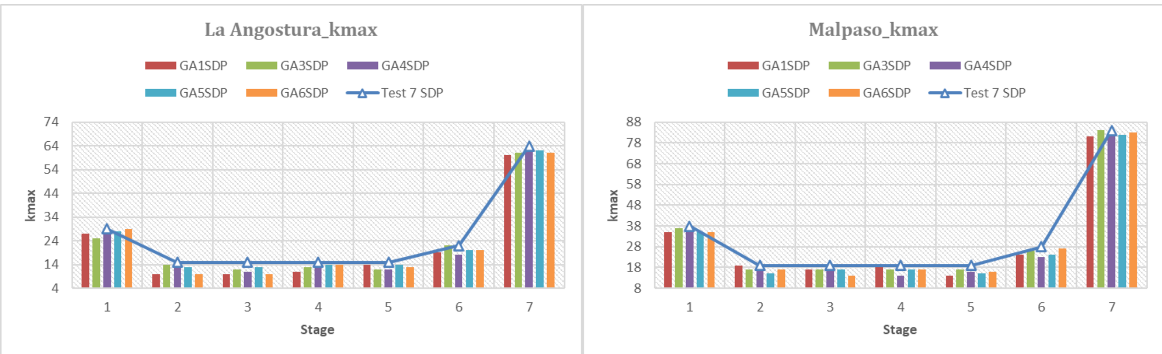

Fig. 4. Comparison of kmáx used with SDP and GASDP for both dams

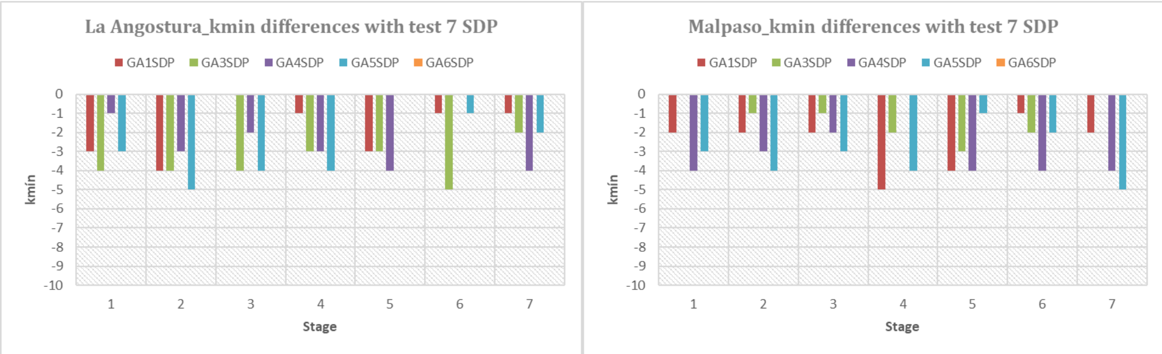

Fig. 5. Differences vs test 7, kmin

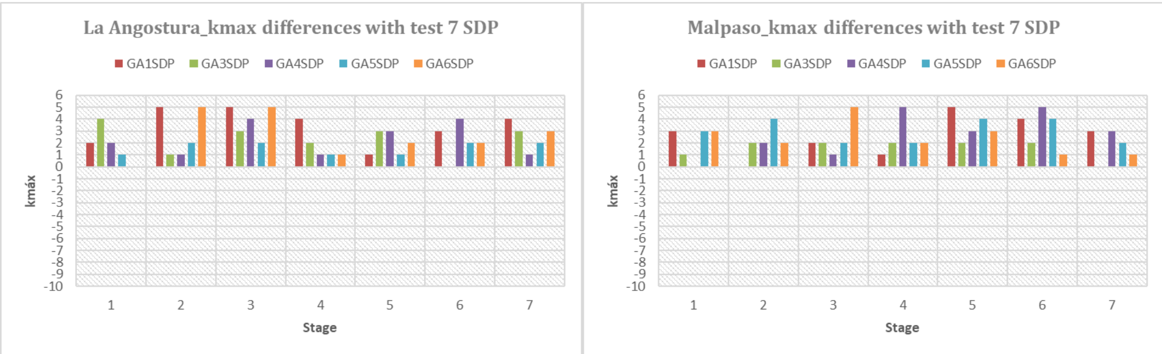

Fig. 6. Differences vs test 7, kmax

4. Conclusions

The GA6SDP policy, calculated with the hybrid algorithm, allowed obtaining optimal operation policies with lower values for maximum extraction, without spills or deficits, although with a reduction in the average total energy generation in the system vs test 7 with SDP, but presented improvements in the value of the maximum storage registered, being lower by 0.4% than that obtained with SDP. Individually, the minimum initial storage in Malpaso decreased with the GA6SDp policy vs test 7 while the maximum increased slightly. In the case of La Angostura, the opposite happened in the maximum initial storage.
When using SDP with the kmin and kmax obtained with GA6 SDP, a reduction of almost one hour was observed in the calculation times with respect to that obtained in test 7, that is, in this sense, the advantage of using GA in hybrid form was observed. with SDP for the selection of the kmax.

Acknowledgments

The authors would like to thank the DGAPA, UNAM for the support given for the publication of this work within the PAPIIT IN100422 project.

References

[1] Hall, W. A., and N. Buras. “The dynamic programming approach to water resources development.” *J. Geophys. Res.* 66 (1961): 517–520.
[2] Nouh, Mamdouh. “Stochastic Approach to Reservoir Design and Management.” *IFAC Proceedings Volumes* 13, no. 11 (1980): 329-332.
[3] Simonović, S. P., and L .M. Miloradov. “Optimization in Water Resources Master Plans.” *IFAC Proceedings Volumes* 18, no. 14 (1985): 221-225.
[4] Chang, F.J., and L. Chen. “Real-Coded Genetic Algorithm for Rule-Based Flood Control Reservoir Management.” *Water Resources Management* 12 (1998): 185–198.
[5] Lin, Nay Myo, and Martine Rutten. “Optimal Operation of a Network of Multi-Purpose Reservoir: A Review.” *12th International Conference on Hydroinformatics (HIC 2016) - Smart Water for the Future. Procedia Engineering* 154 (2016): 1376 – 1384.

[6] Dehghani, M., H. Riahi-Madvar, F. Hooshyaripor, A. Mosavi, S. Shamshirband, E. K. Zavadskas, and K. w. Chau. “Prediction of hydropower generation using Grey wolf optimization adaptive neuro-fuzzy inference system.” *Energies* 12, no. 2 (2019): Article ID 289.
[7] Bellman, Richard Ernest. *Dynamic Programming*. Princeton, New Jersey, Princeton Univ. Press, 1957.
[8] Labadie, John W. “Optimal Operation of Multi-reservoir Systems: State of the Art Review.” *Water Resources Planning and Management* 130, no. 2 (2004): 93-111.
[9] Doraszelski, U., and K. L. Judd. “Avoiding the Curse of Dimensionality in Dynamic Stochastic Games.” *Quantitative Economics* 3, no. 1 (March 2012): 53-93.
[10] Zéphyr, Luckny, Pascal Lang, Bernard F. Lamond, and Pascal Côté. “Approximate Stochastic Dynamic Programming for Hydroelectric Production Planning.” *European Journal of Operational Research* 262, no. 2 (October 2017): 586-601.
[11] Saadat, M., and K. Asghari. “Feasibility Improved Stochastic Dynamic Programming for Optimization of Reservoir Operation.” *Water Resources Management* 33 (2019): 3485–3498.
[12] Chang, Fi-John, Shyh-Chi Hui, and Yen-Chang Chen. “Reservoir operation using grey fuzzy stochastic dynamic programming.” *Hydrological Processes* 16 (March 2002): 2395–2408.
[13] Li, He, Pan Liu, Shenglian Guo, Bo Ming, Lei Cheng, and Yanlai Zhou. “Hybrid Two-Stage Stochastic Methods Using Scenario-Based Forecasts for Reservoir Refill Operations.” *Journal of Water Resources Planning and Management* 144, no. 12 (December 2018): 04018080 1-04018080 11.
[14] Babamiri, Omid, Arash Azari, and Safar Marofi. “An integrated fuzzy optimization and simulation method for optimal quality-quantity operation of a reservoir-river system.” *Water Supply* 22, no. 4 (2022): 4207–4229.
[15] Holland, John H. *Adaptation in Natural and Artificial Systems*. Ann Arbor, MI, The University of Michigan Press, 1975.
[16] Goldberg, David E. *Genetic Algorithms in Search, Optimization and Machine Learning*. Reading, MA, Addison-Wesley Publishing Company, 1989.
[17] Arganis, M. L., and R. Domínguez. “Hydropower System Management Considering the Minimum Outflow.” *American Journal of Environmental Sciences* 4, no. 3 (2008): 178-184.
[18] Mendoza Ramírez, Rosalva, Ramón Dominguez Mora, Maritza Liliana Arganis Juárez, and Eliseo Carrizosa Elizondo. “Quantification of excess and deficit volumes in guide curves to determine operating policies in a hydroelectric system in Mexico / Cuantificación de los volúmenes de exceso y déficit en curvas guía para determinar políticas de operación en un sistema hidroeléctrico en México.” Proceedings of the XXVIII Latin American Congress of Hydraulics, IAHR, UCA, Buenos Aires, Argentina, September 18-21, 2018.
[19] Observatorio de Inteligencia del Sector Energético (OISE). Intelligence, Smartdata. 2022. “Energía Hidroeléctrica.” Accessed May 12, 2022. https://www.oise.mx/hidraulica.
[20] The MathWorks. *MATLAB Reference Guide*. The MathWorks, Inc., 1992.

ISSN 1453 – 7303 **"HIDRAULICA" (No. 2/2022)**
Magazine *of Hydraulics, Pneumatics, Tribology, Ecology, Sensorics, Mechatronics*

Wastewater and Abrasive Sludge Recycling Solutions from Abrasive Water Jet Cutting Machines (AWJCM)

Assoc. Prof. PhD. Eng. **Adriana TOKAR**[1,*], Lect. PhD. Eng. **Luminița FEKETE-NAGY**[1], Assoc. Prof. PhD. Eng. **Cătălin BADEA**[1], Assis. Prof. Eng. **Dănuț TOKAR**[1], Postgrad.Stud.Eng. **Alexandru FEKETE-NAGY**[1]

[1] University Politehnica Timisoara, Romania

* adriana.tokar@upt.ro

Abstract: *Due to the pressure that landfills have on the environment, the article deals with the possibility of recycling waste from abrasive water jet cutting machines (AWJCM) because this waste either takes the path of storage (abrasive sludge) or is discharged into public sewer systems (wastewater). Thus, for the abrasive sludge, two new mortar recipes were proposed, made by replacing fractions of sand with abrasive sludge. The series of cast samples R1 and R2 were subjected to mechanical tests and an increase in bulk density was found with the replacement of parts of the sand component with abrasive sludge, a decrease in mechanical tensile strength in bending and compression, which can be explained by the fact that wet abrasive sludge was used. Another line of research addressed the study of the possibility of reusing discharged wastewater. From this point of view, chemical analyzes were performed for two water samples on the basis of which it could be concluded that the recovered wastewater can be reused in the water supply installation of the abrasive water jet cutting machines. Based on the results obtained, it can be said that the resulting waste can be a raw material for the construction of building materials and can contribute to a considerable reduction in drinking water consumption.*

Keywords: *Waste recycling, abrasive sludge, wastewater, new mortars, AWJCM*

1. Introduction

Compared to conventional cutting processing techniques, abrasive water jet cutting with all the advantages it offers (precision, speed, obtaining complex geometries / shapes, non-modification of the structure of processed materials or diversity of materials) has the disadvantage of large quantities of water and abrasives used, but also the large volume of waste generated in the form of wastewater and sludge (mixture of water, organic/inorganic materials resulting from the discharged materials and abrasive), waste that currently has its way of storage.

In abrasive water jet cutting technology the main parameters are water pressure and its stability, but also the amount of water, the parameters that actually determine the energy of the water jet in the cutting head, energy that is transformed into kinetic energy [1], [2]. The principle of abrasive water jet cutting technology is presented in Fig.1 [1]. As abrasive water jet processing is the result of the interaction between the jet and the material being processed, the speed of the jet and the abrasive material used play an essential role in the quality of the product and the cost-effectiveness of the process. The efficiency of the cutting technology is also ensured by the use of dedicated software used for 2D contour drawing, 3D engraving, multi-axis processing, etc.

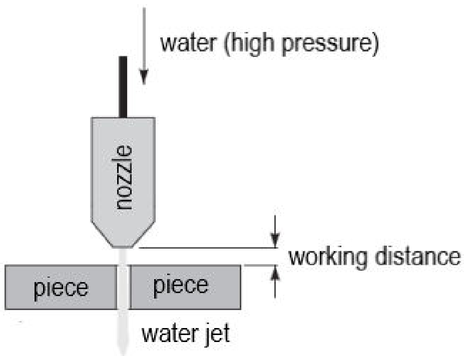

Fig. 1. The principle of abrasive water jet cutting technology [1]

However, with all its advantages, from the point of view of the disadvantage of the large quantities of waste generated, it can be said that the abrasive water cutting industry contributes to the pressure that the industrial sector puts on the environment.
From the analysis of the specialized literature, but also of the previous researches of the authors, it was concluded that, at present, no recycling practices are used, but they are evacuated, collected and temporarily stored in the company in barrels or bags, after which they take the storage final [3], [4], [5], [6]. On the other hand, it has been found that the route of abrasive sludge (disposal-collection-storage) has the greatest negative influence on the environment and for this reason these amounts should be reduced as much as possible.
From the point of view of the recycling of waste generated by abrasive water jet cutting machines / installations, two directions of analysis can be deduced:
- wastewater recycling;
- recycling of abrasive sludge.

With regard to recycling options, the following directions can be addressed:
- on-site recycling:
    - reuse of wastewater after settling and filtration;
    - reuse of the abrasive after drying the sludge and separating the abrasive;
    - reuse of processing waste;
    - the use of dry sludge to stabilize the soil.
- off-site recycling:
    - the use of abrasive sludge in construction materials.

In this context, of the options presented above, it is necessary to consider for the on-site recycling option, whether the abrasive sludge producer has the necessary space for sludge storage and drying and whether the benefit of reducing abrasive costs is substantial, and for off-site recycling, an analysis of the cost of transporting the abrasive sludge to the recycling site is important.
However, we should look at the environmental benefits of recycling and reusing this waste. For this reason, the article addresses on-site recycling options for wastewater and off-site recycling for abrasive sludge. Thus, chemical analyzes were taken and performed for the wastewater samples, and for the integration of the sludge in building materials, recipes were proposed that integrate the sludge in its state of collection, after the separation of the manufacturing waste, for which they were made tests on which mechanical strength tests were performed (tensile strength by bending and compressive strength).
Previous studies by some of the authors of this article have proposed a plant for the separation of the components of the mixture of wastewater, sludge and solid metals [3], so that the resulting waste is a raw material for new or classic building materials and contributes to the considerable reduction of drinking water consumption. Basically, the purpose of this article is to study whether the separate components can be used to make new mortars and whether the recovered wastewater can be reused in the water supply installation of abrasive water jet cutting machines.

2. Methods of analysis for the determination of solutions for the recycling of components of the mixture of wastewater and abrasive sludge

2.1. Analysis methods for wastewater recycling and reuse

The method of analyzing the composition of the wastewater resulting from the abrasive water jet cutting process is atomic absorption spectrophotometry AAS. The AAS atomic absorption spectrophotometry method, compared to classical methods, is much more accurate and uses a smaller amount of reagents, being used to control water quality. The method is part of the optical methods that are based on measuring the radiant power adsorbed by a population of free atoms; practically in absorption the main role is to atomize the sample.
In the first stage, the calibration curves were drawn based on which the concentrations of the metals present in the wastewater were determined. The possible metals present in the wastewater were sought, taking into account the materials that were cut.

For an assessment of the quality of the decanted wastewater and the evaluation of the presence of metals in the wastewater, two samples P1 and P2 were collected, in two different periods, periods in which the quantity and type of material discharged were followed. Samples P1 and P2 were collected in plastic containers which were filled to the brim.
Sample P1 was taken after settling the abrasive sludge resulting from the cutting of 50% stainless steel and 50% carbon steel. The P2 sample was taken after settling the abrasive sludge resulting from the cutting of 65% aluminum, 30% stainless steel and 5% carbon steel.
Thus, for the P1 sample, the concentration of Fe, Ni and Cr was monitored, and for the P2 sample, the concentration of Ca, Mg, Fe, Mn, Cr and Ni was monitored.
Given the possible reuse of the decanted water in the water supply installation of the abrasive water jet cutting machine, for the P1 test the water TDS was performed for the purpose of a general evaluation of the total inorganic salts, but also of the organic matter dissolved in water (Ca, Mg, etc.).
The possible presence of natural dissolved solids that may occur from the dissolution of components resulting from the cutting of materials or from abrasive material used for water jet cutting may cause some problems in cutting water supply installations with increasing TDS. In addition, for these reasons, the pH and conductivity of the water samples P1 and P2 were determined within 4 hours from the time of sampling.
Electrical conductivity is useful as an overall assessment of the quality of wastewater analyzed and has only been determined for the P1 sample because it remains relatively constant. Once established, it can be used as a basis for comparison with common conductivity measurements. Significant changes in conductivity could be an indicator if the range of materials cut is diversified.

2.2. Methods of analysis for recycling and reuse of abrasive sludge

In the literature, regarding the recycling and reuse of abrasive sludge there is an overview of the indicators and methods of analysis used in assessing the sustainability of sludge management in wastewater [7], while indicators that directly address the sustainability of abrasive sludge were less approached. However, four methods are generally used to assess the sustainability of the sludge part of wastewater treatment, namely: Life Cycle Assessment (LCA), Exergy Analysis (ExA), Economic Analysis or Cost-Benefit Analysis (CBA) and Analysis of Wastewater emergency (EmA), and a fifth method was later added, namely Environmental Risk Assessment (ERA), as it was used to assess the wastewater treatment process, including sludge treatment.
Life cycle assessment (LCA) is a common assessment method for wastewater treatment with the main application of assessing different categories of environmental impacts, such as the impact on global warming potential, depletion of resources or the ozone layer, ecotoxicity or degradation of the landscape. The main advantages of LCA are that the assessment process is described and standardized (ISO 14040, 2006 / AMD1,2020), that it can be applied to a wide range of areas, in terms of wastewater use and sewage sludge.
The main advantage but also the limiting factor of the Exergy Analysis (ExA) is that the whole assessment is based on a single quantifiable indicator: exergy but it only measures the efficiency of the processes, without giving an assessment of the various impacts on the environment. Emergency analysis (EMA) has recently become a more popular method of analysis, but its conclusion is that an outside investment is needed to repair the damage and replace the natural and human capital lost due to pollution.
Economic analysis (CBA), in the context of the environment, has only one indicator, all aspects of sustainability being expressed in monetary terms (called internalization in economic evaluation). The main environmental economic tools are cost-benefit analysis, life cycle cost and total cost assessment and the fifth method, Environmental Risk Assessment (ERA) examines the risk that threatens ecosystems and society related to technology, processes, or risk substances qualitatively or quantitatively.
Regarding the field of research done by us on this abrasive waste resulting from the use of abrasive water jet cutting machines and taking into account the resulting abrasive sludge, it is observed that it is composed of abrasive sand type Garnet. For the research presented in this article, the abrasive sludge was collected manually and stored for 7 days for settling (Fig.2).

Fig. 2. Abrasive sludge storage for settling

The decanted abrasive sludge was chemically analyzed to determine the concentration of metal components, and the results are presented in Table 1.

Table 1: Concentration of metals present in the abrasive sludge

Metal components	Zn	Cu	Ni	Fe	Mn	Cr	Ti
Concentration	175±10ppm	84±10ppm	207±15ppm	41.4±1%	0.7±0.02%	0.1±0.01%	1.3±0.04%

The analyzed abrasive sludge test is the result of the technological process of cutting 65% aluminum, 30% stainless steel and 5% carbon steel.
Three new mortar recipes were made, of which this article presents the first two recipes, R1 and R2. The structure of the recipes is a combination between the mortar recipe for determining the cement class (according to SR EN 196-1) and the sludge composition resulting from the chemical analysis (Table 1) correlated with the experience of the research team in the field.
The stages of the mortar tests are:
- establishing the recipes for the R1 and R2 test series (Table 2);

Table 2: Proposed recipes

New mortars Recipes	Cement CEM II A-LL 42.5R [g]	Sand 0.5/1-Sort 3 [g]	Abrasive sludge with a moisture content of 12.7% [g]	Superplasticizer Additive Master Glenium 27 [g]	Mixing water [ml]
R1	450	900	450	4.5	175
R2	450	675	675	4.5	175

- weighing of the materials used (Fig. 3) which was made with the Kern EW electronic balance with the precision of 0.1 g;

a) b) c) d) e)

Fig. 3. Weighing materials used
cement, b) sand, c) abrasive sludge, d) additive, e) water

- mixing the mixture (Fig. 4) which was made with the Auto-Mortar Mixer;

Fig. 4. Mixing materials used

- casting the samples (Fig. 5) in molds previously greased with BASF Master Finish RL 450 stripping agent

Fig. 5. Pour mixture

- compacting of the mixture by mechanical shocks (60 + 60 shocks) (Fig. 6);

Fig. 6. Compaction by mechanical shocks

- the samples were removed at the age of 1 day; it is observed that they do not show edge degradation (Fig. 7);

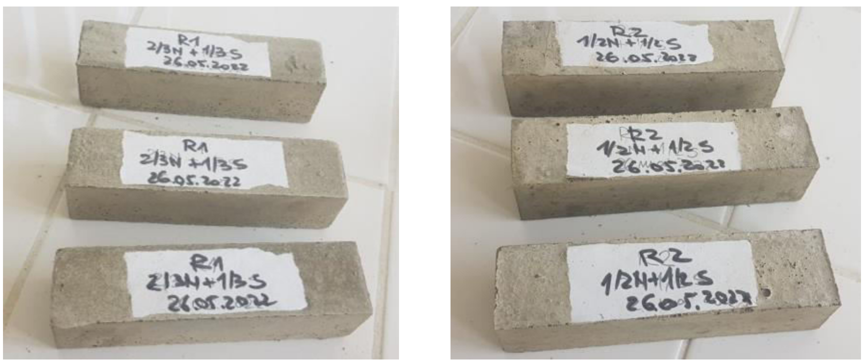

Fig. 7. The appearance of the samples after stripping

- immersing the samples in the pool with drinking water at a temperature of + - 20°C, until the moment of their testing (Fig. 8);

Fig. 8. Immersion of samples

- performing mechanical tests (Fig. 9) with a hydraulic press, using a loading speed of (50 + -10) N/sec for the bending test and (2400 + -200) N/sec for the compression test. The results obtained represent the arithmetic mean of the individual results in N/mm^2. The humidity of the abrasive sludge used for the samples is 12.7%.

a) b) c)

Fig. 9. Mechanical tests
a) bending tensile test, b) compression test, c) hydraulic press

3. Results and discussions

3.1. Results and the establishment of solutions for recycling and reuse of wastewater

The concentrations of metals present in the wastewater resulting from the cutting process, corresponding to the two samples taken are presented in Table 3 and Table 4, respectively.

Table 3: Concentration of metals present in decanted water - Sample P1

Sample	Content of Sample P1 [mg/l]			TDS (totally dissolved solids) [mg/l]
	Fe	Ni	Cr	
OLC wash water	0.045	sld(*)	sld(*)	333
	Detection limit [mg/l]			
	0.001	0.001	0.001	

sld$^{(*)}$ = below the detection limit

Table 4: Concentration of metals present in the decanted water - Sample P2

Sample	Content of Sample P2 [mg/l]					
	Ca	Mg	Fe	Mn	Cr	Ni
OLC wash water	14.8	3.9	sld(*)	sld(*)	sld(*)	0.01
	Detection limit [mg/l]					
	0.003	-	0.001	0.001	0.001	0.001

sld$^{(*)}$ = below the detection limit

The detection limits specified in Table 3 and Table 4 are below the maximum allowable concentrations for the detected metals. The concentrations below the detection limit, indicated in the two tables can be considered zero.

The pH and conductivity of the two wastewater samples, P1 and P2, were performed in order to compare the values obtained for the wastewater that is proposed to be reused with their values required for abrasive water jet cutting machines.
As indicators of general appreciation and not of water potability, pH and conductivity were determined only for sample P1, determined at 23 °C. For pH, a value of 8.5 was determined, which indicates a moderate alkaline character, and the determined value of electrical conductivity is 6 μS/cm. The Romanian drinking water law [8] specifies for water quality values lower than 2500 μS/cm, which means that the TDS is approximately 1250 mg/l, and the EPA (United States Environmental Protection Agency) [9] recommends performing laboratory tests for TDS greater than 500 mg/l or a conductivity greater than 1000 μS/cm.
As mentioned above in Chapter 2.1, the value of 333 mg/l determined for the P1 water sample, being below the limits established by both the Romanian drinking water law and the EPA, which means that in a general assessment, wastewater decanted meets drinking conditions.
From the point of view of the presence of metals (Fe, Ni, Cr) and the main ions (Ca, Mg), in the two water samples, it is observed in Table 5 that the allowed values for industrial waters [10] from technological processes of mechanical processing, but not the permissible ones for surface waters [11].

Table 5: Comparison of values for metals detected in wastewater

Contaminate	**U.M.**	**Measured values**		**Permissible limit values**	
		P1	**P2**	**Surface water**	**Industrial water from mechanical processing**
Metals					
Fe	**[mg/l]**	0.045	sld(*)	0.1	5
Ni	**[mg/l]**	sld(*)	0.01	0.01	0.5
Cr	**[mg/l]**	sld(*)	sld(*)	0.005	1
Main ions for the sample P2					
Ca	**[mg/l]**	14.8		180	300
Mg	**[mg/l]**	3.9		40	100
Mn	**[mg/l]**	sld(*)		-	1

The comparative analysis between the permissible limits for industrial and surface water was carried out in view of the direction of sludge recycling on the one hand to stabilize the land and on the other hand to analyze its reuse for feeding the abrasive water jet cutting machine in safety conditions.
Following the results obtained on the basis of chemical analyzes, it can be seen that the waste water resulting from the technological process of cutting with abrasive water jet can be reused to supply the cutting machine or for other technological processes. These measures will contribute to a considerable reduction in the consumption of drinking water and thus of the energy consumed for its production.

3.2. Results and the establishment of solutions for recycling and use of abrasive sludge

The attempt to recycle and use abrasive sludge on new construction materials materialized in these researches by making three series of new mortar recipes, three samples each, of which in this article are presented the series of samples R1 and R2. The structure of their recipes is a combination between the mortar recipe for determining the cement class (according to SR EN 196-1) and the composition of the abrasive sludge resulting from the chemical analysis, correlated with the experience of the research team in the field. Thus, in the sample series R1 (2/3N + 1/3S) 1/3 of the total amount of sand (N) with abrasive sludge (S) was replaced and in the sample series R2 (1/2N+1/2S) 1/2 of the total amount sand (N) was replaced with abrasive sludge(S).
The average values by series of the physical-mechanical characteristics of the samples were determined at the age of 7 days (Table 6).

Table 6: Physical-mechanical characteristics at 7 days on the R1 and R2 mortar sample series

Sample series	Apparent density ρ_a [Kg/m^3]	$\Delta\rho_a$ [%]	Bending tensile strength f_{ti} [N/mm^2]	Δf_{ti} [%]	Compression strength f_c [N/mm^2]	Δf_c [%]
R1	2331.25	4.13	4.48	-19.19	32.88	-31.99
R2	2427.73		3.62		22.36	

From the comparative analysis of the values of the physical-mechanical characteristics determined at the age of 7 days (Table 6), respectively of the apparent density, of the tensile strengths in the bending and of the compressive strengths, for the series of new mortar samples made R1 and R2 can be seen that by switching from the R1 mortar recipe to the R2 mortar recipe, with the increase in the amount of abrasive sludge in the recipe and the decrease in the amount of sand at the same time, the apparent density increased by 4.13% while the tensile strength from bending decreased by 19.19% and compressive strength by 31.99%.

It is observed that the apparent density of the samples from the two studied series exceeds 2000 kg/m^3 and the compressive strengths exceed the value of 20 N/mm^2, as such the abrasive sludge resulting from the technological process of cutting with abrasive water jet can be reused to make new materials such as new mortars that could be included in the field of construction repair mortars.

The physical-mechanical characteristics are to be determined at the age of 28 days and the experimental program that is in progress will continue with other new mortar recipes.

4. Conclusions

Currently, the wastewater and abrasive sludge, analyzed in this paper is a problem, but the results obtained and presented above show that they are a resource in terms of both wastewater and abrasive sludge.

Unfortunately, in Romania there are no major concerns regarding the prevention, reduction and recycling of industrial waste. Redesigning the entire chain of current production systems could lead to the concept: waste from one process can be a raw material for another or even for itself. In this regard, the results presented above show that wastewater resulting from the process of cutting abrasive water jet can be a resource for the cutting machine or other technological processes dependent on drinking water, after a simple decantation.

From the point of view of the current abrasive sludge route, it can be said that its integration into the construction materials proposed in the article could significantly contribute to reducing the amount of landfilled waste, which puts pressure on the environment.

Therefore, the waste that is the subject of this article may be a shortcoming or a resource only depending on how we manage it.

As future research directions, the authors aim to create new recipes for obtaining construction materials that use this waste and the results to form a basis for other researchers and research in the field.

References

[1] Frățilă, Domnița. *Manufacturing technologies / Tehnologii de fabricație*. Cluj-Napoca, U.T. Press Publishing House, 2019.

[2] Xu, Jiazhong, Bo You, and Xiangbing Kong. "Design and Experiment Research on Abrasive Water-jet Cutting Machine Based on Phased Intensifier". Paper presented at the 17th World Congress The International Federation of Automatic Control, Seoul, Korea, July 6-11, 2008.

[3] Tokar, Adriana, Mirela Toropoc, Daniel Muntean, Danut Tokar, and Simona Popa-Albu. "Proposals for the Separation of Inorganic Components from Technological Wastewater in order to Reduce Landfills." Paper presented at the 7th World Multidisciplinary Civil Engineering-Architecture-Urban Planning Symposium, Prague, Czech Republic, September 5-9, 2022.

[4] Osazee, Iyenoma ThankGod. ”Landfill in a Sustainable Waste Disposal.” *European Journal of Environment and Earth Sciences* 2, no. 4 (2021): pp. 67-74.
[5] The European Commission. *Evaluating the implementation of environmental policies* / *Evaluarea punerii în aplicare a politicilor de mediu*. Country Report Romania. Bruxelles, 4.4.2019 SWD 130 final, pp. 8-12, 2019.
[6] The Government of Romania. ”HG 856/2002 on waste management records and for approval of the list of wastes, including hazardous waste” / ”HG 856/2002 privind evidența gestiunii deșeurilor și pentru aprobarea listei cuprinzând deșeurile, inclusiv deșeurile periculoase”, 2002.
[7] Grönlund, Sven Erik. “Indicators and methods to assess sustainability of wastewater sludge management in the perspective of two systems ecology models.” *Ecological Indicators* 100 (May 2019): 45-54.
[8] The Parliament of Romania. ”Law no. 458/2002 updated in 2011 on drinking water quality” / ”Legea nr. 458/2002 actualizată 2011 privind calitatea apei potabile.” *The Official Gazette* / *Monitorul Oficial*, Part I, no. 875, on December 12, 2011.
[9] United States Environmental Protection Agency. ”National Aquatic Resource Surveys”. Accessed June 11, 2022. https://www.epa.gov/national-aquatic-resource-surveys/.
[10] ***. The norm regarding the establishment of the loading limits with pollutants of the industrial and urban wastewater at the discharge in the natural receptors NTPA-001/2002, on 28.02.2002 - part of HG 188/2002 / Normativul privind stabilirea limitelor de încărcare cu poluanţi a apelor uzate industriale şi orăşeneşti la evacuarea în receptorii naturali NTPA-001/2002, din 28.02.2002 - parte din HG 188/2002. *The Official Gazette* / *Monitorul Oficial*, Part I, no. 187, on March 20, 2002.
[11] Serviciul Hidrometeorologic de Stat din Republica Moldova. “Maximum permissible concentrations of surface water pollutants monitored in the DMCM and their influence on the environment and human health.” / “Concentraţiile maxim admisibile ale poluanţilor apei de suprafaţă, monitorizaţi în cadrul DMCM şi influenţa lor asupra mediului şi sănătăţii omului.” Accessed June 11, 2022. www.meteo.md/images/uploads/pages_downloads/Normele_pentru_apa.pdf.

Measuring Robot Development

Attila LAKATOS[1]

[1] Ányos Jedlik Mechanical and Information Technology and Technical College, Győr, Hungary, lakatosattila2004@gmail.com

Motto:

"Imagination is more important than knowledge. Knowledge is limited. Imagination encircles the world."
Albert Einstein

Abstract: *Last year, my self-developed energy robot, HEAT SPOTTER, won high commendation at the 30th INTERNATIONAL SCIENTIFIC AND INNOVATION COMPETITION. The robot is patent pending, as recommended by the jury.*
In the meantime, I have improved the robot in many ways. The main aspects of this process have been to improve technical sophistication and usability.
In this article, I present the results of this process.

Keywords: *Energetics, robot, remote control, thermal camera*

1. Introduction

Energy plays a prominent role in the world. Energy losses are a sign of inefficiency, a disruption of operations. In certain cases, we can identify these processes and diagnose the points of failure by means of heat loss.
A good tool for this can be a thermal imaging camera. In many cases, however, it can be useful to use a mobile, remote-controlled robot to introduce the analysis tool into hard-to-reach places. It can also be important to store the results for several analysis points and evaluate them later.
Remote control can also mean not having a direct view of the instrument. This problem also needs to be technically addressed.
HEAT SPOTTER, as the first development version, solved the above-mentioned tasks with simplified technical solutions.
Its main advantages are that it:

- is labour-saving,
- is simple and efficient to use, not only by energy and air chemistry specialists,
- It provides objective and documentable measurement results.

In this article, I describe the subject, the tools, and the results of the nearly one-year development process that has taken place since then.

2. Improving the basic and energy operation of HEAT SPOTTER

I have also upgraded the basic and energy operation in the following areas:

- improved image transmission technology,
- enhanced thermal imaging camera with higher resolution,
- improved on-board electronics (design of printed circuit boards instead of the previous prototype electronics)
- reducing the robot's risk of collision with front and rear ultrasonic distance sensors,
- making the mechanical structure suitable for the new functions (design and construction of new supports and structural elements),
- LIDAR-based environmental detection (in this case, the first phase of development is currently under way).

The above listed objectives were achieved by carrying out the following professional tasks.

- Mechanical design (Autodesk Inventor) and construction, 3D printing (Anycubic Chiron 3D printer),
- Programming (image transfer, teleoperation, LIDAR, data acquisition, processing),
- Electronic design (new camera and thermal camera, improved image transmission and teleoperation, LIDAR-based environmental assessment, ultrasonic range finders).

3. How it is implemented

3.1. The initial design (HEAT SPOTTER 1.0)

Main features of version 1.0:

- The structure of the robot is easy and cheap to manufacture, but at the same time robust and aesthetically pleasing anodised aluminium sheet to withstand the stresses of use.
- The equipment is remote-controlled, six-wheeled, differential-driven. This type of drive facilitates manoeuvrability in tight spaces.
- Basic IT architecture:
    - An embedded computer (Raspberry Pi 4) is located inside the device and is responsible for on-board image processing.
    - Teleoperation is separated from image transmission:
        - The speed and direction are determined by a 2.4 GHz radio signal.
        - The thermal camera and the camera image are displayed on a display tablet (Archos Oxygen 70).

Fig. 1. HEAT SPOTTER 2.0 (Source: Own development and own photo)

3.2 Mechanical design and implementation

3.2.1 Additions to the robot body to support new functions

The housing (body) of the robot platform I designed was already made from aluminium sheet for the previous competition, using CNC laser cutting. I used Autodesk Inventor to design the mounting and support elements (PLA filament) and the bumper (PETG filament) of each element in the body (fig. 2), and then fabricated them on my 3D printer (Anycubic Chiron 3D). In this respect, version 2.0 (fig. 1) includes a number of newly designed and manufactured elements that improve quality.

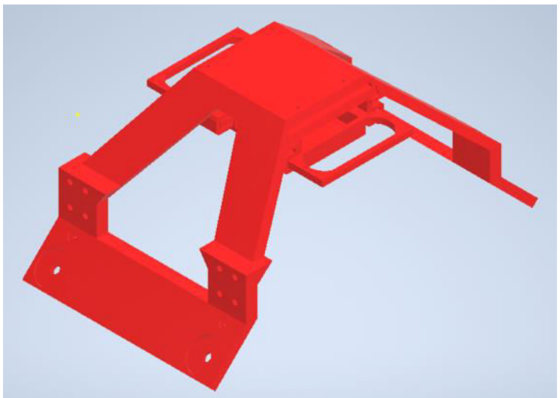

LIDAR and air quality sensor holder (PLA)

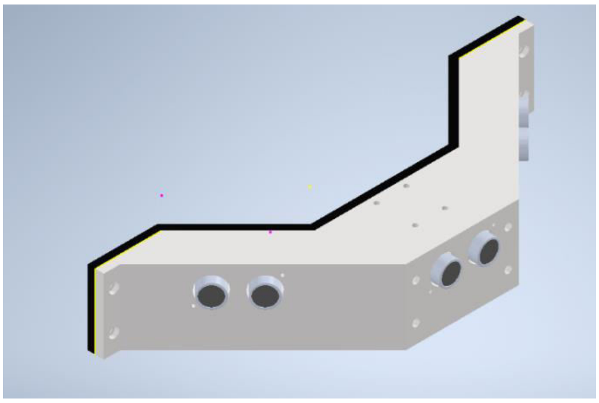

Bumper (PETG)

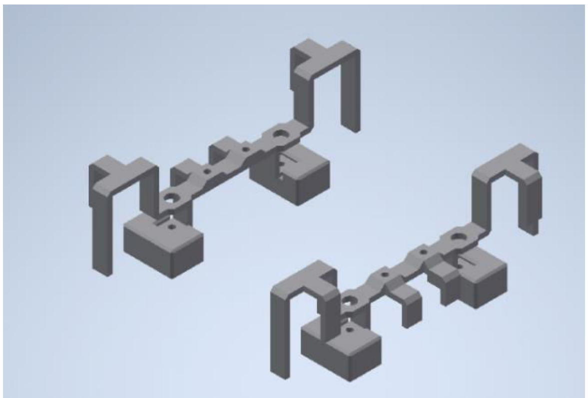

Battery holder (PLA)

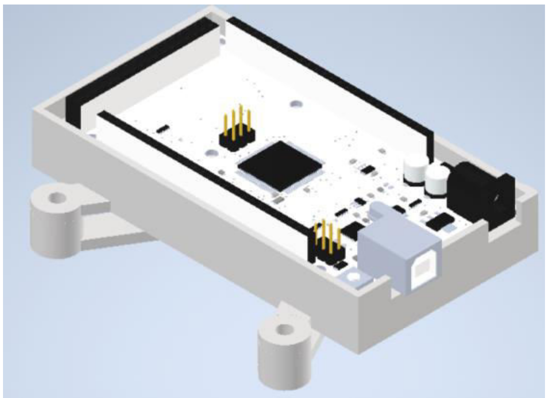

Raspberry holder (PLA)

Fig. 2. Mechanical design and construction

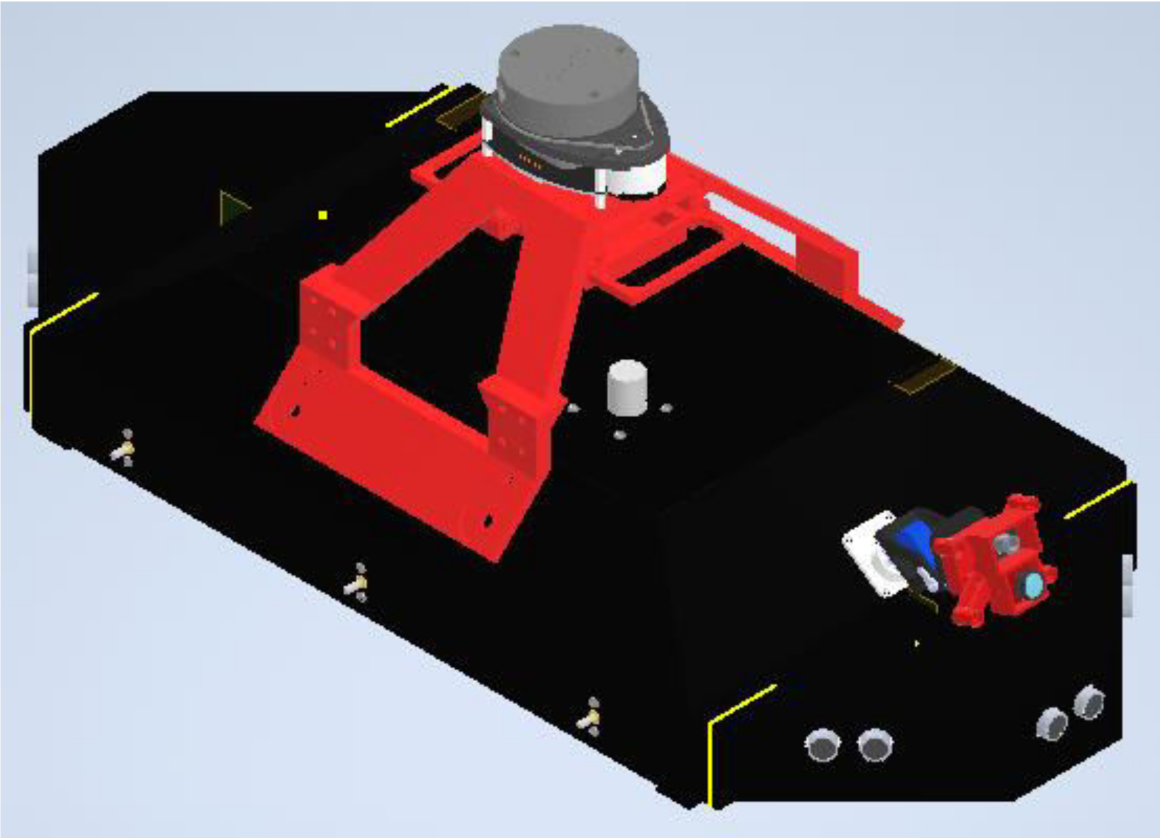

Fig. 3. The robot body with the new LIDAR and camera mounts designed from scratch, the air quality sensor drawer and the bumpers (3D design and printing, PLA material)

3.2.2. Drive

Differentially driven robots are capable of a high degree of mobility with mechanical simplicity. The drive mode makes the robot very manoeuvrable, even when turning in one position, and therefore easy to manoeuvre in confined spaces.

Speed control is achieved by pulse width modulation (PWM) in proportion to the stick positions set by the teleoperator.

As my future plans include the ability to enable the robot to autonomously navigate in the field, which may require odometry, I have equipped the motors with Hall-effect quadratic rotary encoders

3.3 Electronic design and implementation (fig. 4)

The on-board electronics were developed using printed circuit boards of my own design. The printed circuit boards were created using Autodesk Eagle software.

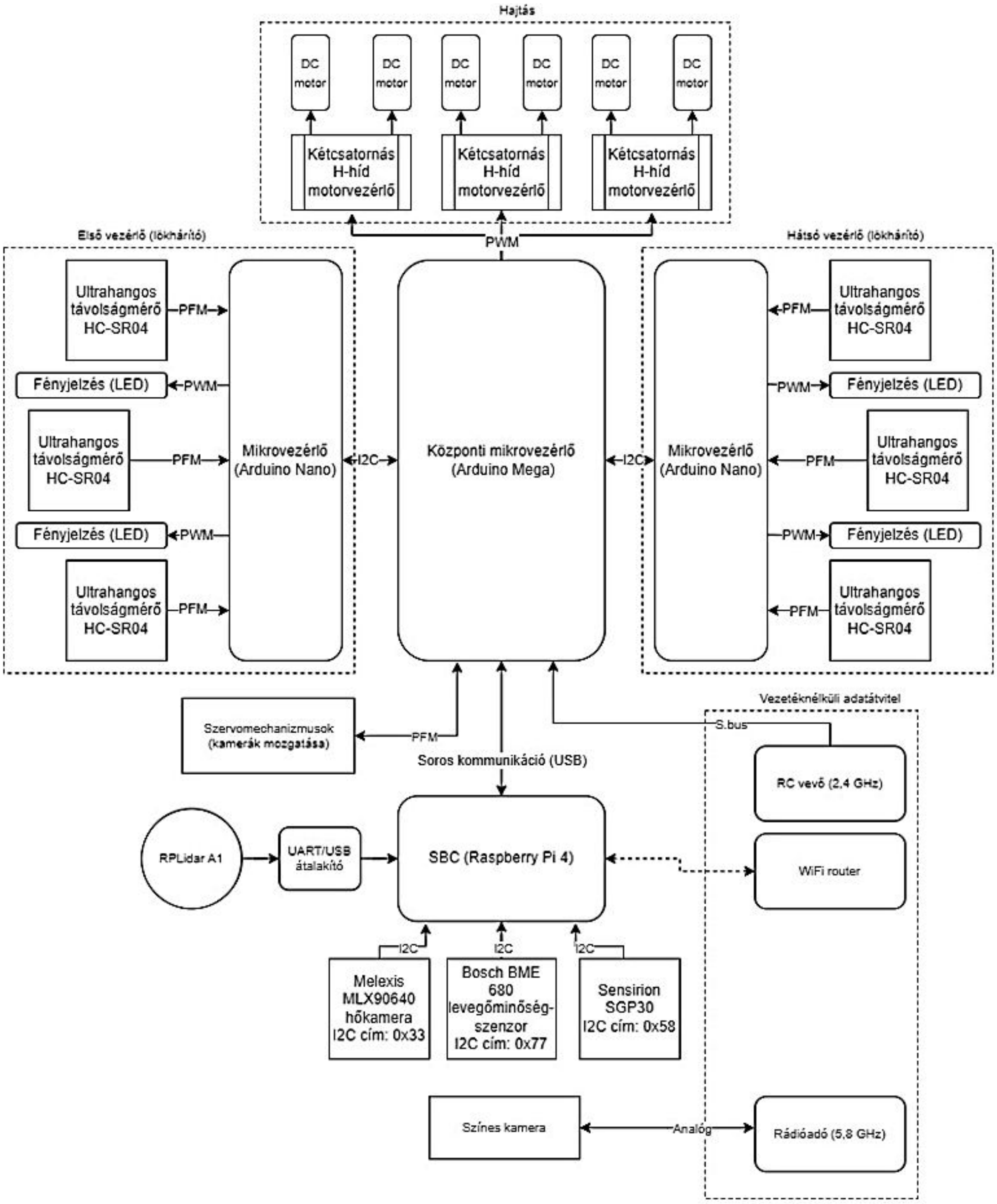

Fig. 4. Block diagram of the robot's electronic architecture (Own picture)

Components of the on-board electronics of the robot:

- **High-level control - Raspberry Pi 4**
  - Processing and transmission of sensor data,
  - Later: environment sensing, route planning for autonomous/semi-autonomous operation,
- **Low-level control - Arduino Mega**
  - Real-time guarantee,
  - Motor actuation,
  - Custom PCB.
- **Control of distance sensors on the front and rear of the robot (in the bumpers)**
  - Arduino Nano, custom PCB,
  - I2C communication between front and rear controllers and central low level,
  - Improved reliability, avoiding problems with wiring, analog signal transmission.

Data transmission is an essential part of a remote-controlled robot. Its solutions are designed and developed in a modular way:

- Camera image transmission - 5.8 GHz radio frequency transceiver
- Teleoperation - 2.4 GHz radio frequency transceiver
- Other on-board sensors data transmission - WiFi, using on-board router. Two possible solutions
- Currently with screen sharing, GUI on Raspberry
- later in the form of UDP packets, GUI on the host PC,
- C# Windows Form Application.

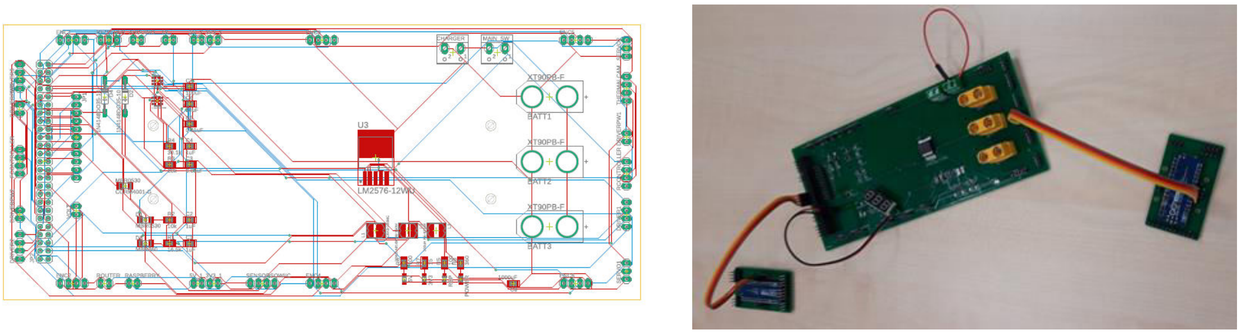

Fig. 5. Design and construction of a centralised substation (Own design)

3.4. LIDAR

I have chosen the following LIDAR for the robot, which offers the best value for money: SLAMTEC RPLIDAR A1 - 360 LASER RANGE SCANNER

This laser scanner development kit is capable of 360-degree scanning within a range of 12 m with a sampling rate of 2-10 Hz (this is for a full revolution). This LIDAR is capable of 0.2 cm range, 1-degree angular resolution and a range of 12 m.

Power supply is 5V. Via a USB cable, the data can be processed on a Raspberry Pi computer.

To hold the LIDAR and the air sensors, I designed a holder with Inventor, with the LIDAR mounted in the upper part (with a suitable robot-around-robot view) and a lower (pull-out) "drawer" to hold the air sensors. The holder also has integrated robot mounting tabs for easier handling of the robot. The design features a hinged construction for easy access to the robot's interior when needed.

3.5. Multifunctional bumpers

I wanted to keep the aluminium frame of the robot, but the redesign of the layout and the development of new functions required an extension. This is achieved by appropriately designed front and rear bumpers. I designed the main switch, the charging socket (so that the battery does not have to be removed for charging), the front and rear ultrasonic distance sensors (4-4) and the printed circuit boards designed to operate them into the front and rear bumpers.

3.6. Thermal camera

The 8x8 matrix thermal camera of the HEAT SPOTTER 1.0 was replaced by a higher resolution Adafruit MLX90640 IR thermal camera. The Adafruit MLX90640 IR consists of an array of 24x32 IR thermal sensors. When connected to the Raspberry Pi, it returns 768 individual IR temperature readings via I2C. The selected version 4469 has a wide field of view (110°x70°). The card can measure temperatures between -40°C and 300°C with an accuracy of 2°C (range 0-100°C). Thanks to the maximum frame rate of 16 Hz, it is perfectly suited to be used as a mini thermal imager.

3.7. Colour night vision camera

The Caddx Ratel, chosen to record colour images, is a low weight, compact analogue camera. 1/18"

HDR sensor, with an output signal compliant with the PAL analogue standard.

3.8. Data transmission, communication

To ensure reliable operation, the robot is equipped with a modular telecommunication system.

It includes the following components:

- WiFi communication with on-board wireless router
- Wireless transmission of data recorded by air quality sensors and LIDAR via WiFi connection
- The data transmitted by the LIDLAR sensors, and the LIDARs are transmitted via wireless link. Data transmission can be implemented in two ways to ensure redundancy:
    - UDP (User Datagram Protocol) - the sensor data is transmitted via the
        - The sensor data is sent in packets. The packets are sent via UDP (packets are sent in packets using the protocol "Datagram protocol").
        - The packets are received by a Windows Form application based on C# programming language.
        - The Windows Form application also acts as a graphical user interface.
    - By mirroring the screen of the Raspberry - sensor data is sent using Python code are displayed on the Raspberry desktop, this is mirrored to AnyDesk application.
        - 5.8 GHz radio communication - used to transmit the colour camera image.
        - 2.4 GHz radio communication - allows teleoperation of the robot.

4. Further development plans

In the near future (for next year's competition), I plan to implement the following improvements to achieve an even higher level of readiness:

- Semi-autonomous, autonomous scouting, surveying, data collection,
- Use of odometry and laser scanners,
- Implementation of SLAM algorithm,

- Ultrasonic distance sensors for safety stop, precise manoeuvrability application of ultrasonic remote sensing.

Preparatory operations already implemented for the above:

- Installation of the laser scanner LIDAR,
- Installation of ultrasonic distance sensors,
- Measurement of the wheel angular speed for odometry.

5. Summary

In many areas of industry and construction, a quick and inexpensive energy survey by a target robot can be a useful tool for listing and rating thermal bridges and heat loss factors and structural elements.

The Heat Spotter 2.0 robot, which I designed and implemented, is an affordable and quick payback tool for these tasks.

The Heat Spotter's design is easy and inexpensive to manufacture, yet robust enough to withstand the rigors of use.

The size and dynamic movement of the device, combined with its good maneuverability and remote control, make it an excellent tool for the job.

I spent many hours designing, building and testing the robot.

During the development phase, of course, I also had to deal with problems, which were a real development challenge. These included:

- choosing the right tools for the budget and quality requirements,
- mutual display of the camera image and the thermal image,
- adjusting the colour map of the thermal camera,
- processing the signals from the air quality sensors,
- ensuring an adequate and independent power supply to sensors and actuators and to the on-board computer,
- design and construction of additional mechanical components for the new developments (with the main focus on appropriate functional design and ease of installation)
- design of prototype-compliant, easy-to-understand PCBs and replacement of the HEAT SPOTTER 1.0 wiring with PCBs.

The robot I designed and implemented is affordable, so it is a quick return on investment for many tasks.

Acknowledgement

The research presented in this paper was partly supported by the Carpathian Basin Talent Research Foundation and Hungarian Innovation Association.

References

[1] Lakatos, Attila. "Building energy assessment robot (HEAT SPOTTER 2.0)." 31st Youth Science and Innovation Talent Competition, 2022.
[2] Chen, Min, and Gabriel A. Rincón-Mora. "Design and Planning a Printed-Circuit Board (PCB) Prototype." (2006).
[3] National Oceanic and Atmospheric Administration (NOAA), Coastal Services Center, Coastal Geospatial Services Division. *Lidar 101: An Introduction to Lidar Technology, Data, and Applications*. Coastal Remote Sensing Program, 2012.
[4] Wong, Wai Kit, Poi Ngee Tan, Loo Chu Kiong, Loo Chu Kiong, and Way-Soong Lim. „Effective Surveillance System Using Thermal Camera." Paper presented at 2009 International Conference on Signal Acquisition and Processing, ICSAP 2009, Kuala Lumpur, Malaysia, April 3-5, 2009.

Flood Wave Transit on Trotuș River, with the Left Bank Flood Defence Raised

PhD.Eng. **Marie-Alice GHIȚESCU**[1,*], PhD.Eng. **Gheorghe I. LAZĂR**[1], PhD.Eng. **Albert Titus CONSTANTIN**[1,*], PhD.Eng. **Şerban Vlad NICOARĂ**[1]

[1] Politehnica University Timisoara (UPT), Romania

* alice.ghitescu@upt.ro; albert.constantin@upt.ro

Abstract: *The paper presents a discrete 2D numerical modelling on Trotuș River – in Tg-Ocna, at an accidental flood and known configuration, given by the hydrograph registered between 2–8 June 2016. The purpose of this modelling is to estimate the parameters of transient hydraulics (non-permanent), respectively, specifying some constructive aspects of flood protection by establishing the geometric and hydraulic parameters when raising the flood defence dam in the vicinity of the technological platform on the left bank of Trotuș River.*

Keywords: *2D hydraulic modelling, flood wave transition, flood defence*

1. General Consideration

Discrete numerical modelling is based on the existence of a flood study on the Trotuș River to establish constructive aspects of non-flooding of the technological platform on the left bank, in the southern part of Târgu-Ocna, area with car access on the national road DN12A [1].
A new project will be carried out in the vicinity of the Trotuș riverbed (in the immediate vicinity of the flood defence). The construction site is located at an average elevation of approx. 254.50 maSL and covers a total area of 51.665 m^2 (Fig.1). For the modelling the geometry of Trotuș riverbed, a section with a length of approx. 1566 m; on this section a database was created concretized by a situation plan (topographic survey in Stereo 70), 35 transversal profiles (of which 3 transversal profiles on the Slănic brook - right tributary; 14 transversal profiles that intersect the flood defence dam on the left bank, near the technological platform, 1 longitudinal profile on the route of the existing defence dam, from the transversal profiles the morphology of the minor and major riverbeds is highlighted, respectively, the characteristics of the technological platform (Fig.2).

Fig. 1. Plan view of the area of interest on Trotuș River

In the study of the accidental flood hydrograph transit on the Trotuș River, two discrete numerical models were made.

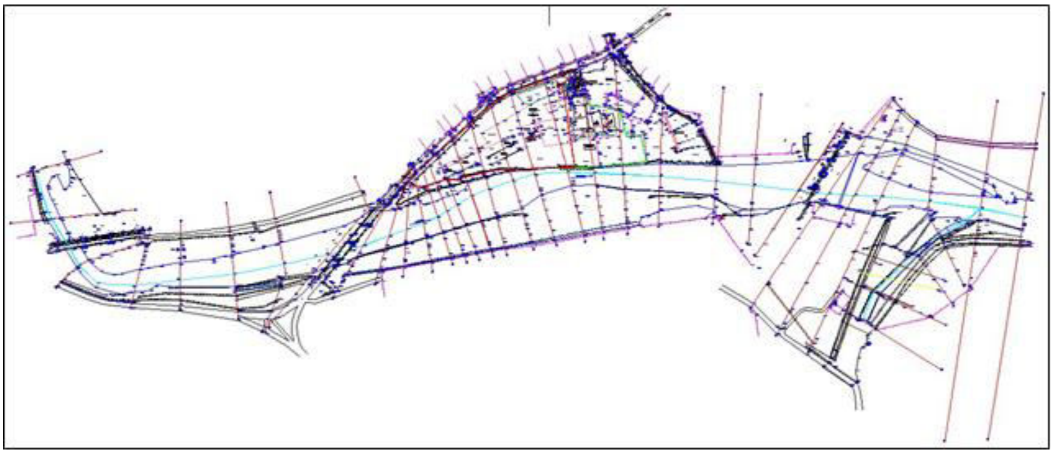

Fig. 2. Plan view with Stereo 70 Survey of cross sections location

The first discrete numerical model was made on a one-dimensional section (1D) and includes the 3 bridges crossing the Trotuș River. This section was divided into 3 sectors: *Raul_Trotuș_am* in length of 1494m; *Raul_Trotuș_av*, in length of 71.85m; and sector *Paraul_Slanic* in length of 220m. These three sectors are connected at the junction and labelled *Jonctiune 1*, (Fig.3).

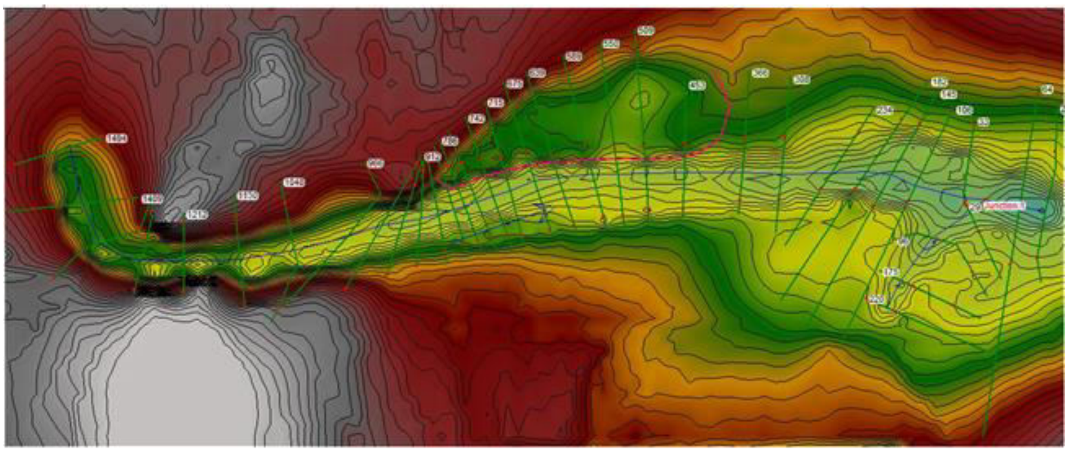

Fig. 3. Numerical model in 1D (HEC-RAS vers.4.1) applied with Ras Mapper cu HEC-RAS vers.6.0 Beta 3

The second discrete numerical model was made on a two-dimensional area (2D) - the graphical representation is presented in Chapter 3; the model contains the 3 bridges crossing the Trotuș River and the end zone of the numerical model (2D) stopping at the cross section S29 not including the confluence zone of the numerical model (1D). Because this area is being downstream of the studied area, respectively, of the confluence where it is made a catchment threshold for the Tg-Ocna Treatment Plant, and because Slănic brook cannot produce a significant turbulence which could have an impact on the analysed area, a fact found on the 1D numerical modelling.
The description flood study only includes the numerical model in (2D). However, geometric references developed in the (1D) model will be made only to describe the generation of the discrete model geometry in (2D). In this discrete numerical model (2D), it will be clearly observed the way of passing the accidental flood wave (the allure of the synthetic flood hydrograph is given by the allure of the flood of June 2-8, 2016). The topographic database (represents about 829 distinct points in geographical coordinates and land elevations) was made by the company SC.Geo Point Expert SRL from Bacău.
For the calculations and hydraulic verifications necessary to determine the variation of water level, the regime of run-off velocities and the transit mode of the flows on the Trotuș river, in the urban area of Târgu-Ocna, the following elements were necessary: maximum flows with different probabilities of exceeding; the appearance of the flood hydrograph; roughness coefficients in the minor and major riverbed; hydrodynamic drainage slope or key curve in the downstream section of

the analysed sector. The hydrological data are provided by the National Administration “Romanian Waters”, the Siret Bacău Water Basin Administration, and the hydrograph is presented in (Fig.4). The flood level hydrograph for June 27, 2005, sent by the National Administration "Romanian Waters", Siret Bacău Water Basin Administration, was registered at the Târgu-Ocna Hydrometric Station and is an important database used to simulate the model numerically discrete.
The geometric shape of the synthetic flood hydrograph was assimilated in all the numerical simulations analysed in the present study, respectively, amplification coefficients (am.coef.) were used to reach the maximum return period flow values for: $Q_{1\%}$ = 1160 m^3 / s (am.coef = 1.6905) and Q_{MAX} = 965m^3 / s (am.coef. = 1.405). When generating the synthetic flood hydrograph for the calibration flow, the June 2016 flood wave configuration was used, with an amplification coefficient of about = 1.405 corresponding to the maximum level H_{max} = 252.996 maSL recorded at S.H. Targu Ocna.

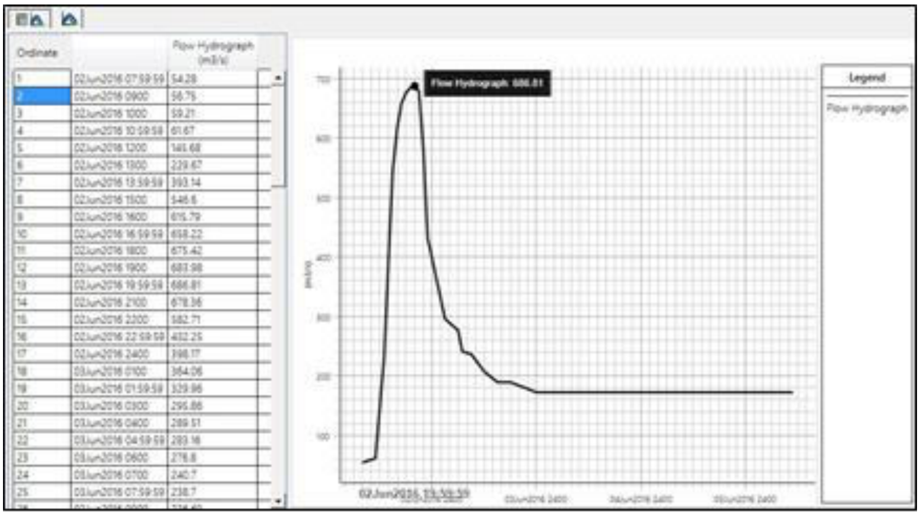

Fig. 4. Graphical representation of flood hydrograph at SH. Târgu-Ocna on 2-8 of June 2016

2. Maximum flows for different return periods

The main hydrotechnical works associated with the project site: "Flood study" were classified in importance class IV and consequently the sizing flow corresponds to the probability of exceeding 5%, respectively, the verification flow with the probability of exceeding 1%. Therefore, the corresponding exceeding probability of 5% is $Q_{5\%}$ = 770m^3 / s, respectively, the corresponding exceeding probability of 1% is $Q_{1\%}$ = 1160 m^3 / s. With the HEC-RAS program vers. 4.1 [2] modeled the transit of flows in transitional regime (flood wave), in modified regime. The use of numerical modeling in the current study aimed to establish cross sections on the Trotuș River and Slănic tributary with real-scale graphical representation (terrain representation in (1D) from survey).

3. Building the numerical model

For building the discrete numerical model, a section of the Trotuș River, Târgu-Ocna urban location, was considered; with a length of 1566m. The analysed sector of Trotuș River and of Slănic tributary was divided into sectors (34) limited by 35 cross-sections obtained in accordance with the actual topographic surveys. The topographic sections on the route are visible (red colour) in the linear interpolation representation of the terrain presented in (Fig.5). The natural terrain model in the representation (2D) with the afferent surface obtained from a two-dimensional interpolation is modified within the HEC-RAS vers program. 6.0 Beta 3 by using several facilities described in particular in the documentation [4] and which may be applied to a known watercourse (in this case the Trotuș River). Therefore, the adjustment operations were performed in two stages:

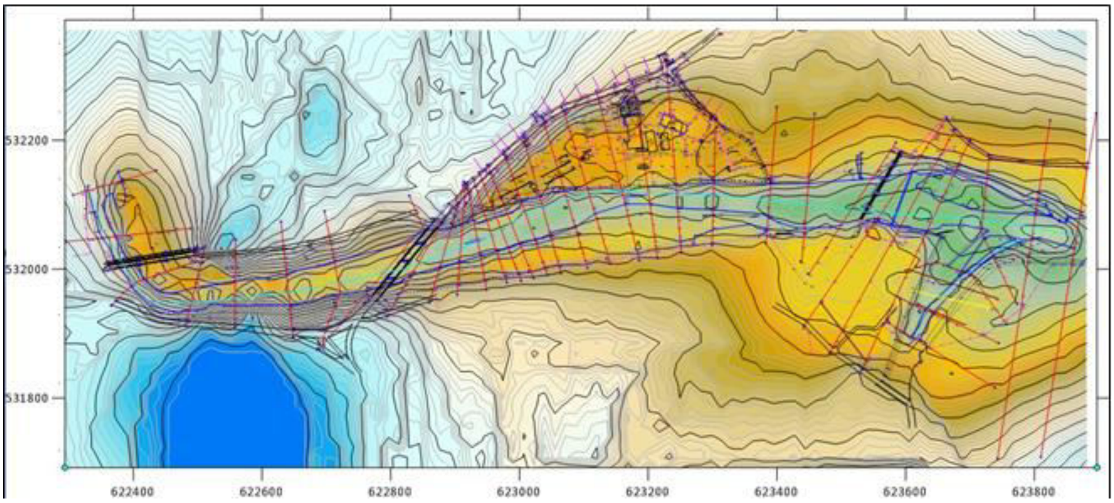

Fig. 5. Plan view of the terrain with level lines and interpolated cross sections

In the first stage, the natural terrain model resulting from the two-dimensional interpolation using the surface domain (2D) called Zona_2SD_Tg_Ocna is used. A perimeter area is defined that includes only the upstream sector of the Trotuș River (which was developed in the discrete 1D model). Select the grid spacing points in meters (Dx = 20, Dy = 20), generate the points associated with the facility (Generate Computations Ponts) as well as the corresponding property tables for points (Compute Property Points). The Refinement Regions facility is used, and an additional region is defined for the thickening of the grid in the area of the minor river bed of Trotuș River (from the beginning to the confluence area). This region is used to perform an additional network thickening operation (Dx = 10, Dy = 10).

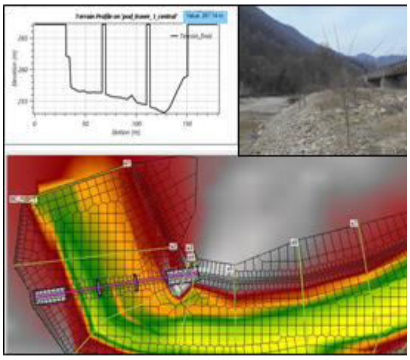

Fig. 6. Overpass structure – Railway bridge

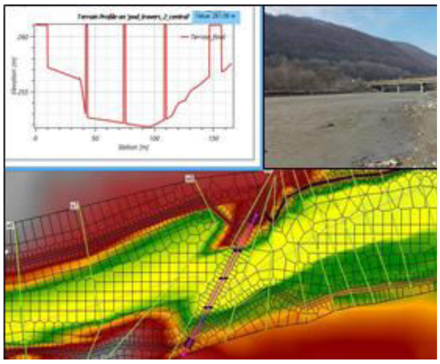

Fig. 7. Overpass structure - Road bridge

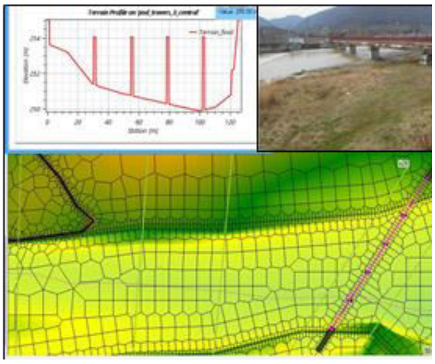

Fig. 8. Overpass structure - Pedestrian bridge

In the second stage, the new additional facilities of HEC-RAS ver. 6.0 Beta 3, adjust the banks of the watercourse in accordance with the known geometric data from the topographic survey, along the entire length of the banks; the three overpass structures are introduced in accordance with the topographic elevations as one can observe in the graphic presentation in (Fig.6). In the graphical representations (Fig.7 and Fig.8), are represented in detail the three areas related to the discrete numerical model that contain the crossing elements in (2D), both in plan view, and cross sections; the cross sections intersect the central area of the overpass structures.

The mode of flows transit on the numerical model (2D) was carried out in 3 stages, namely:

Stage 1 Model calibration to the transit of the historical hydrograph where the maximum level reaches the registered value H_{max} = 252.966 maSL and corresponds to a maximum flow value of. Qmax = 965 m^3 /s.

Stage 2 Transit of the synthetic flood hydrograph and identification of floodable areas on the discrete numerical model and where the flow reaches the maximum value of $Q_{1\%}$ = 1160 m^3 /s.

Stage 3 Synthetic flood hydrograph transit the on the improved discrete numerical model, in which a lateral connection structure was introduced - simulates the elevation of existing defence dam to protect the technological enclosure from flooding when maximum flow reaches $Q_{1\%}$ = 1160 m^3 /s.

3.1. Initial and boundary conditions

Currently, the boundary conditions on the river path are given by: the transit flow with a certain probability of exceeding entered as a known flood hydrograph, values that are introduced in the upstream area of the numerical model; in the present case (2D) - the condition on line BC_S2D_1 which is also associated with the hydrodynamic slope necessary for the distribution of flows on the line; hydrodynamic slope in the downstream area of the numerical model in (2D) - condition on line BC_S2D_2 (see Fig.9); In this discrete numerical model in (2D), no initial conditions are required.

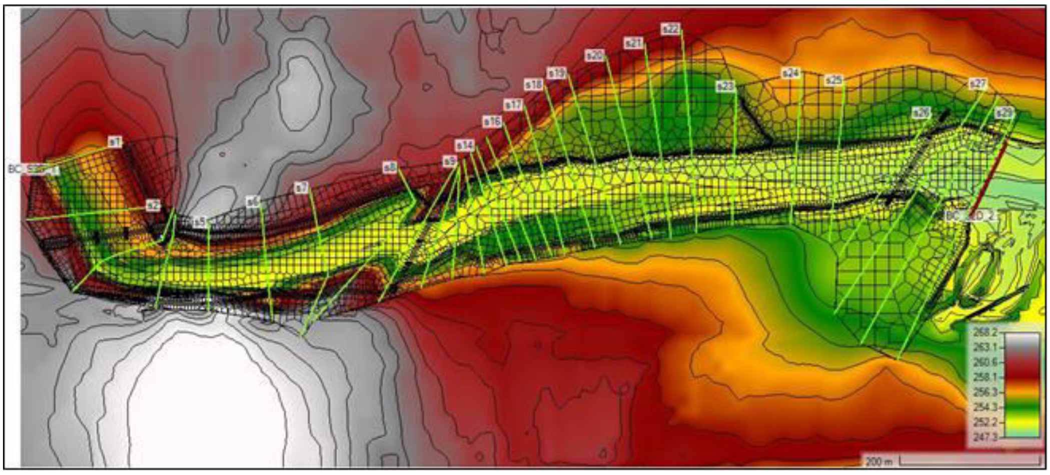

Fig. 9. Model discretization with the boundary location- upstream BC_S2D_1 and downstream BC_S2D_2

Stage 1 – Model calibration - Simulation of the runoff on the Trotuș River, in the situation of the existing flood defence system, in non-permanent regime, for the flow corresponding to the historical flood hydrograph from 2005, registered at SH. Târgu-Ocna where the maximum value of water level is reached → H_{max} = 252.966 maSL and corresponds to a maximum flow of Q_{max}=965m^3/s - in the location marked with “pod_travers_central_3” (value of the historical level was received from the National Administration " Romanian Waters ", Siret Bacău Water Basin Administration) includes:

• a historical flood wave introduced in the upstream section, on line BC_S2D_1, where the maximum level reached was H_{max} = 252.966 maSL, resulting in the associated flow Q=965m^3/s, and the hydrodynamic slope for the flow distribution on the boundary condition is: J = 0.0076;

Stage 2 - Transit of the synthetic flood hydrograph that corresponds as an allure to the hydrograph registered between 2-8 of June 2016 at SH. Târgu-Ocna (approx. 1.6905) and where the flow reaches the maximum verification value of $Q_{1\%}$ = 1160 m^3/s. Therefore, the simulation of the runoff on the Trotuș River in the situation of the existing dam system, non-permanent regime, for the maximum flow $Q_{1\%}$ = 1160 m^3/s includes:

• a wave of synthetic flood generated in the upstream section located on the line BC_S2D_1 with the maximum flow reached at the value of $Q_{1\%}$ =1160 m^3/s and the hydrodynamic slope for the distribution of the flow on boundary condition, located on line BC_S2D_at the value: J = 0.0076;

Stage 3 - Transit of the synthetic flood hydrograph on the discrete numerical model in which a lateral connection structure was introduced which simulates the elevation of the existing defence dam to protect the technological enclosure from flooding when the maximum flow reaches $Q_{1\%}$ = 1160 m^3/s. The simulation of the runoff on the Trotuș River in the situation of the existing dam system, non-permanent regime, with a lateral connection structure at the maximum flow $Q_{1\%}$ = 1160 m^3/s includes:

• a synthetic flood wave generated in the upstream section located on the line BC_S2D_1 with the maximum flow reached at the value of $Q_{1\%}$ =1160 m^3/s and the hydrodynamic slope for the distribution of the flow on boundary condition, located on line BC_S2D_at the value: J = 0.0076;

3.2. Numerical model simulation

The initial conditions and boundary conditions have been applied for all three stages. The numerical modeling for the situation of the flood waves (Stage: 1,2 and 3) takes place in time, for a known period starting from June 2, 2016 at 8.00 am until June 8, 2016 at 6.00 am. The actual (reduced) execution analysis was performed only between 8-21 o'clock, has a time step Δt = 0.5 seconds, the internal mapping interval Δt = 5 minutes, and the results are stored at a time interval of 10 minutes.

3. Results presentation

Following the execution of the numerical simulations, all the constant or time-varying parameters were obtained, referring to: levels, flows and speeds, on the whole discrete numerical model, for all the three stages of water transit along the Trotuș river in the area of Târgu- Ocna. The presentation of the results obtained after the post-processing in graphic form are presented for the 2 stages (Stage 2 and Stage 3) as follows:

Stage 2 - Transit of the synthetic flood hydrograph corresponding to the hydrograph registered between 2-8 of June 2016 at SH. Târgu-Ocna (approx. 1.6905) and where the flow reaches the maximum verification value $Q_{1\%}$ = 1160 m^3/s is included in this stage.

- Plan view with the visualization of the transit mode of the flood hydrograph; water depth distribution (in m); visualization of floodable areas - graphical representations at the current time: June 2, 2016, 20.00, Q = 1160m^3 / s – (Fig.10).

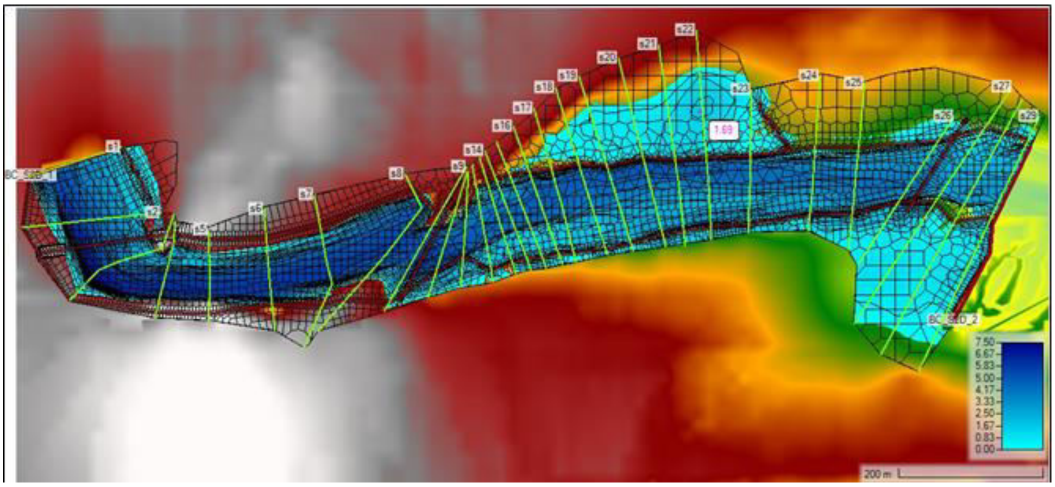

Fig. 10. Plan view with water depth distribution -Stage 2

It is observed on the model that the maximum depth in the area of the technological platform is 1.69 m when reaching the flow value Q_{max} = 1160 m^3 / s at which the maximum level reached is H_{max} = 253.37maSL in the location of S.H. Târgu-Ocna.

- Plotting the trajectories of overlapping particles over the velocities variation (in m/s) - graphical representations at the current time: June 2, 2016, 20.00, Q= 1160m^3/s – (Fig.11)

It is found that the water level at S.H. Târgu-Ocna (the 2005 flood reaches a maximum level of 252.966 maSL) increases to 253.37 maSL, so it is higher by Δ = 0.404m. Therefore, in Stage 2, the water discharges over a significant area of approx. 200 m, over the flood protection dams on the left bank of the river, to the technological area, as in accordance with the current topographic situation of the terrain elevation.

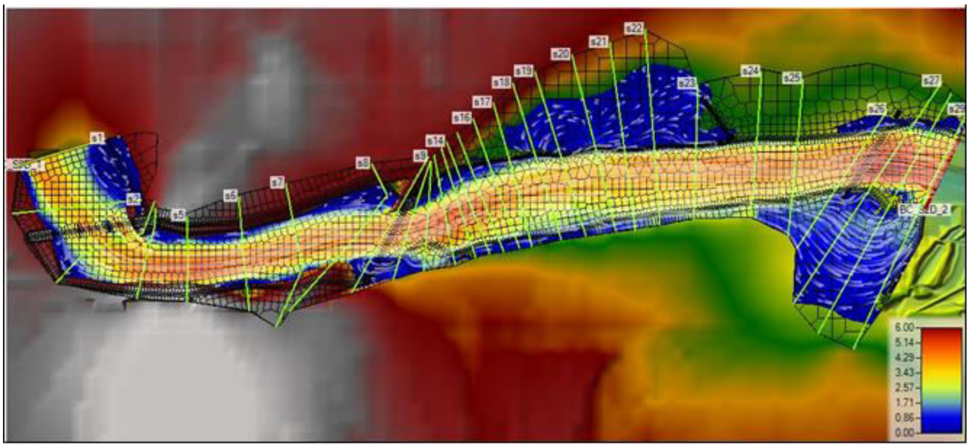

Fig. 11. Plan view of velocities distribution - Stage 2

Stage 3 - Transit the synthetic flood hydrograph on the discrete numerical model in which a lateral connection structure was introduced to simulate the elevation of the existing defense dam, to protect the technological enclosure from flooding when the maximum flow reaches the value of $Q_{1\%} = 1160\ m^3 / s$.

- Plan view with the visualization of the transit mode of the flood hydrograph; water depth distribution (in m); visualization of floodplains (Fig.12).

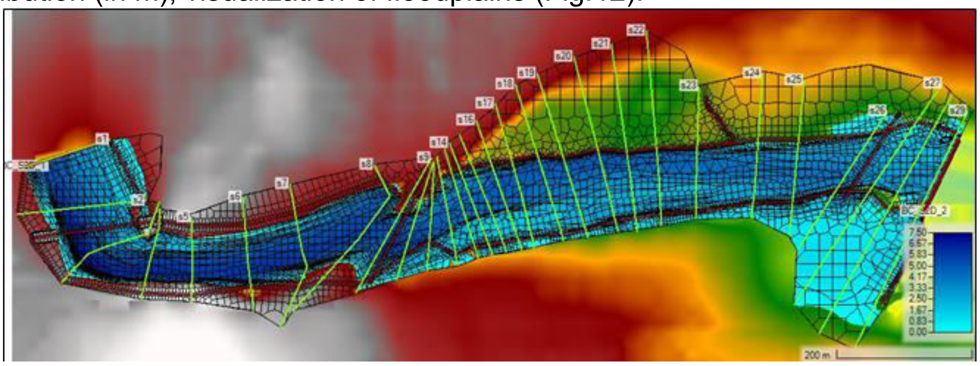

Fig. 12. Water depth distribution map -Stage 3

- Plotting the trajectories of overlapping particles over the velocity's variation (in m/s) - graphical representations at the current time: June 2, 2016, 20.00, Q= 1160m^3/s – (Fig.11)

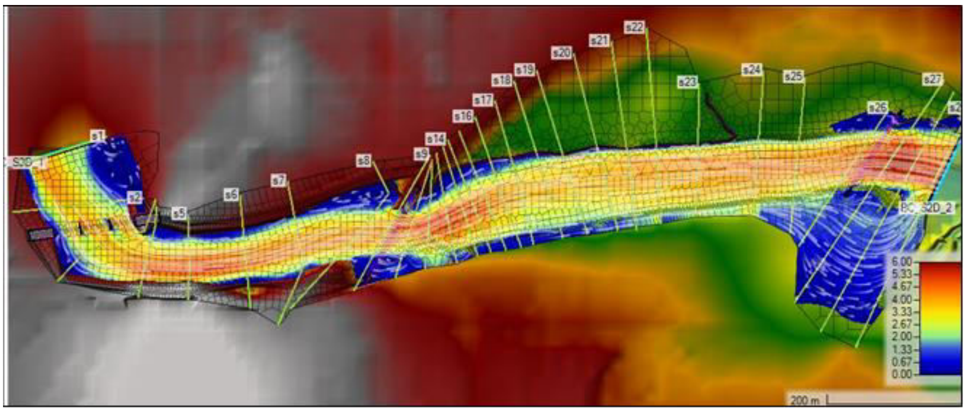

Fig. 13. Plan view of velocities distribution - Stage 3

At this stage it is found that the water transits through the minor riverbed, the major riverbed on the left bank, where the dam was raised ,and that the water no longer passes over the dam, and the area of the technological enclosure is no longer floodable and becomes a flood protected enclosure, corresponding to flow rate $Q_{1\%} = 1160\ m^3 / s$.

The graphical representation in (Fig.14) shows the configuration in plan as well as in cross section through the lateral connection structure that simulates the profile of the raised defence dam on the left bank of the river Trotuș.

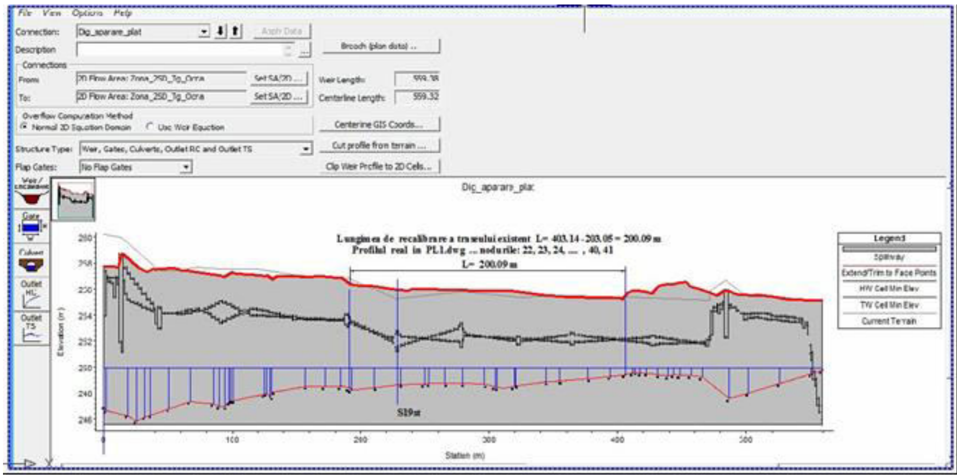

Fig. 14. Longitudinal profile through lateral structure along flood defence structure

It can be observed that the area which the flood defence should be raised extends over 200m (22-41 nodes).

A comparative graphical presentation of the results from Stage 2 and Stage 3, in several characteristic sections (notation: S21 and S22) with the variation of levels (in maSL) and velocities variation (in m/s) - at the current time: June 2, 2016, 20.00, when the maximum flow is Q = 1160m^3/s – (Fig.15).

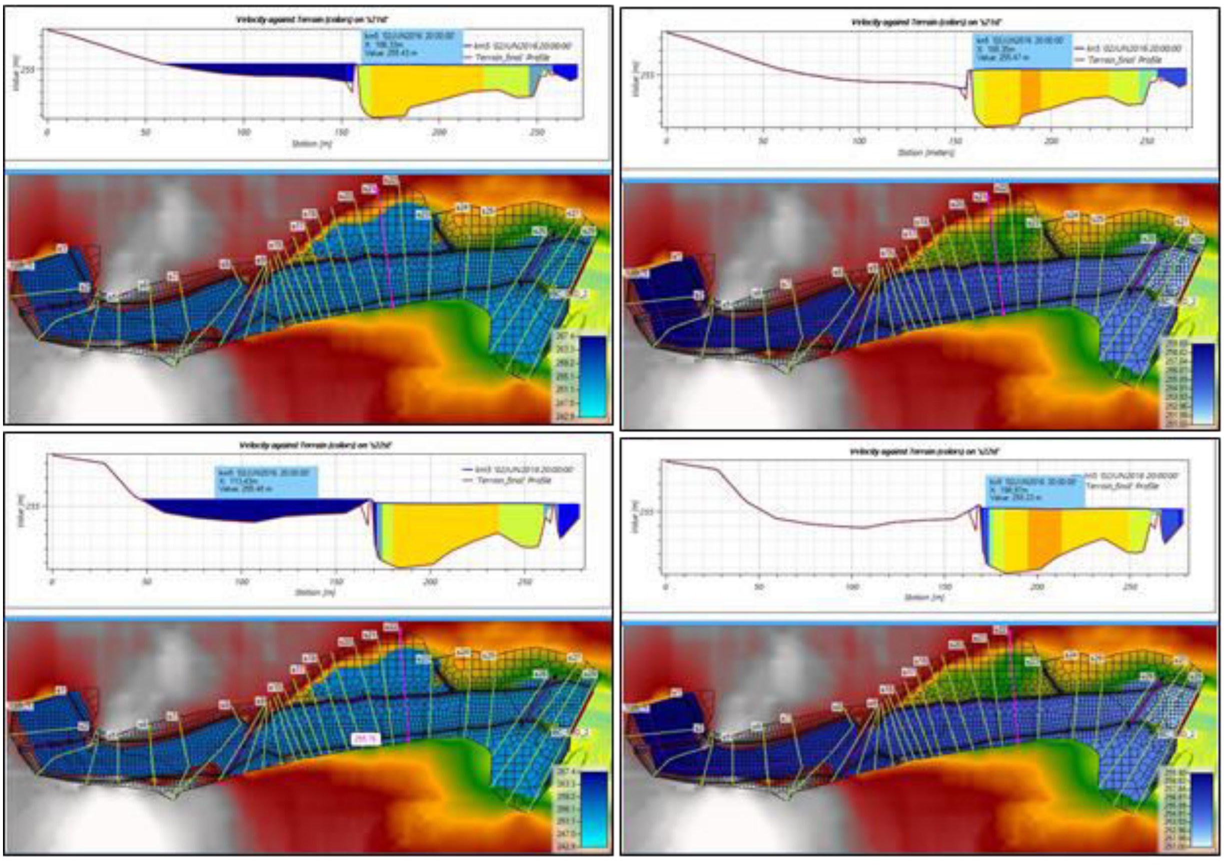

Fig. 15. Water level variation (in maSL) and velocities variation (in m/s) in cross sections S21 and S22-Stage 2 on left side and Stage 3 on right side

6. Conclusions

From the analysis of the comparative results associated with the technological enclosure, the length of the raised area of the flood defence dam was obtained. Fig. 16 also presents in tabular the geometric and hydraulic characteristics necessary to raise the dam in the vicinity of the technological enclosure which represent: topographic number; partial distances; topographic coordinates; the existing elevation of the dam on the left bank; the share of water in the transit regime with the dam raised; the elevation of the dam in the water discharge area; a safety guard of 0.20 m was pre-tapered and resulted in the current heights in the elevation sections. One can also observe that the elevation area of the dam has a length of approx. 200 m, and the maximum height elevation reaches a value of approx. 1.06 m.
Therefore, given the lateral connection structure in the area of the technological enclosure (with the topographic nodes: 22 - 41 resulting from the actual lifting) which simulates the necessary portion of the elevation of the floods defence structure, it is justified to raise the existing flood defence dam over a length of approx. 200 m.

Nr.topo.	Distante cumulate (m)	Coord. X	Coord. Y	Cota existenta dig stanga (mdM)	Cota hidro. (mdM)	Cota dig final (mdM)	Δ (m)
	203.05			256.290	255.95	256.29	0.00
23	211.29	623095.223	532117.798	255.860	255.90	256.21	0.35
24	230.46	623111.874	532119.455	255.260	255.86	256.06	0.80
25	248.16	623130.905	532121.793	255.620	255.84	256.04	0.42
26	251.49	623148.607	532121.880	254.960	255.82	256.02	1.06
27	255.12	623148.797	532125.205	255.320	255.80	256.00	0.68
28	263.26	623160.560	532125.091	255.755	255.78	255.98	0.22
29	275.81	623173.111	532125.152	256.220	255.75	256.22	0.00
30	291.87	623189.150	532124.272	255.660	255.70	255.90	0.24
31	301.43	623198.442	532122.032	255.460	255.64	255.84	0.38
32	306.45	623203.426	532121.451	255.367	255.58	255.83	0.46
33	314.56	623211.425	532122.788	255.520	255.45	255.83	0.38
34	315.18	623211.889	532123.209	255.700	255.45	255.83	0.46
35	337.38	623233.926	532125.837	255.570	255.42	255.62	0.05
36	347.46	623243.974	532126.671	255.458	255.35	255.55	0.09
37	368.41	623264.848	532128.402	255.300	255.26	255.46	0.16
38	384.88	623281.246	532129.947	255.280	255.21	255.41	0.13
39	395.63	623291.926	532131.242	255.190	255.15	255.35	0.16
40	401.26	623297.372	532132.651	255.100	255.13	255.33	0.23
41	403.14	623299.147	532133.269	255.351	255.12	255.35	0.00

Fig. 16. Geometric and hydraulic parameters of flood defence dam

In conclusion, the area of the technological enclosure bordered by the retaining wall to be raised (upper elevations that will respect the geometric and hydraulic characteristics in Fig.16) becomes not flooded when the accidental flood hydrograph passes with the maximum flow value exceeding capacity $Q_{1\%}$ = 1160m^3 / s.
Therefore, it is necessary to redesign a retaining wall whose upper dimensions comply with the indications of this study.

References

[1] Constantin, A.T., Gh. I. Lazăr, Ş.V. Nicoară, A.I. Popescu, M.A. Ghiţescu, and C. A. Gîrbaciu. Beneficiary: RC Europe Development S.R.L, “*Flood study on the Trotuș river, Tg-Ocna area adjacent to the perimeter CF62653, CF62654, protected area of 5166sqm (RO).” Contract of UPT, 2021*.
[2] Brunner, Gary W. *HEC–RAS 4.1 River Analysis System: Hydraulic Reference Manual*. US Army Corps of Engineers - Institute for Water Resources, Hydrologic Engineering Center, November 2002.
[3] Nicoară, Ş.V., Gh.I. Lazăr, and A.T. Constantin. “Comparative Study of a 1D and 2D Numerical Analysis Modelling a Water Flow at a River Confluence under Accidental High Waters.” *“Hidraulica” Magazine,* no. 4 (December 2018): 90-97.
[4] Brunner, Gary W. *HEC-RAS River Analysis System: User’s Manual. Version 6.0 Beta*. US Army Corps of Engineers - Institute for Water Resources, Hydrologic Engineering Center, December 2020.

Increasing the Oxygen Transfer Rate to Stationary Water

PhD Std. **Marilena Monica BOLTINESCU (ROZA)**[1], Prof. Dr. Eng. **Nicolae BĂRAN**[1], Dr. Eng. **Albertino Giovani ROZA**[1], Ș.l. Dr. Eng. **Mihaela CONSTANTIN**[1,*]

[1] University Politehnica of Bucharest

* i.mihaelaconstantin@gmail.com

Abstract: *The paper analyzes the equation of the oxygen transfer rate to water; the factors that lead to the increase of this speed are specified.*
Further, a single factor is studied, namely "shrinking the orifice diameter" in the perforated plate of a fine bubble generator.
Two versions are studied:
- version I: the perforated plate has orifices with a diameter of 0.1 mm;
- version II: the perforated plate has orifices with a diameter of 0.05 mm.
The constructive solutions for the two versions are presented and the methodology of experimental researches is exposed.
The experimental results obtained regarding the increase of the concentration of dissolved oxygen in water, as a function of time, reveal that version II is more favorable here.

Keywords: *Water aeration; fine bubble generators; oxygen transfer rate.*

1. Introduction

Aeration plants aim to increase the content of dissolved oxygen in water, this increase ensuring a favorable development of all forms of life in water.
Water aeration can be achieved as follows [1] [2]:
- by mechanical aeration;
- by pneumatic aeration;
- by mixed aeration.

The most effective is pneumatic aeration and it consists in the introduction of air bubbles into the water.
Water can be stationary (in pools) or moving (flowing through pipes) [3-5].
Pneumatic aeration includes:
A) Aeration installations constructed of pipes with orifices;
B) Aeration installations with porous diffusers;
C) Aeration systems with bubble generators.
Bubble generator aeration systems include [6]:
a) Aeration equipment's producing nanobubbles (Ø <100 nm);
b) Aeration equipment's producing fine bubbles (Ø <1mm);
c) Aeration equipment's producing medium bubbles (Ø <1 - 3 mm);
d) Aeration equipment's producing large bubbles (Ø <3 - 120 mm).
To obtain fine bubbles, the diameter of the orifice must be as small as possible (d_0 <1 mm) and the distribution of the orifices in the plate must be uniform.
These two conditions can be achieved with the help of advanced micro-processing technologies [7] [8]:
- spark erosion processing;
- electrochemical processing;
- laser processing;
- electron beam processing;
- machining with micro-drilling machines in coordinates, with drills of Ø <0.5 mm.

Any of the above technologies must solve the problem of machining precision of the parts.

The processing precision means the extent to which the conditions provided in the execution drawing of the part have been ensured; these conditions refer to the shape of the part, the dimensional accuracy, the reciprocal positions of the surfaces and the quality of the surface [7] [8].
The permissible deviations are also indicated under the conditions provided in the drawing; it indicates the proximity degree required by processing for size, shape, etc., to an optimal constructive solution of the respective part [9].

2. Materials and methods

2.1 Materials

Paragraph: In the first version, a fixed fine bubbles generator is used for aeration of stationary water; it emits air bubbles in the water through a plate with orifices Ø 0.1 mm (figure 1). The plate thickness s = 2 mm, has 113 orifices with a diameter of d_0 = 0.1 mm, and the distance between the orifices is d = 2 mm. Thus, the two conditions were met [10]:

$$\frac{s}{d_0} > 3 \rightarrow \frac{2}{0.1} = 20 \tag{1}$$

$$\frac{d}{d_0} > 3 \rightarrow \frac{2}{0.1} = 20 \tag{2}$$

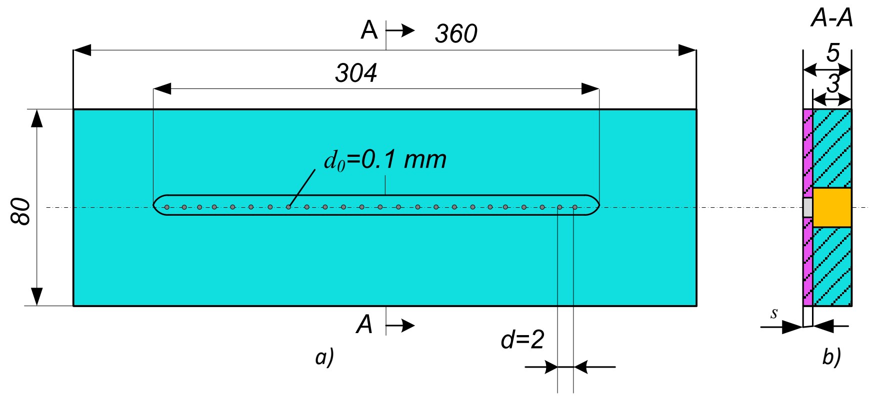

Fig. 1. Plate with orifices with a diameter of 0.1 mm
a) plane view; b) cross section.

In figure 2, one can observe the constructive solution of the fine bubble generator for version I:

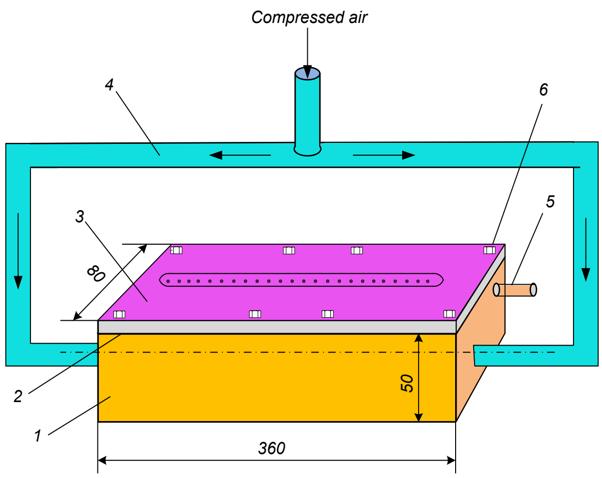

Fig. 2. Fine air bubble generator
1-compressed air tank; 2- sealing gasket; 3- plate with orifices Ø 0.1 mm;
4- G.B.F compressed air supply pipe; 5-connection for measuring the compressed air pressure; 6- screws for fixing the tank plate.

To perform the orifices of Ø 0.1 mm in the plate, a channel was created with a depth of 3 mm and a length of 304 mm; the orifices through which the air comes out has a thickness of 2 mm. Subsequently, with the help of a special machine used for micro processing, KERN Micro type, the 113 orifices with Ø 0.1 mm were made in the channel.
Figure 3 shows the scheme of the installation for version I; for the compressed air entering the fine bubbles generator, the pressure is measured with a digital manometer, the temperature with a digital display thermometer and the flow rate with a rotameter.

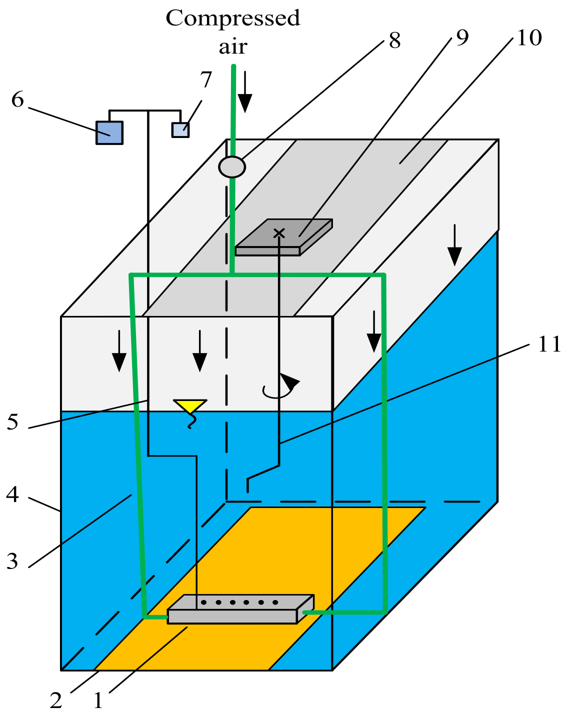

Fig. 3. The location of a FBG in the water tank
1-FBG; 2- the FBG support platform; 3- compressed air pipe; 4- water tank; 5- connection for measuring the pressure and temperature of the air in the FBG body; 6- digital device for pressure measuring; 7- digital device for temperature measuring; 8- rotameter; 9- mechanism of actuation of the oxygenometer probe; 10- support platform; 11- oxygenometer probe.

Figure 4 shows the fine bubbles generator in function.

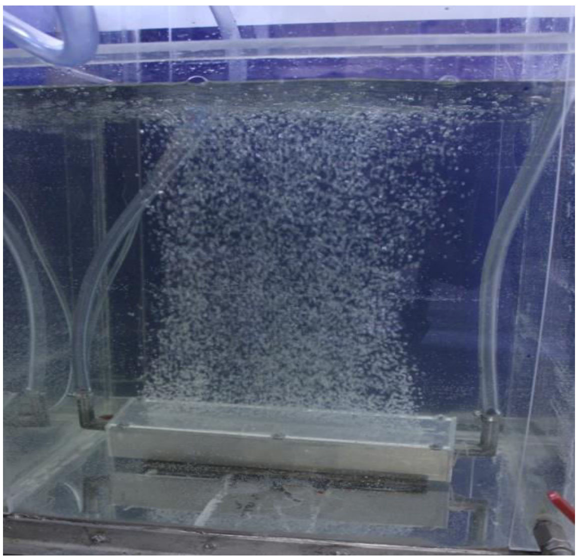

Fig. 4. FBG with orifices Ø 0.1 mm, in operation.

In version I, the area of the air-to-water outlet section will be:

$$A_I = n_I \cdot \frac{\pi}{4} \cdot d_I^2 = 113 \cdot \frac{\pi}{4} \cdot (0.1 \cdot 10^{-6})^2 = 0.887 \cdot 10^{-6} m^2 \quad (3)$$

To make a comparison between the two versions, the area of the air outlet section in the water will have to be the same ($A_I = A_{II}$) [11].

In version II, in which the orifices have Ø 0.05 mm, the number of orifices will be four times higher, i.e., 452 orifices.

$$\frac{A_I}{A_{II}} = \frac{n_I \cdot \frac{\pi}{4} \cdot d_I^2}{n_{II} \cdot \frac{\pi}{4} \cdot d_{II}^2} = \frac{113 \cdot 0.1^2}{4 \cdot 113 \cdot 0.05^2} = 1 \quad (4)$$

The total number of orifices (452) is divided into 4 circular plates, each containing 113 orifices with Ø 0.05 mm. Each plate has a thickness s = 2 mm; the location of the orifices complies with the conditions:

$$\frac{s}{d_0} > 3; \frac{d}{d_0} > 8 \quad (5)$$

Horizontally, the distance between two orifices on the same line is 10 mm and d_0 = 0.05 mm. The conditions become:

$$\frac{s}{d_0} = \frac{2}{0.05} = 40 > 3; \frac{d}{d_0} = \frac{10}{0.05} = 200 > 8 \quad (6)$$

In the vertical direction, the distance between two orifices is also 10 mm. In the oblique direction (the line AB in figure 5) one can obtain:

$$\frac{d}{d_0} = \frac{\sqrt{5^2 + 5^2}}{0.05} = 141.4 > 8 \quad (7)$$

Figure 5 shows the orifices plate, made of transparent plexiglass; the plate is mounted on a cylinder with an outer diameter of 105 mm.

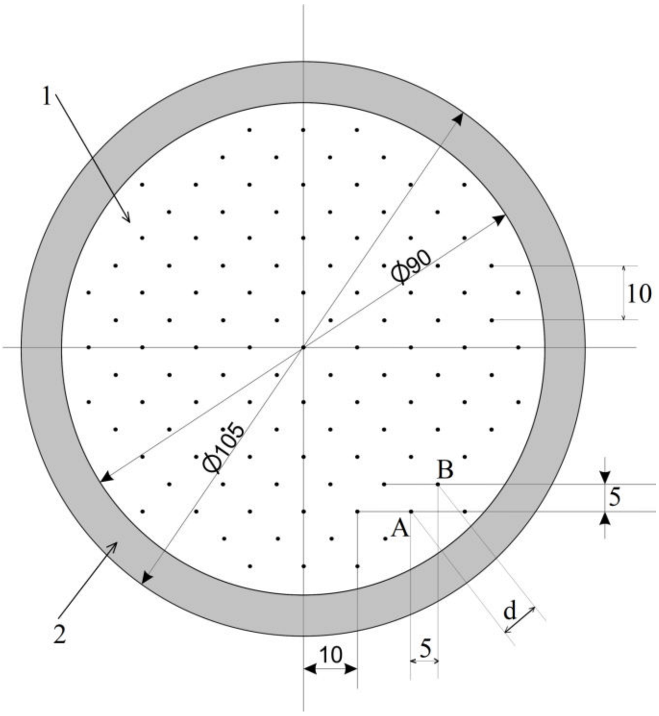

Fig. 5. The orifice plate: n = 113; Ø 0.05 mm
1 - plate with orifices; 2- frame for fixing the plate.

Figure 6 shows the scheme of the experimental installation, designed for the second version (set of four microbubble generators). The compressed air supplied by the electrocompressor (2) passes through the pressure reducer (4) to the four-cylinder assembly (7); the compressed air pressure must overcome the hydrostatic load (H), i.e., the height of the water layer in the tank (8) and the loss of air pressure when passing through the orifices.

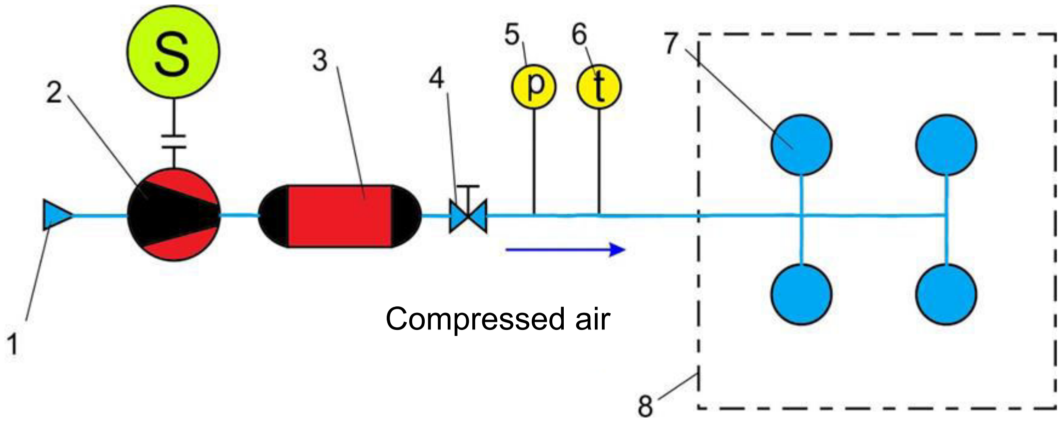

Fig. 6. The scheme of the experimental installation for water aeration using fine bubble generators.
1 - air filter; 2 - electrocompressor; 3 - compressed air tank; 4 - pressure reducer; 5 - pressure measuring device; 6 - temperature measuring device; 7 - set of four cylinders each supporting a plate with orifices of Ø = 0.05 mm; 8 - water tank.

In version II, atmospheric air (21% O_2 and 79% N_2) is introduced into the water tank by means of the fine bubble generator which has 4 cylinders, each cylinder having a perforated plate with 113 orifices Ø 0.05 mm (figure 7).
Figure 7 shows a side image of the fine bubble generator with plates with orifices Ø = 0.05 mm. In the second version, the 4 cylinders with the perforated plate at the top can be seen.

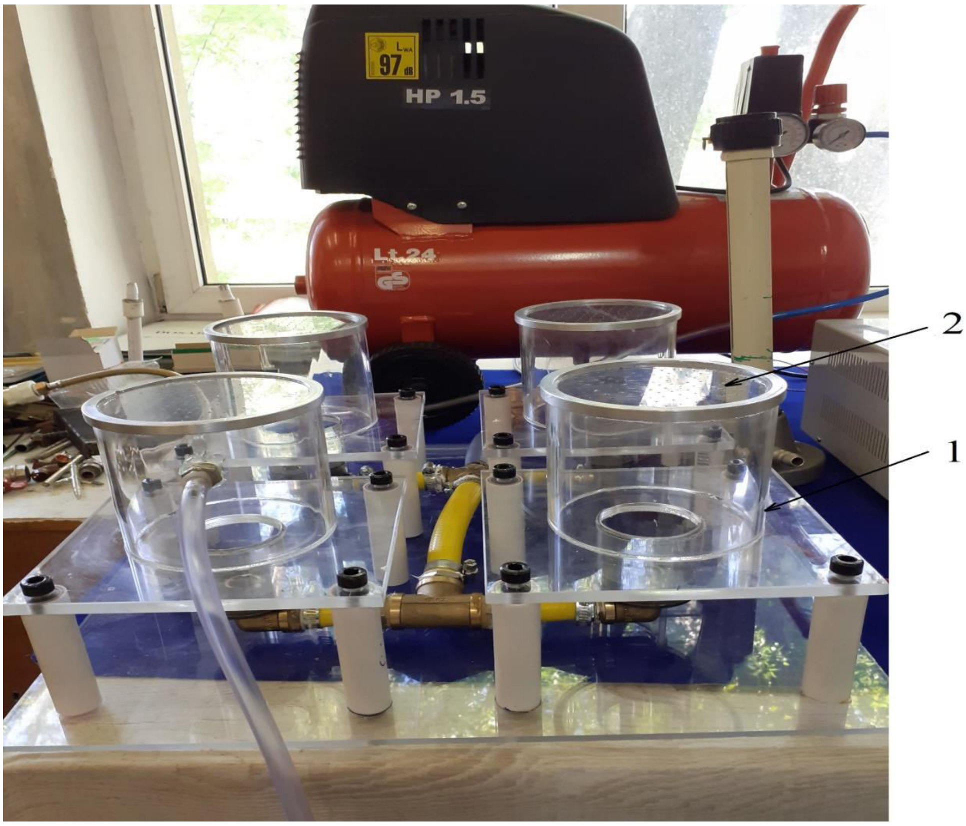

Fig. 7. Side view of the fine bubble generator
1 - cylinder with Ø = 105 mm; 2- perforated plate with Ø = 90 mm.

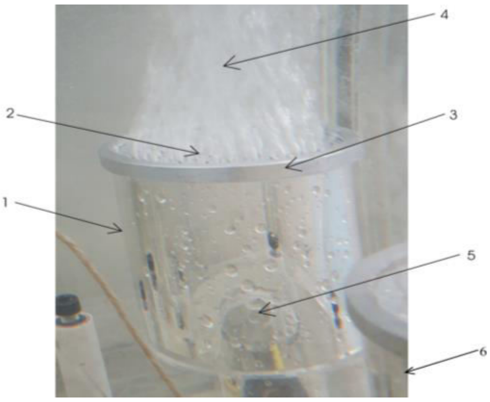

Fig. 8. One FBG element with Ø 0.05 mm in operation
1 - cylinder body; 2 - plate with 113 orifices Ø 0.05 mm; 3 - clamping ring; 4 - bubble column; 5 - compressed air connection; 6 - water tank.

The operation of a component (one cylinder) of the fine bubble generator is shown in figure 8.

2.2. Methods

The rate of oxygen transfer to water is specified by the relation [2] [12]:

$$\frac{\mathrm{d}C}{\mathrm{d}\tau} = a \cdot k_L \left(C_s - C\right) \tag{8}$$

where:
C –the concentration of dissolved oxygen at time τ;
$a \cdot k_L$ –the volumetric mass transfer coefficient;
C_s – the oxygen concentration in water, at saturation.

$$a = \frac{A}{V}\left[\frac{m^2}{m^3}\right] \tag{9}$$

where:
a – the specific interfacial area between air and water;
A – the area of gas bubbles [m^2];
V– the volume of the biphasic system (air + water) [m^3];
k_L – the mass transfer coefficient [m / s].
Relation (8) indicates the change of the oxygen concentration in time, because of the molecular diffusion of oxygen from the area with high concentrations to the area with low concentrations.
Analyzing the relation (1) one can observe a series of factors that influence the change in the rate of oxygen transfer to water; these factors are presented in table 1.

Table 1: Solutions for increasing dC/dτ.

No.	The pursued goal	The theoretical solution	The practical solution
1	The increase of C_s	Increasing the O_2 concentration in the air introduced into the water.	Introduction of oxygen, ozone (O_3) into water
2	The decrease of C_0	Minimum values for C_0 depending on the nature of the micro-organisms present in the water	Decreased initial water temperature; Introduction of C_0-reducing substances into water.
3	The increase of k_L	Intensification of turbulence	FBG rotation Using mobile FBG
4	The increase of a	Decrease the gas bubble diameter	Decreasing of the FBG orifices diameter.

From table 1 it results that, to increase the concentration of dissolved oxygen in water, it is necessary to reduce the diameter of the orifices of the fine bubble generators, therefore, implicitly to decrease the diameter of the air bubbles immersed in water [13].

As a result, the use of micro technologies in water aeration processes is considered for creating aeration installations that produce air bubbles with a diameter of less than 1 mm.
For a sphere of radius "r" and diameter "d", the relation (9) becomes:

$$a = \frac{A}{V} = \frac{4\pi r^2}{\frac{4}{3}\pi r^3} = \frac{3r^3}{r^3} = \frac{3}{\frac{d}{2}} = \frac{6}{d} \tag{10}$$

From relation (10) one can observe that for a spherical air bubble "a" it will increase if the diameter of the air bubble will decrease. The diameter of the air bubble is proportional to the diameter of the air bubble outlet in the water.
The paper studies two versions:
-Version I: FBG has a plate with orifices with a diameter d_I = 0.1 mm
-Version II: FBG has a plate with orifices with a diameter d_{II} = 0.05 mm
The relation (10) for the two versions becomes:

$$a_I = \frac{6}{d_I} = \frac{6}{0.1} = 60 \tag{11}$$

$$a_{II} = \frac{6}{d_{II}} = \frac{6}{0.05} = 120 \tag{12}$$

Because a_{II} is higher than a_I it is predicted that the oxygen transfer rate to water will be higher in the case of version II [14].

3. Results and discussion

3.1. Results

As initial data, at the beginning of the experimental measurements there are specified:
- The volume of water in the tank: V_{H2O} = 0.125 m^3;
- The height of the water layer in the tank: H = 0.5 m;
- The initial concentration of the dissolved oxygen in water: C_0 = 5.84 mg / dm^3;
- The water temperature;

Because the experimental measurements were performed on different days, the water temperature was different, as follows:
- for version I: t_{H2O} = 23.7 °C, which corresponds to a concentration of dissolved oxygen at saturation f C_s = 8.4 mg / dm^3 [1];
- for variant II: t_{H2O} = 19.5 °C, which corresponds to a concentration of dissolved oxygen at saturation C_s = 9.2 mg / dm^3;

e) The air flow rate introduced into water: $\dot{V}$= 0.6 m^3 / h;
f) The air pressure, measured in the body of the fine bubble generator: p = 583 mmH_2O
g) The duration of the experiments: τ = 120 min.
The results of the experimental measurements are presented in Tables 2 and 3:

Table 2: Experimental data for version I: C = f (τ).

No.	τ [min]	0	15	30	45	60	75	90	105	120
1	*C* [mg/dm^3]	5.89	6.89	7.65	8.01	8.10	8.26	8.31	8,.35	8.39
2	*Cs* [mg/dm^3]	8.4	8.4	8.4	8.4	8.4	8.4	8.4	8.4	8.4

Table 3: Experimental data for version II: C = f (τ).

No.	τ [min]	0	15	30	45	60	75	90	105	120
1	*C* [mg/dm^3]	5.84	7.90	8.20	8.35	8.53	8.71	8.75	8.85	9.00
2	*Cs* [mg/dm^3]	9.2	9.2	9.2	9.2	9.2	9.2	9.2	9.2	9.2

The results presented in Tables 2 and 3 fall within the range of values obtained in other specialized papers [15-19].

3.2. Discussion

The aim of experimental researches is to evaluate the variation of the concentration of dissolved oxygen in water, as a function of time: C = f (τ).
Performing the measurements involves the following steps:
1. Check that the 113 orifices with Ø = 0.1 mm function, i.e., the atmospheric air is introduced into the bubble generator;
2. Fill the tank with water up to H = 500 mm H_2O;
3. Measure C_0, t_{H2O}, t_{air};
4. Insert the fine bubble generator into the water tank and note the time (τ);
5. Every 15 minutes, take the fine bubble generator out of the tank and measure the dissolved oxygen concentration; subsequently, reinsert the fine bubbles generator in the water tank.
6. When a horizontal level of the function C = f (τ) is reached, the measurements stop, with the condition: C ≈ Cs;
7. From previous researches [20-21], the concentration of dissolved oxygen in water tends to saturate after two hours. Therefore, the measurement of the oxygen concentration will be performed at the moments: 15, 30, 45, 60, 75, 90, 105, 120 minutes.
8. At the end of the measurements, clean the oxygenometer probe and drain the water from the tank. Figure 9 shows that the values of the dissolved oxygen concentration in water are higher in version II, red curve, than those of version I, blue curve.

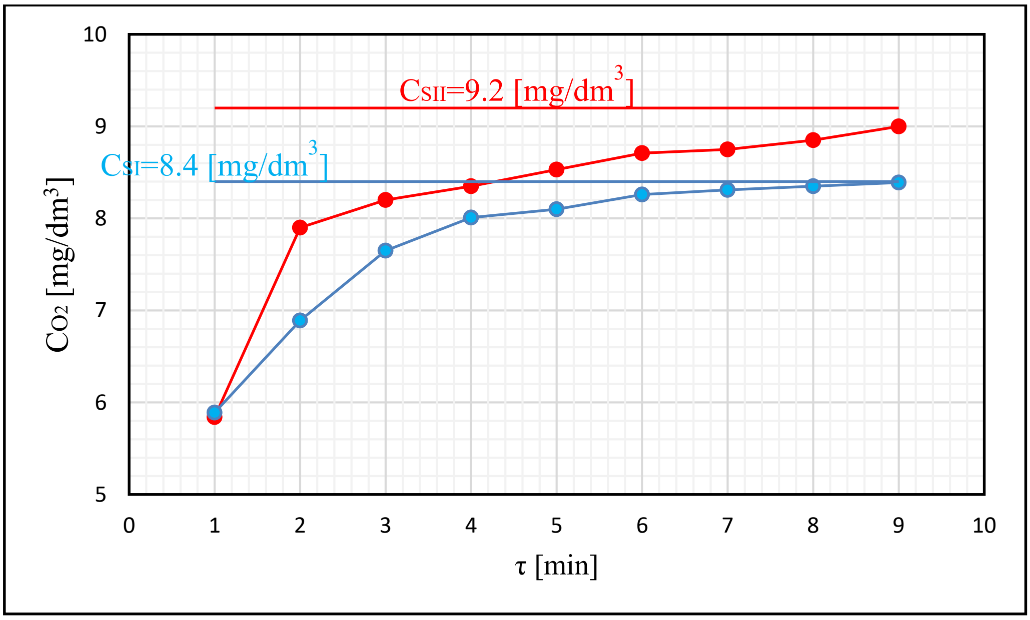

Fig. 9. Graphical representation of the function = f(τ) for version I curve 1 și and for version II curve 2
Blue curve: C= f(τ) for FBG with ø = 0.1 mm;
Red curve: C= f(τ) for FBG with ø = 0.05 mm.

Comparing the values of C mg / dm^3 in table 2 with those in table 3, one can observe that those in Table 3 are higher, so the aeration in version II is more efficient.

4. Conclusions

Any process of aeration of water aims at an increase in the content of the dissolved oxygen in the water.
This oxygen concentration must be maintained within normal limits, because its increase or decrease affects the quality of the water, so implicitly the existence of life forms in the water.
Tables 2 and 3 show the following values of the function C = f (τ):

- in table 2, the value of C tends to C_s after 105 min: 8.35 → 8.4 [mg / dm^3]
- in table 3, the value of C reaches the value of 8.35 [mg / dm^3] after a time of 45 min.

Therefore, the aeration process has a shorter duration by about 50%, i.e. the duration of the aeration process is reduced by half.

As a result, a sure way to improve the stagnation of stagnant water is to make fine bubbles generators to introduce air bubbles with a diameter as small as possible; this involves making plates with orifices as small as possible.

In the paper, a diameter of the orifices of 0.05 mm was reached, which the authors hope will be exceeded, tending to orifices of the order of nanometers.

References

[1] Oprina, G., I. Pincovschi, and Gh. Băran. *Hydro-Gas-Dynamics Aeration systems equipped with bubble generators / Hidro-Gazo-Dinamica Sistemelor de aerare echipate cu generatoare de bule*. Bucharest, Politehnica Press, 2009.

[2] Robescu, D.L., F. Stroe, A. Presura, and D. Robescu. *Wastewater treatment techniques / Tehnici de epurare a apelor uzate*. Bucharest, Technical Publishing House, 2011.

[3] Besnea, D., Gh.I. Gheorghe, M. Constantin, N. Băran, and B. Tănase. "Researches regarding the placement of fine bubble generators in water tanks." *Review Precision Mechanics, Optics and Mechatronics*, no. 50 (2016): 48-52.

[4] Voicu, C.R., R. Cusma, I.L. Grigore, N. Băran, N. Albu, F. Șelea, and M. Petroșel. "Theoretical and experimental research regarding the water oxygenation through pipes." Paper presented at the 25th International Conference on Hydraulics and Pneumatics HERVEX, Băile Govora, Romania, November 13-15, 2019.

[5] Donțu, O., R. Cusma, C.R. Voicu, I.L. Grigore, F. Șelea, N. Băran, M. Petroșel, and T.C. Cioienaru. "Researches regarding the design and construction of air dispersion devices in the transported water through pipes." Paper presented at the 25th International Conference on Hydraulics and Pneumatics HERVEX, Băile Govora, Romania, November 13-15, 2019.

[6] Miyahara, T., Y. Matsuha, and T. Takahashi. "The size of bubbles generated from perforated plates." *International Chemical Engineering* 23 (1983): 517-523.

[7] Micu, C.A., and L. Bogatu. *Materials processing technology in fine mechanics / Tehnologia procesării materialelor în mecanica fină*. Bucharest, Printech Publishing House, 2002.

[8] Besnea, D., O. Donțu, and D. Cioboată. *Mechatronic technologies and their applications / Tehnologii mecatronice si aplicatiile lor*. Bucharest, Printech Publishing House, 2017.

[9] Tănase, B., D. Besnea, R. Mlisan, M. Constantin, and N. Băran. "Constructive solutions for the achievement of fine bubble generators based on micro-drilling technologies." *IJISET - International Journal of Innovative Science, Engineering & Technology* 2, no. 2 (2015): 46-50.

[10] Băran, N., I.M. Călușaru, and G. Mateescu. "Influence of the architecture of fine bubble generators on the variation of the concentration of oxygen dissolved in water." *Scientific Bulletin of the University Politehnica of Bucharest, Series D, Mechanical Engineering* 75, no. 3 (2013): 225-236.

[11] Băran, N., M. Constantin, E. Tănase, and R. Mlisan. "Researches regarding water oxygenation with fine air bubbles." *Scientific Bulletin of the University Politehnica of Bucharest*, *Series D, Mechanical Engineering* 78, no. 2 (2016): 167-178.

[12] Călușaru, I.M. *The influence of the physical properties of the liquid on the efficiency of the oxygenation processes / Influenţa proprietăţilor fizice ale lichidului asupra eficienţei proceselor de oxigenare*. Doctoral thesis. Politehnica University of Bucharest, Faculty of Mechanics and Mechatronics, Bucharest, 2014.

[13] Pătulea, Al.S. *The influence of functional parameters and the architecture of fine bubble generators on the efficiency of aeration installations / Influenţa parametrilor funcţionali şi a arhitecturii generatoarelor de bule fine asupra eficienţei instalaţiilor de aerare*. Doctoral thesis. Politehnica University of Bucharest, Faculty of Mechanics and Mechatronics, Bucharest, 2012.

[14] Mlisan (Cusma), R. *The influence of fine bubbles generators architecture on the dissolved oxygen concentration in water / Influenţa arhitecturii generatoarelor de bule fine asupra creşterii concentraţiei de oxigen dizolvat în apă*. Doctoral thesis. Politehnica University of Bucharest, Faculty of Mechanics and Mechatronics, Bucharest, 2017.

[15] Călușaru, I.M., N. Băran, and Al. Pătulea. "The influence of the constructive solution of fine bubble generators on the concentration of oxygen dissolved in water." *Advanced Materials Research* 538-541 (June 2012): 2304-2310.

[16] Droste, L.R. *Theory and Practice of Water and Wastewater Treatment*. Hoboken, New Jersey, John Wiley & Sons, Inc., 1996.

[17] Stenstrom, M.K., and D. Rosso. *Aeration* (online presentation). University of California, Los Angeles, 2010.

[18] Tănase, E. Beatrice*. The influence of the instilled gas composition in water on the dissolved oxygen content / Influența compoziției gazului insuflat în apă asupra conținutului de oxigen dizolvat*. Doctoral thesis. Politehnica University of Bucharest, Faculty of Mechanics and Mechatronics, Bucharest, 2017.

[19] Oprina, G. *Contributions to the hydro-gas-dynamics of porous diffusers* / *Contribuţii la hidro-gazo-dinamica difuzoarelor poroase*. Doctoral thesis. Politehnica University of Bucharest, Faculty of Power Engineering, 2007.

[20] Constantin, M., N. Băran, and B. Tănase. "A New Solution for Water Oxygenation." *International Journal of Innovative Research in Advanced Engineering (IJIRAE)* 2, no. 7 (2015): 49-52.

[21] Căluşaru, I.M., N. Băran, and Al. Pătulea. "Researches regarding the transfer of oxygen in water." Paper presented at the 3rd International Conference on Mechanic Automation and Control Engineering (MACE 2012), Baotou, China, July 27 -29, 2012.

[22] Pătulea, Al., N. Băran, and I.M. Căluşaru. "Measurements of Dissolved Oxygen Concentration in Stationary Water." *World Environment* 2, no. 5 (2012): 104-109.

FLUIDAS

NATIONAL PROFESSIONAL ASSOCIATION OF HYDRAULICS AND PNEUMATICS IN ROMANIA

fluidas@fluidas.ro